INFORMATION TO USERS

This manuscript has been reproduced from the microfilm master. UMI films the text directly from the original or copy submitted. Thus, some thesis and dissertation copies are in typewriter face, while others may be from any type of computer printer.

The quality of this reproduction is dependent upon the quality of the copy submitted. Broken or indistinct print, colored or poor quality illustrations and photographs, print bleedthrough, substandard margins, and improper alignment can adversely affect reproduction.

In the unlikely event that the author did not send UMI a complete manuscript and there are missing pages, these will be noted. Also, if unauthorized copyright material had to be removed, a note will indicate the deletion.

Oversize materials (e.g., maps, drawings, charts) are reproduced by sectioning the original, beginning at the upper left-hand corner and continuing from left to right in equal sections with small overlaps.

Photographs included in the original manuscript have been reproduced xerographically in this copy. Higher quality 6" x 9" black and white photographic prints are available for any photographs or illustrations appearing in this copy for an additional charge. Contact UMI directly to order.

ProQuest Information and Learning
300 North Zeeb Road, Ann Arbor, MI 48106-1346 USA
800-521-0600

UMI®

DISSERTATION

CARRIER INTERFEROMETRY FOR NEXT GENERATION CDMA AND TDMA WIRELESS SYSTEMS: A MULTI-CARRIER FRAMEWORK

Submitted by

Balasubramaniam Natarajan

Department of Electrical and Computer Engineering

In partial fulfillment of the requirements

for the Degree of Doctor of Philosophy

Colorado State University

Fort Collins, Colorado

Spring 2002

COLORADO STATE UNIVERSITY

March 27, 2002

WE HEREBY RECOMMEND THAT THE DISSERTATION PREPARED UNDER OUR SUPERVISION BY BALASUBRAMANIAM NATARAJAN ENTITLED **CARRIER INTERFEROMETRY FOR NEXT GENERATION CDMA AND TDMA WIRELESS SYSTEMS: A MULTI-CARRIER FRAMEWORK** BE ACCEPTED AS FULFILLING IN PART REQUIREMENTS FOR THE DEGREE OF DOCTOR OF PHILOSOPHY.

Committee on Graduate Work

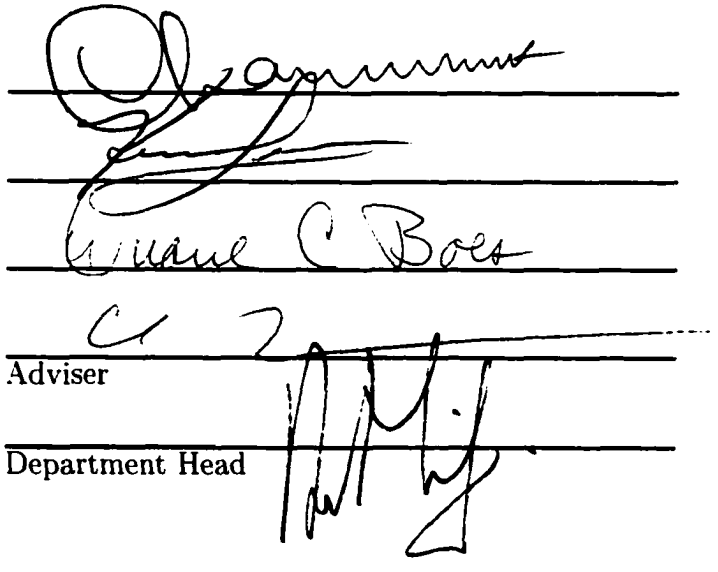

Adviser

Department Head

ABSTRACT OF DISSERTATION

CARRIER INTERFEROMETRY FOR NEXT GENERATION CDMA AND TDMA WIRELESS SYSTEMS: A MULTI-CARRIER FRAMEWORK

In this thesis, we introduce an enabling technology called Carrier Interferometry, that has the potential to satisfy many of the requirements of next generation wireless systems. The objective of this work is not only to present the technology, but also demonstrate the benefits it offers to multiple access schemes like MC-CDMA and TDMA, and modulation schemes like FSK.

We first introduce the Carrier Interferometry (CI) signal, the basic building block for the Carrier Interferometry approach. This signal corresponds to the superposition of N orthogonal carriers equally spaced in frequency. A theoretical analysis of the orthogonal and pseudo-orthogonal properties of this CI signal is provided and it is shown how as a result, this signal can support many practical applications.

We apply the CI approach to an MC-CDMA system in the form of a powerful set of complex spreading codes (referred to as CI codes). These CI spreading codes of length N have a unique feature which allows the CI/MC-CDMA system to (1) support N users orthogonally; (2) then, as system demand increases, codes can be selected to accommodate up to an additional N users pseudo-orthogonally. Furthermore, the performance of CI/MC-CDMA shows minimum degradation when capacity is doubled.

We also introduce the CI signal into TDMA systems as a multi-carrier implementation of the sinc pulse shape. We demonstrate that this proposed multi-carrier pulse

shape along with frequency domain receiver processing, provides significant performance gains relative to TDMA systems employing traditional pulse shapes. The CI approach in TDMA also results in a doubling of throughput via pseudo-orthogonality.

The CI approach is also applied to fundamental FSK modulation to yield significant performance and throughput gains. We demonstrate that, by introducing a multi-carrier implementation of FSK using the CI approach, along with a novel coherent receiver, we can successfully employ an FSK system in a frequency selective channel and exploit frequency diversity benefits.

Finally, we demonstrate how our CI-based multi-carrier approach can be extended to the synthesis of any arbitrary pulse shape. We demonstrate a corresponding signal decomposition at the receiver side leading to dramatic performance gains.

These are definitely exciting times in the wireless world. There is a large gap emerging between public expectations for mobile communications and available technologies. The work presented in this thesis is extremely significant as we introduce a fundamental technology that can play a big part in closing this gap.

Balasubramaniam Natarajan
Department of Electrical and Computer Engineering
Colorado State University
Fort Collins, Colorado 80523
Spring 2002

ACKNOWLEDGEMENTS

There are many people who I would like to thank for their love and support throughout this five-year journey.

First and foremost, I am very grateful to Dr.Carl R.Nassar for being an understanding advisor and a good friend. A loving and caring man, Carl helped me unearth my research potential and nurtured my spiritual growth. Through both rough and happy times, he helped me find my peace within. My self confidence in my academics and in my research has grown, thanks to his encouragement.

I am very fortunate to have wonderful people in my committee and I would like to thank all of them. Dr.Chandrasekhar has always welcomed me and my questions with an open heart and encouraged me to excell in my academics. I will carry his words of advice with me long after my Ph.D. days. Dr.Kevin L.Lear has been a solid support through my academic life. His inputs and ideas were extremely valuable. He set a very good example for how to organize and articulate my thoughts, words and actions. Dr.Boes, thanks for your kindness. You have been an inspiration and you demonstrated how exciting and fun Statistics can be.

My PhD experience was not only an academic journey, but a journey of personal growth as well. Here, again, there are many people who I want to acknowledge for their love and support.

First, I would like to thank my parents for the sacrifices they have made and for imparting the values and morals that guide my life. Amma and Appa, thank you for sharing your selfless love and affection. Thanks to my sister Bharathi and her wonderful family for being there for me, through all the challenging years of my life.

Thanks Ammamma, for all the blessings.

A special thanks to Rekha, for being my best friend and my spiritual companion through the last year and for many more years to come. The love we share has helped me overcome all the hurdles and find bliss within ourselves. You are an endless source of joy in my life.

Thanks, Wendy, Jeremy, Rama, Hari, Sundar, Padma, Chandra and Bhagya for making me one with your family. You are all a bundle of joy and have given me strength in this long journey.

Thanks to many other people who have provided me with warm companionship and lots of fond memories. There are so many, I can only begin with this list that is never-ending: Karen, Beth, Nancy, Tom, Dr.Lile, Dr.Wilmsen, Dr.Bringi and Sreedevi Bringi, Jong, David, Reza, Julie, Marco, Kishor, Chetan, Shamal, Kripa, Maha, Greg, Jason, Cho, Sai Group of Fort Collins, Bhavani, Babbu, Siva, and many others.

Last but not the least, my very existence and life is indebted to my God and Guru, Sri Sathya Sai Baba. Thank you, Swami, for your infinite grace and compassion. Thank you for being with me, around me and in me.

Thank you all, for giving me a place in your lives. That completes mine.

TABLE OF CONTENTS

LIST OF FIGURES

LIST OF TABLES

Chapter 1

Introduction

This first chapter introduces the area of interest in this thesis, namely enabling technologies for wireless communication systems. This is followed by a summary of the original contributions of this thesis.

1.1 History of Wireless Systems

Radio communications began with the discovery of electromagnetic waves by Hertz in 1888. Since then there has been tremendous growth in the demand for wireless communication services. The desire to communicate and be connected at all times and places has fueled this demand.

Commercial wireless communication systems have exhibited tremendous growth over the past decade. Currently, there are more than 100 million users in the USA and Europe and this figure is increasing daily [1]. Throughout the world, wireless communication systems are enabling developing countries to provide instant telephone access to new subscribers who otherwise would have to wait years for wireline access. The number of new wireless subscribers is growing 15 times faster than wireline subscribers and analysts predict that, by the year 2006, there will be equal number of wireless and wireline connections throughout the world [2].

The evolution of wireless mobile telephone systems can be divided into three generations as discussed in the following subsections.

1.1.1 First Generation Systems

The first analog cellular system went into operation in Chicago in 1983 and was governed by AMPS (advanced mobile phone system) standards. The AMPS cellular standard uses analog FM (frequency modulation)and full duplex radio channels. The frequency division multiple access (FDMA) technique (see section 2.2) enables multiple users to share the same spectrum.

This standard supported clear communication and inexpensive mobile telephones, but the transmissions were easy to intercept and therefore prone to eavesdropping. The systems were also severely limited with respect to capacity and coverage.

The European cellular service, which pre-dated the AMPS system, used the nordic mobile telephone (NMT) standard beginning in 1982. Japan and few other nations also developed their own analog standards.

1.1.2 Second Generation Systems

The evolution of second generation systems was spurred by the need to satisfy consumer demands and to better utilize spectrum. The most widespread second generation techniques are based on (1) the European standard, GSM (global system for mobile communications) (2) IS-136, based on a TDMA (see section 2.3) backbone, or (3) IS-95 supporting a CDMA (see section 2.4) backbone. The GSM standards were released in 1990 and are deployed in the 900 and 1800 MHz bands. The IS standards used in USA are employed in the 800 and 1900 MHz bands. Japan operates different cellular systems in the 800 MHz and 1500 MHz bands.

These second generation systems use digital processing techniques, compression,

coding, and network-control techniques to conserve bandwidth, prevent eavesdroppings and unauthorized use of networks, and also to support additional services (three-way calling, voice mail, text transmission).

The commercial success of the second generation systems has stimulated widespread interest in making these systems more attractive for data services and providing wireless Internet access. The technology will continue to grow as research and development organizations worldwide try to make the transition to third generation systems.

1.1.3 Third and Future Generation Systems

The international mobile telecommunications - 2000 (IMT-2000) is the standard being developed by the ITU (international telecommunication union) to set the stage for the third generation of mobile communication systems. IMT-2000 lays down the goals for third generation systems. These goals provide insight into the basic requirements of next generation systems.

Next generation wireless systems represent both an evolution of and an enhancement to present systems. These include -

- increased capacity and coverage
- support of high bit rate data, for Internet and multimedia services
- higher quality of service, especially for voice
- increased security
- improved ease of operation
- worldwide common frequency bands
- flexibility for evolution

Another important objective of next generation wireless systems is to support the

idea of "unification". Currently, there are a large number of wireless systems and applications that service a wide variety of communication needs. Different transmission protocols and frequency bands characterize the communication markets in different countries. There are significant differences in the physical layer design of these different systems. This presents a compatibility problem and it is not possible to use the same mobile equipment in different countries. One of the concepts that has received widespread attention is "Software Radio" [3]-[10]. Here, engineers envision a simple piece of software capable of switching mobiles from TDMA to DS-CDMA (direct-sequence CDMA) to MC-CDMA (multi-carrier CDMA) to OFDM (orthogonal frequency division multiplexing), while maintaining a common hardware platform [11]. This enables roaming, with a single inexpensive phone, between different networks worldwide - a concept referred to as "Global Roaming".

1.1.4 Personal Area Networks

Another market that promises to flourish in the future is that of personal area networks. Based on the Bluetooth standard [12], the vision here is to provide short-range wireless connectivity between different electronic devices in an ad-hoc fashion at home or in an office. This personal area network also serves as a wireless bridge to existing data networks.

Bluetooth enabled devices will automatically seek each other out and configure themselves into networks. Though small, these networks can be quite useful. For example, they can forward email received on a cellular phone in a person's pocket to the notebook or laptop computer in a briefcase; they can download data from a digital camera to a PC or a cell phone; or they can alert their owners as they pass by a Bluetooth enabled vending machine.

More than 2000 organizations have joined the Bluetooth special interest group

(SIG) and most of them are currently developing Bluetooth-enabled products under a specification developed by the group. The IEEE 802.15 personal area networks working group, formed in early 1999, has made Bluetooth the foundation for a range of portable products. They are developing a 1Mbps as well as a 20 Mbps standard, that can be widely deployed for short range networks.

The expectations for Bluetooth are huge. Analyst's market projections place Bluetooth-enabled products in the "next big thing" category, with sales expected to top a billion units by 2005.

1.2 Enabling Technologies

In the previous section, we presented the evolution of wireless communication systems and services and provided a glimpse of the future. This rapid growth in wireless communications has been aided by the timely emergence of enabling technologies. These technologies are extremely vital, as they equip next generation systems to meet the demands of new subscribers and services. For example, spectrum is becoming a rare commodity. Therefore, these technologies aim at extracting the most out of the limited spectrum, in terms of capacity and performance.

Perhaps the two most well founded technologies that have been successfully deployed in wireless systems are TDMA and CDMA. These technologies are also the basis for next generation (3G) systems. Specifically, DS-CDMA is the backbone for 3G (third generation) wireless telephony in most parts of the world. TDMA is also proposed for 3G in some parts of the world, and more recently, it has been adopted for the IEEE 802.16 standard for fixed broadband wireless services.

With a hope of enhancing the capacity and the quality of service in these multiple access schemes, researchers have been working on novel transmission and reception strategies. For example, in TDMA systems like GSM, considerable work and efforts

have focussed on novel receiver designs to improve performance [13]-[17]. However, in all these works, the nominal performance gains achieved via time domain signal processing come at the cost of increased complexity and fall short of the expectations for the future. Furthermore, in [18] and [19], a technique to increase throughput in TDMA using the idea of "oversaturation" or "channel overloading" have been proposed. Yet the gains in throughput are minimal (less than 50%) when considering the tremendous cost in complexity, making this technique unattractive.

Similarly, many enabling techniques have emerged to enhance CDMA systems. For example, Multi-user detection strategies have become an extremely popular area of research. In Multi-user detection, receivers are designed to cancel out the interference introduced by unwanted users, enabling increases in performance and capacity [20]. Significant research has been and continues to be focussed in this area ([21]-[23]).

The enabling technology in Bluetooth (personal area network) systems is a frequency hopping/FSK (frequency shift keying) modulation technique. Now, FSK is not a spectrally efficient modulation technique, but the need for simplicity in Bluetooth transceivers motivated this choice. Some researchers have focussed their efforts in improving FSK performance in multipath wireless channels by novel receiver designs ([24]-[28]). However, in all these works, the system performance degrades rapidly as the time delay spread of the channel approaches the symbol duration. Recently, in [29],[30], a RAKE architecture is employed to exploit path diversity in FSK systems. But, the impact of inter-path interference along with hardware limitations (restricting the number of RAKE fingers that can be implemented) reduces this system's ability to benefit from the available diversity. So, there remain some vexing technical issues that plague FSK modulation which in turn limits the attractiveness of the much hyped Bluetooth technology.

1.3 The Emergence of Multi-Carrier Technologies

One emerging technology is catching the attention of wireless system engineers around the globe: multi-carrier communications, and its application to multiple access. In particular, there has been a great deal of research and development of late in the areas of OFDM (orthogonal frequency division multiplexing)([31]-[38]) and MC-CDMA (multi-carrier code division multiple access)([39]- [48]).

One of the catalysts for the popularity of OFDM is its adoption in different wireless system standards. The IEEE 802.11a wireless local area network (WLAN) [49] standard has adopted OFDM as its technology of choice. Additionally, the IEEE 802.15 standard is considering OFDM for its high rate 20 Mbps PAN system. OFDM is also being considered as a viable technology for 4G wireless systems [50].

MC-CDMA is also gaining in popularity. The objective of current research is to enhance CDMA capabilities in terms of capacity and performance: With regard to performance, MC-CDMA significantly outperforms DS-CDMA (see [51]-[54], section 2.4.3) by employing frequency domain signal processing at the receiver and exploiting frequency diversity gains instead of path diversity gains. Some researchers believe that it is only a matter of time before MC-CDMA surpasses DS-CDMA in popularity.

Developing new spreading codes for MC-CDMA is another approach that engineers have been diligently working on, with the goal of increasing capacity in MC-CDMA. In [55], a thorough analysis and comparison of existing MC-CDMA codes is presented: specifically, [55] examines the use of Hadamard Walsh, Gold, Orthogonal Gold and Zadoff Chu sequences in MC-CDMA systems. In all cases, the MC-CDMA codes are designed to be either orthogonal, supporting N users (where N is the processing gain or code length), or pseudo-orthogonal, supporting greater than N users, at the cost of degraded performance. Furthermore, N is limited to 2^n or $2^n \pm 1$

$(n \in I)$.

1.4 Thesis Overview: The Multi-Carrier Revolution

In this thesis, using an enabling technology called Carrier Interferometry, the scope and power of multi-carrier technologies is significantly enhanced.

The building block for this approach is the Carrier Interferometry (CI) signal. This signal corresponds to the superposition of N orthogonal carriers equally spaced in frequency. The orthogonal and pseudo-orthogonal properties of this CI signal lends itself to support multiple access techniques [56].

Specifically, this approach can be incorporated in an MC-CDMA system as a powerful set of complex spreading codes (referred to as CI codes) ([57]-[61]). These CI spreading codes of length N have a unique feature which allows the CI/MC-CDMA system to (1) support N users orthogonally; (2) then, as system demand increases, codes can be selected to accommodate up to an additional N users pseudo-orthogonally. Additionally, there is no restriction on the length N of the CI code (i.e.,$N \in I$), making it more robust to the diverse requirements of wireless environments. Furthermore, the performance of CI/MC-CDMA is not degraded even after doubling capacity.

We also introduce the CI signal into TDMA systems as a multi-carrier implementation of the sinc pulse shape ([62]-[66]). We demonstrate that this proposed multi-carrier pulse shape along with frequency domain receiver processing, provides significant performance gains (in the order of 5-8 dB) relative to TDMA systems employing traditional pulse shapes. The CI approach in TDMA also results in doubling of throughput via pseudo-orthogonality.

The approach is also applied to fundamental FSK modulation to yield significant

performance and throughput gains in PANs ([67]-[69]). We demonstrate that by introducing a multi-carrier implementation of FSK using the CI approach, we can successfully employ an FSK system in a frequency selective channel. Specifically, using a novel coherent receiver introduced in this work, we show that the new FSK system exploits frequency diversity gains in such multipath channels.

We also show how our CI-based multi-carrier approach can be extended to the synthesis of any arbitrary communication signal [70]. We demonstrate a corresponding signal decomposition at the receiver side that leads to dramatic performance gains.

1.5 Contributions of this Thesis

This section summarizes, in point-form, the key contributions of this dissertation.

- The carrier interferometry signal is introduced and its orthogonality and pseudo-orthogonality properties are presented. A novel way of utilizing this signal for multiple access is demonstrated (Chapter 3, [58],[61]).
- The CI signal is incorporated into MC-CDMA, and is shown to correspond to a powerful set of complex CI spreading codes. This CI/MC-CDMA scheme is shown to support twice the number of users relative to traditional MC-CDMA employing orthogonal spreading codes, with no cost in bit-error-rate performance. The minimum-mean-squared error and maximal ratio combining receivers are derived for CI/MC-CDMA (Chapter 4, [57],[59],[60]).
- The CI/MC-CDMA system is tested in the presence of phase jitters and frequency offsets and robustness in both cases is demonstrated (Chapter 5, [57]).
- The signal compactness in CI/MC-CDMA is determined in terms of crest factor measure. An analysis of the CI/MC-CDMA downlink shows that the crest factor is well within tolerable levels for today's power amplifiers. On the other hand, the CI/MC-CDMA uplink suffers from high (poor) crest factor (CF) values. However,

applying Schroeder's crest factor reduction technique, we demonstrate that the uplink CF is easily brought to very low values (close to that of a pure sine wave) (Chapter 5, [71]).

• The carrier interferometry (CI) signal is introduced as a pulse shape in the design of a TDMA system (Chapter 6, [62]-[66]). The resulting CI/TDMA system, with its frequency-based signal processing is (1) bandwidth efficient, (2) significantly enhances performance, and (3) has the ability to double throughput by positioning CI pulse shapes pseudo-orthogonally in time. Even when the throughputs are doubled, performance still exceeds that of traditional TDMA systems (by 3-6 dB). By application of the multi-carrier approach found in OFDM and MC-CDMA, and by using the pseudo-orthogonality concept that has found widespread use in DS-CDMA, TDMA systems now benefit from significant gains in performance and throughput.

• The CI approach is applied to FSK modulation to enhance personal area network performance and throughput (Chapter 7, [67]-[69]). Specifically, the new CI/FSK scheme is (1) spectrally efficient relative to traditional FSK, and (2) supports increased throughputs through pseudo-orthogonal symbol positioning. It is also shown that (3) the carrier interferometry envelope of the CI/FSK signal maintains excellent peak to average power ratios. (4) The novel coherent receiver designed for CI/FSK makes it suitable for use in frequency selective channels, with the system benefiting from the available frequency diversity.

• The CI approach is extended and a more general multi-carrier signal synthesis/decomposition concept is introduced (Chapter 8, [70]). Here, we develop a multi-carrier implementation of basic pulse shapes such as sinc and raised cosines based on spectral sampling of their Fourier spectrums. To implement this at the transmitter, we propose the linear combining of discrete carriers with the appro-

priate weighting. At the receiver, we introduce a frequency domain processor that decomposes the received signal into its constituent carriers and recombines them coherently, similar to MC-CDMA. This creates a uniform multi-carrier hardware platform and extends the applicability of CI approach to multiple access schemes that employ other classical pulse shapes.

Wireless communications has seen explosive growth over the last two decades. In order to meet the challenges of next generation wireless systems, many enabling technologies are coming to forefront. CI is one such multi-carrier technology that significantly enhances different multiple access schemes in terms of performance (measured in terms of probability of error), network capacity (measured in terms of number of users sharing the system, or, equivalently in terms of throughput per user) and overall ease in implementation.

Chapter 2

Multiple Access Techniques

In this chapter, we present an overview of the commonly used multiple access techniques. First, we discuss the operation of an FDMA system in Section 2.2. Next, we present the TDMA system that forms the backbone of today's GSM system. We then introduce the spread spectrum concept and discuss CDMA systems. Specifically, we present an overview of DS-CDMA systems, the basis for the IS-95 standard. Finally, we present MC-CDMA, a multi-carrier CDMA technique that is a strong candidate for next generation wireless.

2.1 Introduction

Multiple access refers to any method which allows multiple users to share a common channel. In wireless communications, multiple access schemes allow multiple users to share the limited radio spectrum.

If user i and user j share a channel, we require that one of the following conditions be met. First, the users can satisfy the orthogonality condition in time. In this case, the k^{th} and j^{th} user's transmitted signals $s_k(t)$ and $s_j(t)$ satisfy

$$\int s_k(t)s_j(t)dt = 0 \tag{2.1}$$

or, alternatively, the users satisfy the orthogonality condition in the frequency domain:

$$\int S_k(f)S_j(f)df = 0 \tag{2.2}$$

where $S_k(f)$ and $S_j(f)$ represent the frequency domain representation of $s_k(t)$ and $s_j(t)$, respectively.

Sometimes, the orthogonality condition is relaxed to accommodate more users. Here, user i and user j's transmitted signals satisfy the pseudo-orthogonality condition:

$$\int s_k(t)s_j(t)dt \leq \epsilon \tag{2.3}$$

where ϵ is a very small non-zero value. The pseudo-orthogonality condition is represented in the frequency domain as follows:

$$\int S_k(f)S_j(f)df \leq \epsilon \tag{2.4}$$

When the orthogonality condition is satisfied, user i's signal does not interfere with user j's signal resulting in strong receiver performance. The drawback is that the number of users that can share the channel in this way is limited. With pseudo-orthogonality, the users interfere with each other slightly causing a degradation in performance. However, with pseudo-orthogonality, more users can share the same channel.

TDMA and FDMA represent two conceptually simple solutions to transmitting users' signals which satisfy the orthogonality condition. In TDMA, user signals are separated in time. That is, each user transmits or receives his or her information only at certain time slots and all other users remain silent during that time slot.

In FDMA, users' signals are separated in frequency. That is, each user is assigned a specific frequency band or channel and during the period of call, no other user can use the same frequency band. In this way, equation (2.2) is satisfied.

In CDMA, all users share the same frequency band and can transmit at the same time. The users are distinguishable from each other by means of what is called a signature waveform or spreading code. This code can be applied in time or in frequency. The former leads to the most popular implementation of CDMA called direct sequence - CDMA (DS-CDMA). The latter leads to the second implementation of CDMA that is growing in popularity, called multi-carrier CDMA (MC-CDMA).

All these multiple access architectures are discussed in the following sections. Since, CDMA and TDMA systems are of primary interest in this thesis, we discuss these multiple access schemes in greater detail relative to FDMA.

2.2 Frequency Division Multiple Access

Figure 2.1 illustrates the idea of frequency division multiple access (FDMA). In FDMA, signals from various users are separated in frequency. Guard bands are maintained between adjacent signal spectra to minimize crosstalk between channels. Typically, these guard bands form 10% of the total bandwidth. If frequency slots are assigned permanently to the users, the system is referred to as fixed assignment multiple access (FAMA). If some type of dynamic allocation scheme is used to assign frequency slots, it is referred to as demand assignment multiple access (DAMA).

For analog transmission in FDMA systems, FM (frequency modulation) is typically employed, while, for digital data transmission, BPSK, MSK, and QPSK are candidate modulation methods. In general, FDMA systems are not bandwidth efficient and suffer severe performance degradation in multipath fading channels (most wireless environments fall under this category).

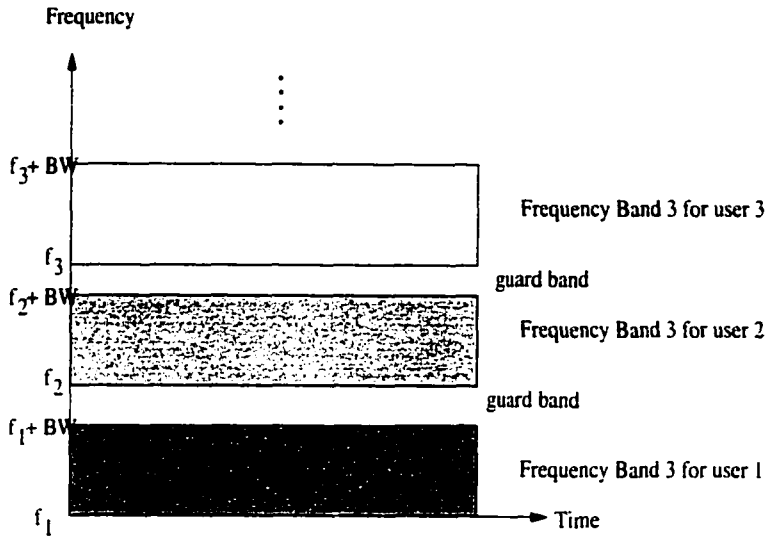

Figure 2.1: FDMA

2.3 Time Division Multiple Access

Time division multiple access (TDMA) systems divide the radio spectrum into time slots, and in each slot only one user is allowed to either transmit or receive. This is shown in Figure 2.2. Each user in TDMA occupies a cyclically repeating time slot that re-occurs every frame, where K time slots comprise a frame. TDMA users buffer the information and send it out as a burst during their allotted time slot. So user transmission is not continuous. Therefore, unlike FDMA systems that can accommodate analog FM, digital data and digital modulation must be used with TDMA.

The user transmissions are interlaced into a frame structure as depicted in Figure 2.3. It is clear that each frame consists of a preamble, an information message, and tail bits. In TDMA/TDD(time division duplex), half of the time slots in the information message are used for the uplink and half for the downlink. In TDMA/FDD(frequency division duplex) different carrier frequencies are used for uplink and downlink transmissions.

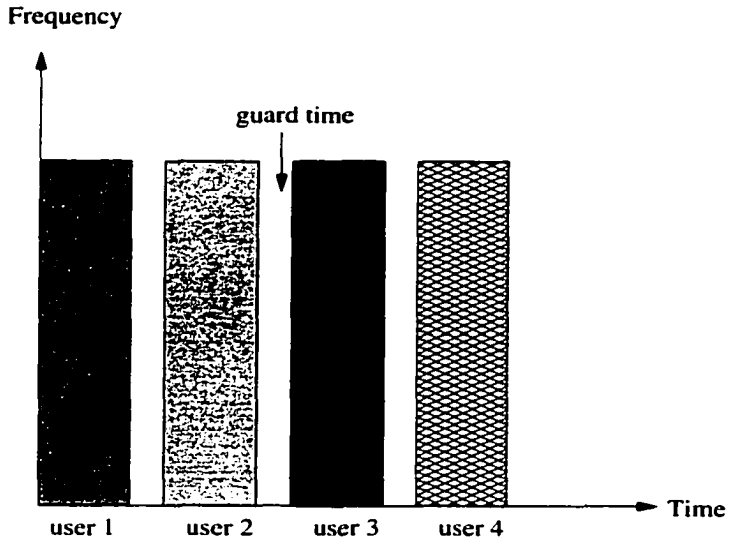

Figure 2.2: TDMA

A typical TDMA transmitter for user k is shown in Figure 2.4. Here, we assume N bits per slot, leading to a transmitted signal given by

$$s_k(t) = \sum_{k=0}^{N-1} \Re e[a_k p(t - kT_b) \cdot m(t) \cdot e^{j2\pi f_c t}] \tag{2.5}$$

where a_k is the k^{th} symbol transmitted in the N symbol TDMA slot; $p(t - kT_b) \cdot m(t)$ is the k^{th} pulse shape (a sinc or raised cosine function) time limited to a slot duration $T_{sl} = NT_b$(where T_b is the symbol duration) by $m(t)$; and f_c is the carrier frequency.

This signal, after transmission through a multipath channel experiences inter-symbol-interference (ISI). In most TDMA systems, this undesirable ISI is combated via equalization. Typically, a decision feedback equalizer [13] is used while in some cases linear equalization techniques may also be employed [17].

The other key features of a TDMA system are given below:

• The non-continuous data transmission in TDMA results in low battery consumption [72]. This is because the subscriber transmitter can be turned off when not in use.

• High synchronization overhead is required in TDMA systems. Since TDMA transmissions are slotted, it requires the receivers to be synchronized for each data burst.

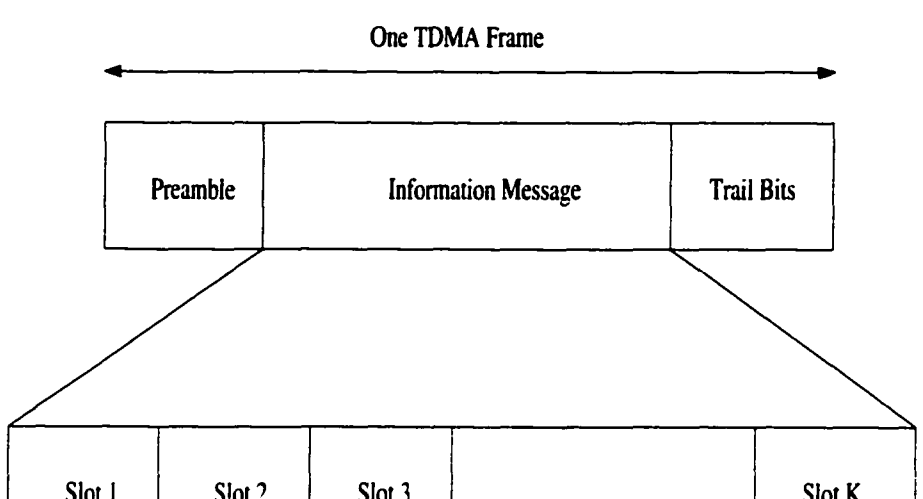

Figure 2.3: TDMA frame structure

In addition, guard slots are necessary to separate users.

TDMA systems are much more bandwidth efficient than FDMA systems. However, they have a hard capacity limit, and thus do not offer flexibility with regard to wireless system design.

2.4 Code Division Multiple Access

Code division multiple access (CDMA) falls under the category of spread spectrum multiple access, where signals have a transmission bandwidth much higher than the minimum required RF bandwidth [73]. Specifically, in CDMA, the narrowband information signal is multiplied by a large bandwidth signal called the spreading signal. This strategy of spreading the transmission spectrum provides immunity to multipath interference and jamming. Eventhough this strategy is wasteful for single user communication, it is extremely bandwidth efficient in a multi-user environment. This is the main reason for the popularity of CDMA systems among wireless system designers.

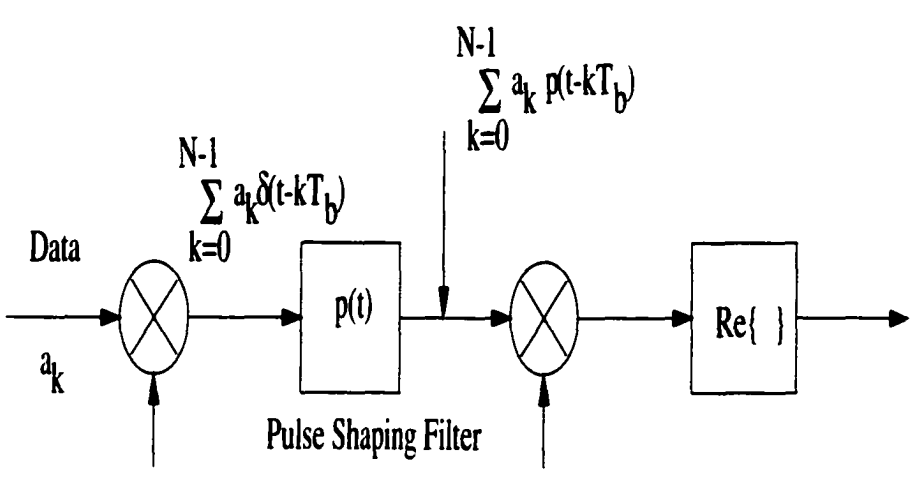

Figure 2.4: TDMA transmitter

The spreading signal is generally a pseudo-noise code referred to as a spreading code (or sequence) that has a chip rate of magnitudes greater than the data rate. As seen in figure 2.5, all users may transmit at the same frequencies, simultaneously, but each user has its own spreading code which is orthogonal to all the other users' spreading codes. At the receiver, a correlation operation allows the receiver to detect the desired user's signal.

If the CDMA spreading codes are applied in time, the system is referred to as direct-sequence CDMA (DS-CDMA) and if the spreading code is applied in frequency, the system is referred to as multi-carrier CDMA (MC-CDMA). We discuss these CDMA techniques next.

2.4.1 DS-CDMA

DS-CDMA has emerged as a dominant player in wireless communications market. Among DS-CDMA's successes is its adoption as the standard of choice in 3G wireless (see, e.g., [74]). The key benefits of DS-CDMA that make it an attractive choice for next generation wireless systems include: enhanced privacy, resistance to multipath

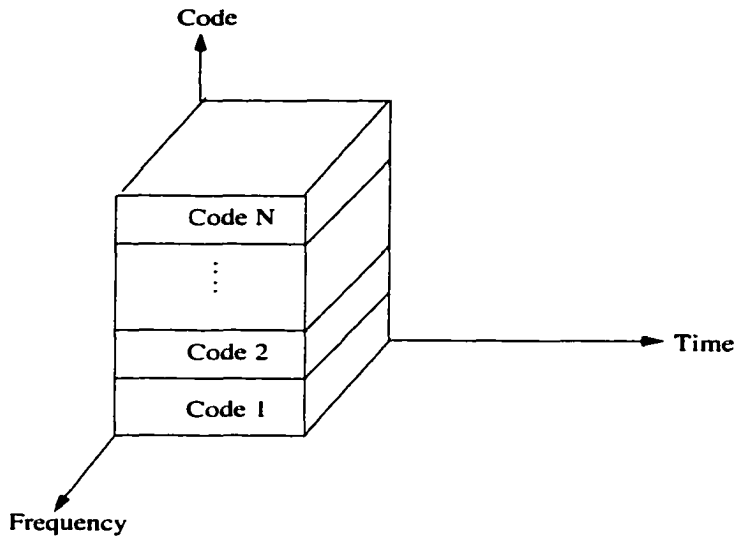

Figure 2.5: CDMA

fading, and improved spectral efficiency relative to TDMA based systems.

The block diagram representation of a DS-CDMA transmitter is shown in Figure 2.6. Here, the DS-CDMA transmitter for user k spreads the original data stream via a spreading code applied in the time domain ($c_k(t)$). Each user is allocated a unique spreading code (usually orthogonal in the downlink and pseudo-orthogonal in the uplink). The ability to suppress multi-user interference is determined by the cross correlation characteristics of the spreading codes.

The code $c_k(t)$ is generally composed of N chips per bit, each modulated by a +1 or -1. Mathematically, this corresponds to

$$c_k(t) = \sum_{i=0}^{N-1} \beta_k^i P_{T_c}(t - iT_c) \tag{2.6}$$

where, $\beta_k^i \in \{-1, +1\}$ is the i^{th} element of user k's spreading sequence $\{\beta_k^0, \beta_k^1, \cdots, \beta_k^{N-1}\}$; T_c is the chip duration, and $P_{T_c}(t)$ is the chip shaping filter. In current DS-CDMA systems, the most commonly used spreading codes are orthogonal Hadamard Walsh codes; the chip shaping filter is either the usual sinc function or raised cosine function.

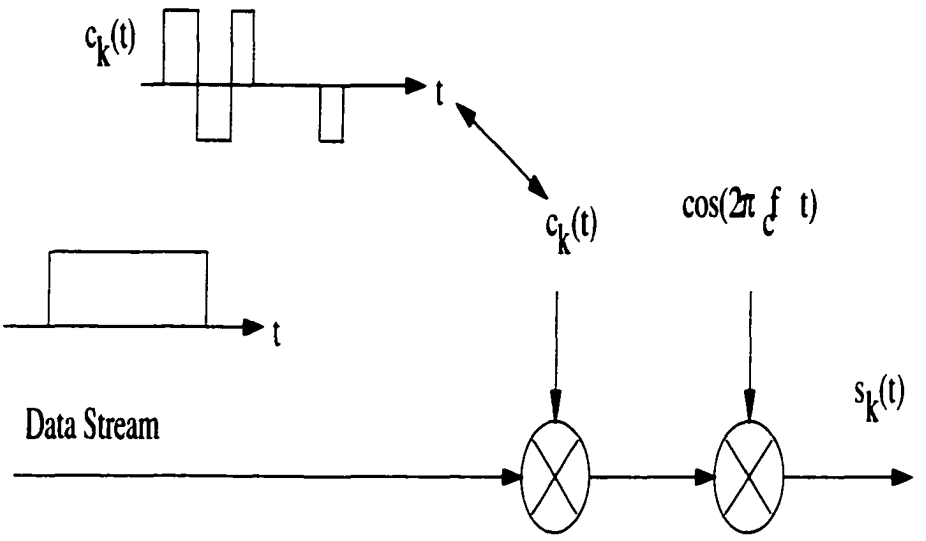

Figure 2.6: DS-CDMA transmitter

Thus, in DS-CDMA, the k^{th} user's transmitted signal for one bit corresponds to (at baseband):

$$s_k(t) = Aa_k \sum_{i=0}^{N-1} \beta_k^i P_{T_c}(t - iT_c) \tag{2.7}$$

where, A is a constant that determines the symbol energy; a_k is the k^{th} user's symbol (and is equal to ± 1 if BPSK is employed). Assuming downlink transmission the total transmit signal with K active users is:

$$s(t) = A \sum_{k=0}^{K-1} a_k \sum_{i=0}^{N-1} \beta_k^i P_{T_c}(t - iT_c) \tag{2.8}$$

Transmitted over a multipath fading channel at carrier frequency f_c, the signal arriving at the receiver side corresponds to

$$r(t) = A \sum_{l=0}^{L-1} \alpha_l s(t - \tau_l) \cos(2\pi f_c t + \phi_l) + n(t) \tag{2.9}$$

where L is the total number of resolvable paths; α_l is the fading parameter of the l^{th} path; τ_l is the time delay of the l^{th} path; ϕ_l is the phase offset of the l^{th} path; and $n(t)$ is the additive white Gaussian noise.

Thus, the received signal is the superposition of several multipath signals arriving with different delays (in the time domain). Here, the cross correlations of different users' signals on different paths are no longer the cross correlations of the time-aligned spreading codes.

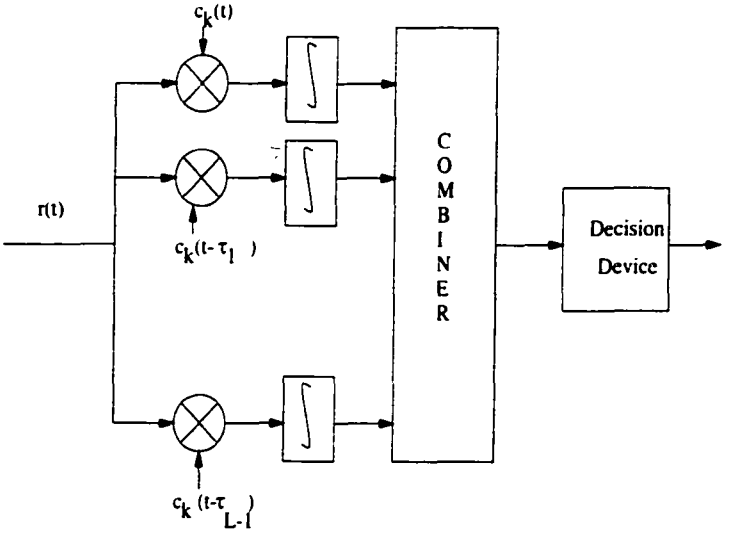

Figure 2.7: DS-CDMA RAKE receiver

The DS-CDMA receiver is shown in Figure 2.7. This tapped delay line RAKE receiver ([73],[75]) is commonly employed to achieve path diversity gains. With L separable multi-paths, the RAKE receiver attempts to provide up to L^{th} order diversity. Specifically, in RAKE receivers, each "finger" extracts one of the multipaths, and the fingers' outputs are recombined coherently using suitable weights (typically maximal ratio combining (MRC)) to exploit path diversity. However, the multipath effect causes a loss of orthogonality between different user's signals (even in the synchronous case) thereby degrading the signal to interference ratio (SIR) on each branch of the RAKE (due to large inter-path interference). This has been presented in detail in [54]. As a result, it is difficult for the DS-CDMA receivers to make full use of the scattered signal energy in time. This directly affects the probability of error

performance in DS-CDMA which, in turn, limits the network capacity.

2.4.2 MC-CDMA

As discussed earlier, CDMA has emerged as a very popular multiple access technique for wireless communications. The benefits offered by CDMA include the ability to combat hostile frequency selective channels and the ability to support higher network capacities relative to the conventional access techniques of TDMA and FDMA. At the same time, Multi-carrier modulation schemes such as OFDM have also gained a lot of attention of late due to the demand for high data rate transmission in mobile radio environments.

Desire is the mother of invention. The desire to combine the benefits of CDMA and OFDM gave birth to the idea of Multi-Carrier CDMA (MC-CDMA) in 1993 [39]. MC-CDMA demonstrates many desirable qualities including: overcoming drawbacks of frequency selective channels, exploiting frequency diversity, and the handling of diverse multimedia traffic [40]. As a result MC-CDMA has emerged as a powerful alternative to current DS-CDMA in wireless communications [52].

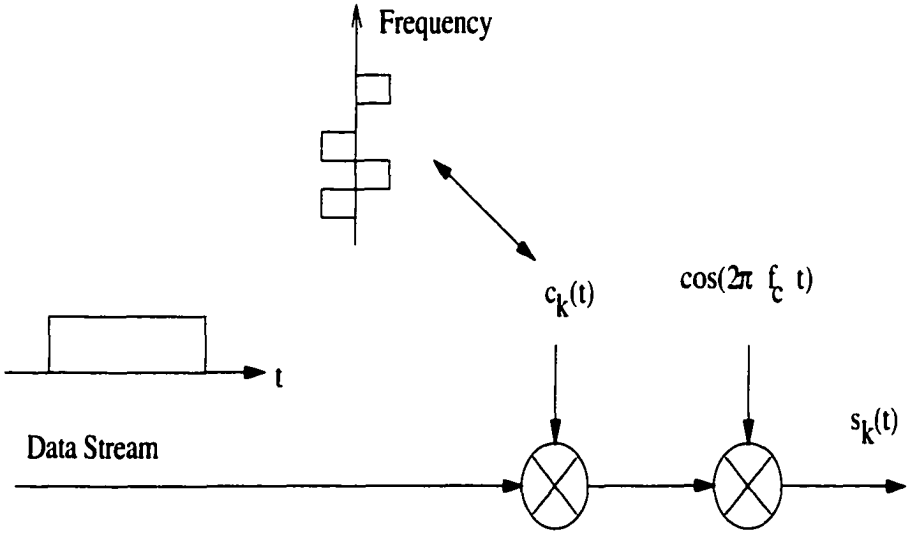

Figure 2.8: MC-CDMA transmitter block diagram

Figure 2.8 shows a block diagram representation of the MC-CDMA transmitter. Much like in DS-CDMA, the MC-CDMA transmitter for user k spreads the original data stream via a spreading code $c_k(t)$. However, the spreading code $c_k(t)$ is applied in the frequency domain instead of the time domain. Each user is allocated a unique spreading code as in DS-CDMA. Mathematically, the spreading code corresponds to

$$c_k(t) = \sum_{i=0}^{N-1} \beta_k^i e^{j2\pi i \Delta f t} \tag{2.10}$$

Here, N is the processing gain, i.e., the total number of narrowband carriers in the MC-CDMA code; β_k^i is the i^{th} value in user k's spreading sequence, typically a +1 or -1 (β_k^i is e^{j0} or $e^{j\pi}$) in accordance with known spreading codes such as Hadamard-Walsh codes; $i\Delta f$ is the frequency position of the i^{th} frequency component (Δf is chosen to ensure carrier orthogonality).

The k^{th} user's transmitted signal corresponds to

$$s_k(t) = \Re e[a_k c_k(t) \cdot e^{j2\pi f_c t} \cdot m(t)] \tag{2.11}$$

where a_k is the information symbol; $m(t)$ is a rectangular pulse that extends over time $[0,T_b]$ (T_b is the symbol duration). Including code creation in the MC-CDMA transmitter side, we can redraw Figure 2.8 in a detailed manner, as shown in Figure 2.9.

The total transmitted signal assuming K users in the downlink, corresponds to

$$s(t) = \Re e[\sum_{k=0}^{K-1} \sum_{i=0}^{N-1} a_k \beta_k^i e^{j2\pi(f_c + i\Delta f)t} \cdot m(t)] \tag{2.12}$$

After transmission through a multipath fading channel, the frequency selectivity over the entire bandwidth is resolved by the narrowband carriers, i.e., each of the N narrowband carriers experience a unique flat fade. The received signal in MC-CDMA

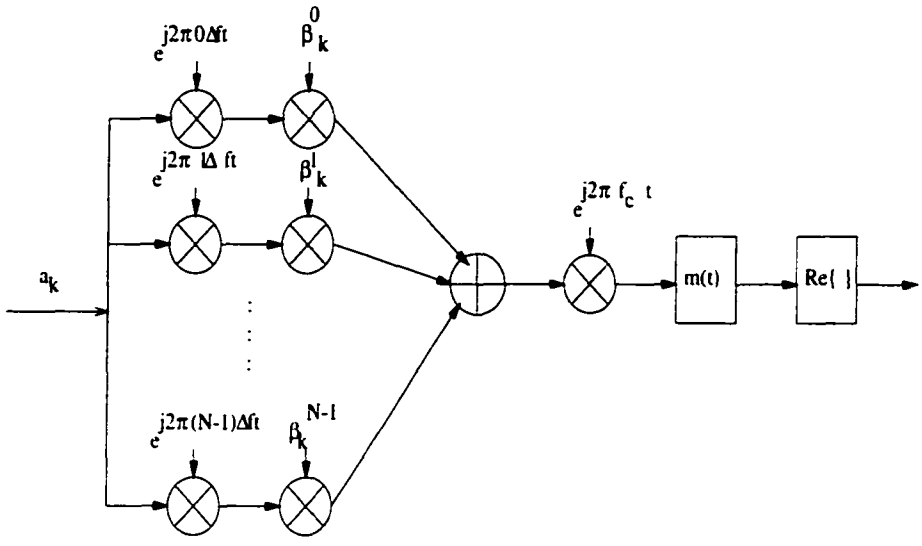

Figure 2.9: MC-CDMA transmitter

thus corresponds to

$$r(t) = \Re e[\sum_{k=0}^{K-1}\sum_{i=0}^{N-1} a_k \alpha_i \beta_k^i e^{j2\pi(f_c+i\Delta f)t+\phi_i} \cdot m(t)] + n(t) \tag{2.13}$$

where, α_i is the gain and ϕ_i is the phase offset on the i^{th} subcarrier due to the channel; and $n(t)$ represents AWGN.

At the receiver side the signal is first decomposed into its N orthogonal carriers and despread by the desired user's spreading code (by multiplying the appropriate β_k^i's on each carrier). Next, a suitable combining strategy (typically minimum mean squared error combining (MMSEC) is used to linearly combine the carrier components. This coherent combining enables MC-CDMA to (1) minimize noise and/or interference from other users and (2) exploit frequency diversity benefits. This receiver is shown in Figure 2.10.

From this receiver design, we observe MC-CDMA receivers exploit frequency diversity in a frequency selective channel by separating carriers and recombining them (while DS-CDMA RAKE receiver use correlators to resolve multiple paths and create path diversity).

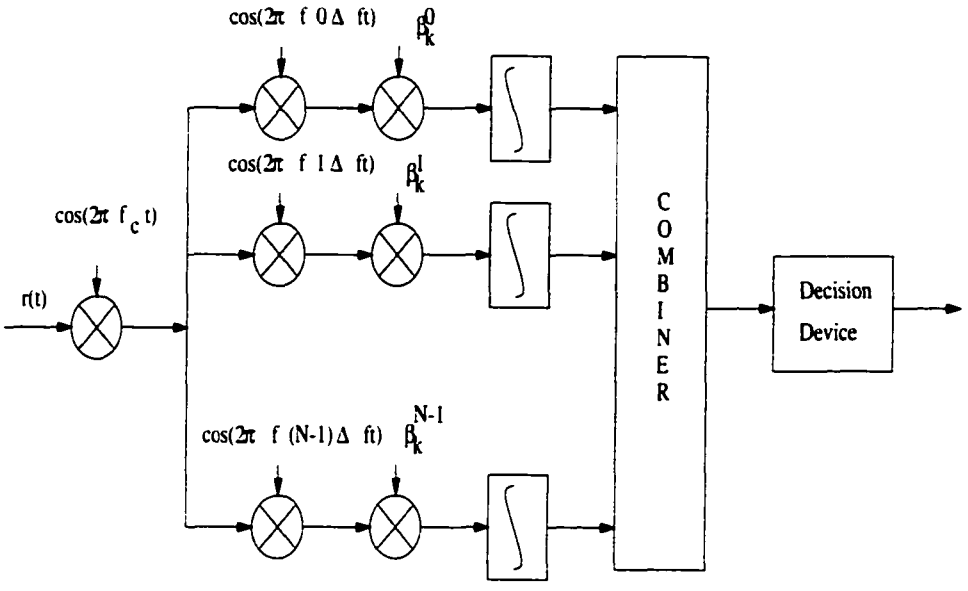

Figure 2.10: MC-CDMA receiver

2.4.3 MC-CDMA vs. DS-CDMA

One common question is, "Can MC-CDMA be better than DS-CDMA in terms of performance - after all, time and frequency domain processing are duals of one another?". The answer follows. When perfectly orthogonal code sequences are transmitted synchronously over slow, flat fading channels with perfect synchronization, the performance of DS-CDMA and MC-CDMA is equivalent. Here, the orthogonal multi-user interference vanishes completely in both MC-CDMA and DS-CDMA [76]. However, in reality, wideband CDMA signals are sent over *multipath* channels, and these signals experience more severe channel distortions. The resulting channel dispersion (i.e., frequency selectivity) erodes the orthogonality of CDMA signals. In such cases, it turns out to be far more beneficial to harness the signal energy in the frequency domain (as in MC-CDMA) than in the time domain (as in DS-CDMA) [53], [54].

Specifically, MC-CDMA receivers exploit frequency diversity in the frequency se-

lective channel by separating carriers and then carefully recombining them, while DS-CDMA RAKE receivers use correlators to resolve multiple paths and create path diversity. The primary reason MC-CDMA receivers outperform their DS-CDMA counterparts is: (1) in DS-CDMA RAKE receivers, large interference results on each diversity branch (each path) due to the presence of other users' signals from other paths as well as one's own signal from other paths; (2) in MC-CDMA, where carriers are separated from one another, receivers can perfectly separate the carrier components by performing an FFT operation (since carriers are designed to be orthogonal to one another). In other words, the SIR (Signal to Interference Ratio) on each diversity branch in MC-CDMA is much higher than the SIR on diversity branches in DS-CDMA. For this reason (primarily) MC-CDMA demonstrates performance gains relative to DS-CDMA.

The performance gains of MC-CDMA over DS-CDMA are discussed in detail in [51]-[54].

2.5 Summary

In this chapter, we provided a brief overview of different multiple access schemes. Specifically, we discussed FDMA, TDMA and CDMA systems. We also emphasized the importance of MC-CDMA and the benefits of exploiting frequency diversity relative to path diversity (as in DS-CDMA). In the next part of this thesis, we demonstrate that, by incorporating the Carrier Interferometry approach, we can benefit in increased capacity and performance in TDMA and MC-CDMA systems.

Chapter 3

Carrier Interferometry - Theory

Interferometry [77], a classical method in experimental physics, refers to the study of interference patterns resulting from the superpositioning of waves. The ideas underlying interferometry extend naturally to multiple access applications in telecommunications. For example, in antenna arrays supporting space division multiple access, EM waves are emitted simultaneously from multiple antenna elements, and initial phases are chosen to ensure that interference patterns create a peak at the desired user location, and nulls at the position of other users. In this chapter, we extend this idea and develop a unified multi-carrier framework to enhance the capabilities of multiple access schemes.

The fundamental theory behind the Carrier Interferometry approach is presented in three parts. First, we describe the properties of Carrier Interferometry (CI) signal, the basic building block for CI based systems discussed in later chapters. Second, we present the CI signal as a multi-carrier pulse shape and introduce the key benefits of using the CI approach in TDMA. Finally, we present the CI signal as a spreading code in MC-CDMA.

3.1 Introducing the CI Signal

As the name suggests, at the heart of the Carrier Interferometry concept is a wave that is created by the superposition of N carriers. We refer to this basic building block as the Carrier Interferometry signal, or, simply, the CI signal. Denoted as $g(t)$, it is the addition of N carriers equally spaced by frequency separation Δf. All carriers are in-phase, each with a zero phase offset. This is illustrated in the frequency domain in Figure 3.1. That is, the CI signal corresponds to

$$g(t) = \sum_{i=0}^{N-1} e^{j(2\pi i \Delta f t)} \tag{3.1}$$

or, equivalently, using the properties of summations and sinusoids,

$$|g(t)| = \left| \frac{\sin\left(\frac{1}{2}N(2\pi\Delta f t)\right)}{\sin\left(\frac{1}{2}(2\pi\Delta f t)\right)} \right| \tag{3.2}$$

Interpreting these results graphically in the time domain, the linear combining of

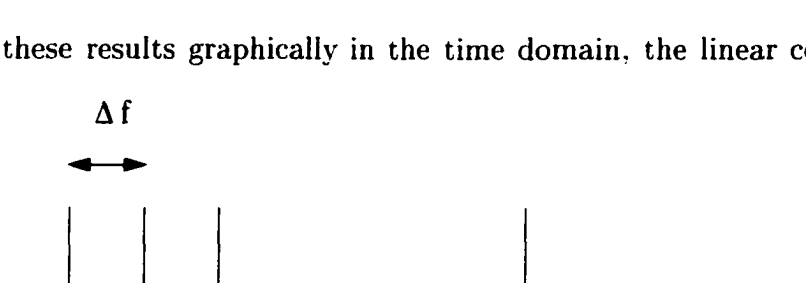

Figure 3.1: Frequency domain representation of the CI signal

these carriers leads to the signal whose envelope is shown in Figure 3.2. Here, we see two periods of the resulting periodic signal: each period, of duration $1/\Delta f$, consists of a mainlobe of duration $2/(N\Delta f)$ followed by times of sidelobe activity, each of duration $1/(N\Delta f)$. The l^{th} side lobe has maximum amplitude (normalized with respect to mainlobe amplitude) of $A(l) = \frac{1}{N \sin \frac{\pi}{N}(l+\frac{1}{2})}$.

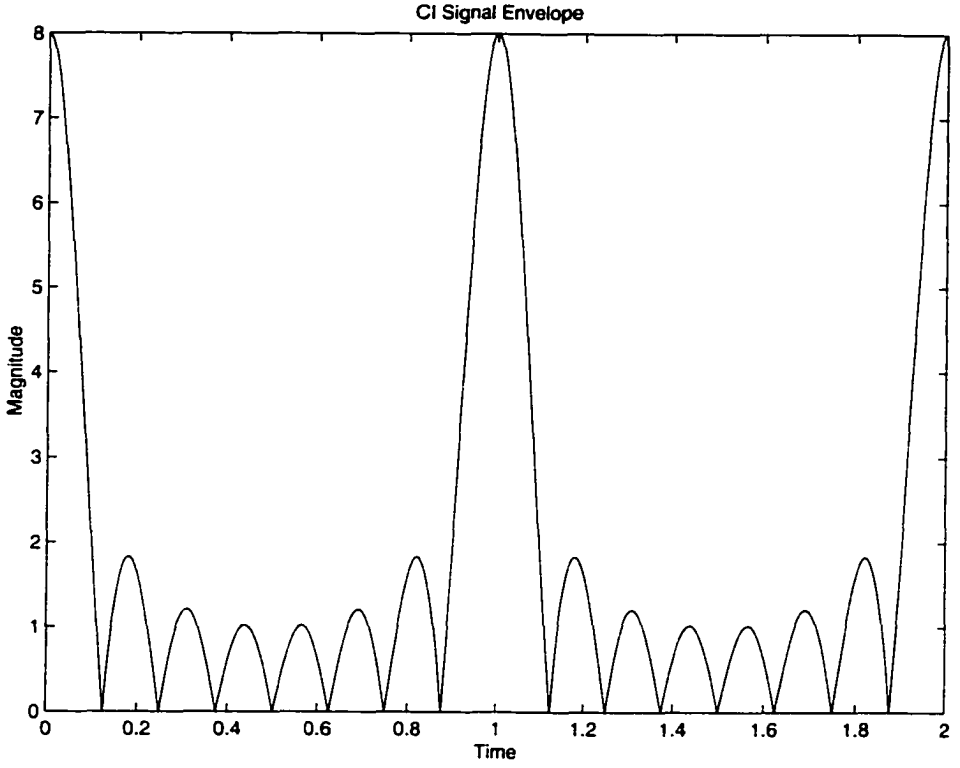

Figure 3.2: Envelope of a CI signal

3.1.1 Orthogonality Properties

Let us now look into the auto-correlation properties of a CI signal. We define the auto-correlation function as

$$Rac(\tau) = \int_0^{1/\Delta f} g(t)g^*(t-\tau)dt \tag{3.3}$$

where, $g^*(t)$ represents the complex conjugate of the CI signal $g(t)$. Substituting for $g(t)$ we get,

$$\begin{aligned} Rac(\tau) &= \int_0^{1/\Delta f} \sum_{m=0}^{N-1} e^{j(2\pi m\Delta ft)} \cdot \sum_{n=0}^{N-1} e^{-j(2\pi n\Delta f(t-\tau))}dt \\ &= \int_0^{1/\Delta f} \sum_{m=0}^{N-1}\sum_{n=0}^{N-1} e^{j(2\pi(m-n)\Delta ft+2\pi n\Delta f\tau)}dt \end{aligned} \tag{3.4}$$

The integral term will be non-zero only when $m = n$. Therefore,

$$\begin{aligned} Rac(\tau) &= \int_0^{1/\Delta f} \sum_{n=0}^{N-1} e^{j(2\pi n \Delta f \tau)} dt \\ &= \sum_{n=0}^{N-1} e^{j(2\pi n \Delta f \tau)} \int_0^{1/\Delta f} dt \\ &= \frac{1}{\Delta f} \sum_{n=0}^{N-1} e^{j(2\pi n \Delta f \tau)} \end{aligned} \tag{3.5}$$

From equation (3.5), we can see that the autocorrelation function of the CI signal is also a CI signal (a change in the variable τ to t, and a multiplicative constant, yield the CI signal of (3.1)). Therefore, the autocorrelation demonstrates the same zeros that are characteristic of $|g(t)|$ in equation (3.2). These zeros correspond to the delays $\tau_k = \frac{k}{N\Delta f}, k = 0, 1, 2, \cdots, N-1$.

Thus, a CI signal positioned with a mainlobe centered at time 0 is *orthogonal* to a CI signal with its mainlobe positioned at time τ, whenever τ is a value in the set $\{\frac{k}{N\Delta f}, k = 1, 2, \cdots, N-1\}$[57]. That is, mathematically,

$$\int_0^{1/\Delta f} g(t)g(t-\tau)dt = 0 \ \ iff \ \ \tau = \frac{k}{N\Delta f}, k = 1, 2, \cdots, N-1 \tag{3.6}$$

Figure 3.3 is a graphical representation of the set of N orthogonal CI signals $\{g(t), g(t-1/(N\Delta f)), g(t-2/(N\Delta f)), \cdots, g(t-(N-1)/(N\Delta f))\}$ drawn over one period (assuming $N = 8$). This property assures us that CI waveforms can be applied to represent information symbols located sequentially in time, without inter-symbol-interference (ISI).

3.1.2 Pseudo-orthogonal Properties

Equation (3.6) provides a strict condition for orthogonality among CI signals. As explained above, this condition enables N CI signals to support N information symbols in one period (without ISI). However, this condition can be relaxed to support more

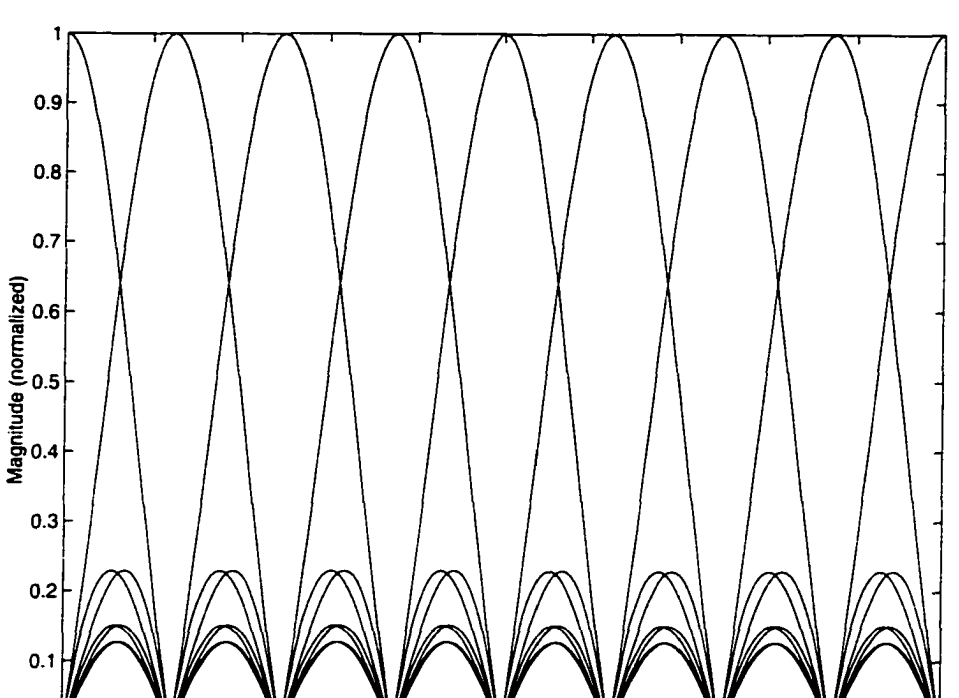

Figure 3.3: N orthogonal CI signals (N=8)

CI signals in a period via pseudo-orthogonality. This directly results in an increase in the amount of information symbols that can be represented in one period, without any cost in bandwidth. The condition for pseudo-orthogonality corresponds to

$$R_{ac}(\tau_n, \tau_m) = \int_0^{1/\Delta f} g(t-\tau_n)g(t-\tau_m)dt < \epsilon \tag{3.7}$$

where ϵ is a small pre-determined value. Now, based on (3.7), we seek to generate pseudo-orthogonal CI signals. Let us take a closer look at the correlation function $Rac(\tau)$. It is evident that the correlation between the CI signals remains zero as long as $\tau_n - \tau_m = \frac{n-m}{N\Delta f}$. If we introduce a fixed delay ζ, i.e., replace each $\tau = \tau_k$ by $\tau = \tau_k - \zeta$, the set of CI signals remain orthogonal to one another. That is the cross correlation between the CI signals remains zero as long as the difference is

$\tau_m - \tau_n = (\frac{m}{N\Delta f} - \zeta) - (\frac{n}{N\Delta f} - \zeta) = \frac{(m-n)}{N\Delta f}$. Of course, there is correlation between an orthogonal set of N CI signals with $\zeta = 0$ and the orthogonal set of N CI signals constructed with arbitrary ζ.

We seek to support $2N$ CI signals in one period, by simultaneously supporting one set of N CI signals with $\zeta = 0$ and another orthogonal set with $\zeta = \zeta$. To do this in an optimal fashion, we determine the value of ζ that minimizes the root mean square cross correlation between the set $\{g(t), g(t - \frac{1}{N\Delta f}), ..., g(t - \frac{(N-1)}{N\Delta f})\}$ and the set $\{g(t - \zeta), g(t - \frac{1}{N\Delta f} - \zeta), ..., g(t - \frac{(N-1)}{N\Delta f} - \zeta)\}$.

Let $R_{1,2}(m, n)$ refer to the cross correlation between the m^{th} CI signal in orthogonal set 1 (constructed with $\zeta = 0$) and the n^{th} CI signal in orthogonal set 2 (constructed with $\zeta = \zeta$). Also let

$$R_{rms} = \left[\frac{1}{N^2}\sum_{m=0}^{N-1}\sum_{n=0}^{N-1} R_{1,2}^2(m, n)\right]^{\frac{1}{2}} \tag{3.8}$$

represent the root-mean-square cross correlation that exists between CI signals in set 1 and set 2. We seek to find the value for ζ that minimizes R_{rms}. Now, it is easily shown that

$$R_{1,2}(m, n) = \sum_{i=0}^{N-1} e^{j(2\pi i\Delta f(\frac{m}{N\Delta f} - \frac{n}{N\Delta f} - \zeta))} \tag{3.9}$$

Furthermore, because real signals are transmitted, the real part of the cross correlation determines the amount of interference and hence

$$R_{1,2}(m, n) = \sum_{i=0}^{N-1} \cos(2\pi i\Delta f(\frac{m}{N\Delta f} - \frac{n}{N\Delta f} - \zeta)) \tag{3.10}$$

It is also easy to show that

$$\sum_{j=0}^{N-1} R_{1,2}^2(m, n) = \sum_{j=0}^{N-1} R_{1,2}^2(m, n') \qquad n \neq n' \tag{3.11}$$

That is, the total cross correlation between the n^{th} CI signal in orthogonal set 2 and all the CI signals in set 1 is identical to the cross-correlation between the $(n')^{th}$ CI

signal in orthogonal set 2 and all the CI signals in set 1. Using equation (3.11), we can rewrite equation (3.8) as

$$R_{rms} = \left[\frac{1}{N}\sum_{m=0}^{N-1} R_{1,2}^2(m,0)\right]^{\frac{1}{2}} \tag{3.12}$$

and using equation (3.10), this becomes

$$R_{rms} = \left[\frac{1}{N}\sum_{m=0}^{N-1}\left(\sum_{i=0}^{N-1}\cos\left(2\pi i\Delta f(\frac{m}{N\Delta f}-\zeta)\right)\right)^2\right]^{\frac{1}{2}} \tag{3.13}$$

We now determine the selection of ζ that minimizes the root-mean-square correlation, R_{rms}. To do this, we select

$$\frac{\partial R_{rms}}{\partial \zeta} = 0 \tag{3.14}$$

$$\frac{\partial R_{rms}}{\partial \zeta} = \frac{1}{2}\left[\frac{1}{N}\sum_{m=0}^{N-1} R_{1,2}^2(m,0)\right]^{-\frac{1}{2}} \frac{1}{N}\cdot I \tag{3.15}$$

where

$$\begin{aligned} I &= \frac{\partial\left[\sum_{m=0}^{N-1} R_{1,2}^2(m,0)\right]}{\partial\zeta} \\ &= \frac{\partial\left[\sum_{m=0}^{N-1}\left(\sum_{i=0}^{N-1}\cos\left(2\pi i\Delta f(\frac{m}{N\Delta f}-\zeta)\right)\right)^2\right]}{\partial\zeta} \end{aligned} \tag{3.16}$$

Now,

$$
\begin{aligned}
I &= \sum_{m=0}^{N-1} 2\left[\sum_{i=0}^{N-1}\cos\left(2\pi i\Delta f(mT_b-\zeta)\right)\right]\cdot\left[\sum_{k=0}^{N-1} k\sin\left(2\pi k\Delta f(\frac{m}{N\Delta f}-\zeta)\right)\right] \\
&= \sum_{m=0}^{N-1}\sum_{i=0}^{N-1}\sum_{k=0}^{N-1} 2k\cos\left(2\pi i\Delta f(\frac{m}{N\Delta f}-\zeta)\right)\sin\left(2\pi k\Delta f(\frac{m}{N\Delta f}-\zeta)\right) \\
&= \sum_{m=0}^{N-1}\sum_{i=0}^{N-1}\sum_{k=0}^{N-1} k\left[\sin\left(2\pi(k+i)\Delta f(\frac{m}{N\Delta f}-\zeta)\right)+\sin 2\pi(k-i)\Delta f(\frac{m}{N\Delta f}-\zeta)\right] \\
&= \Im m\left[\sum_{m=0}^{N-1}\sum_{i=0}^{N-1}\sum_{k=0}^{N-1} k\left(e^{j(2\pi(k+i)\Delta f(\frac{m}{N\Delta f}-\zeta))}+e^{j(2\pi(k-i)\Delta f(\frac{m}{N\Delta f}-\zeta))}\right)\right] \\
&= \Im m\left[\sum_{i=0}^{N-1}\sum_{k=0}^{N-1} ke^{-j(2\pi(k+i)\Delta f\zeta)}\sum_{m=0}^{N-1} e^{j(2\pi(k+i)\Delta f\frac{m}{N\Delta f}}\right]+ \\
&\quad \Im m\left[\sum_{i=0}^{N-1}\sum_{k=0}^{N-1} ke^{-j(2\pi(k-i)\Delta f\zeta)}\sum_{m=0}^{N-1} e^{j(2\pi(k-i)\Delta f\frac{m}{N\Delta f}}\right] \\
&= \Im m\left[\sum_{i=0}^{N-1}\sum_{k=0}^{N-1} ke^{-j(2\pi(k+i)\Delta f\zeta)}\delta(k+i-N)N\right]+ \\
&\quad \Im m\left[\sum_{i=0}^{N-1}\sum_{k=0}^{N-1} ke^{-j(2\pi(k-i)\Delta f\zeta)}\delta(k-i)N\right] \\
&= \Im m\left[\sum_{i=0}^{N-1}(N-i)e^{-j(2\pi N\Delta f\zeta)}+\sum_{i=0}^{N-1} i\right]\cdot N \qquad (3.17)
\end{aligned}
$$

When $\zeta = \frac{k}{2N\Delta f}, k = 0, 1, ...,$ we have $I = 0$ and, therefore from equation (3.15), $\frac{\partial R_{rms}}{\partial \zeta} = 0$.

Seeking to determine which ζ are maxima and which are minima, we calculate the second order partial derivative at $\zeta = \frac{k}{2N\Delta f}$ and determine:

$$
\begin{aligned}
\frac{\partial R_{rms}^2}{\partial^2\zeta} > 0 \quad when \quad \zeta = \frac{(2k+1)}{2N\Delta f} \\
\frac{\partial R_{rms}^2}{\partial^2\zeta} < 0 \quad when \quad \zeta = \frac{2k}{2N\Delta f} \qquad (3.18)
\end{aligned}
$$

Hence, $\zeta = \frac{2k}{2N\Delta f}$ corresponds to a maxima and $\zeta = \frac{(2k+1)}{2N\Delta f}$ provides minima. Selecting $k = 0$, we choose $\zeta = \frac{1}{2N\Delta f}$ as our minima. Therefore, our final result for ζ that

minimizes cross correlation between the two sets of CI signals is

$$\zeta = \frac{1}{2N\Delta f} \tag{3.19}$$

Pictorially, this is shown in Figure 3.4 (assuming N=8). The ability to position CI signals pseudo-orthogonally helps increase network capacity (measured in terms of number of users or throughput per user) as shown in the following chapters.

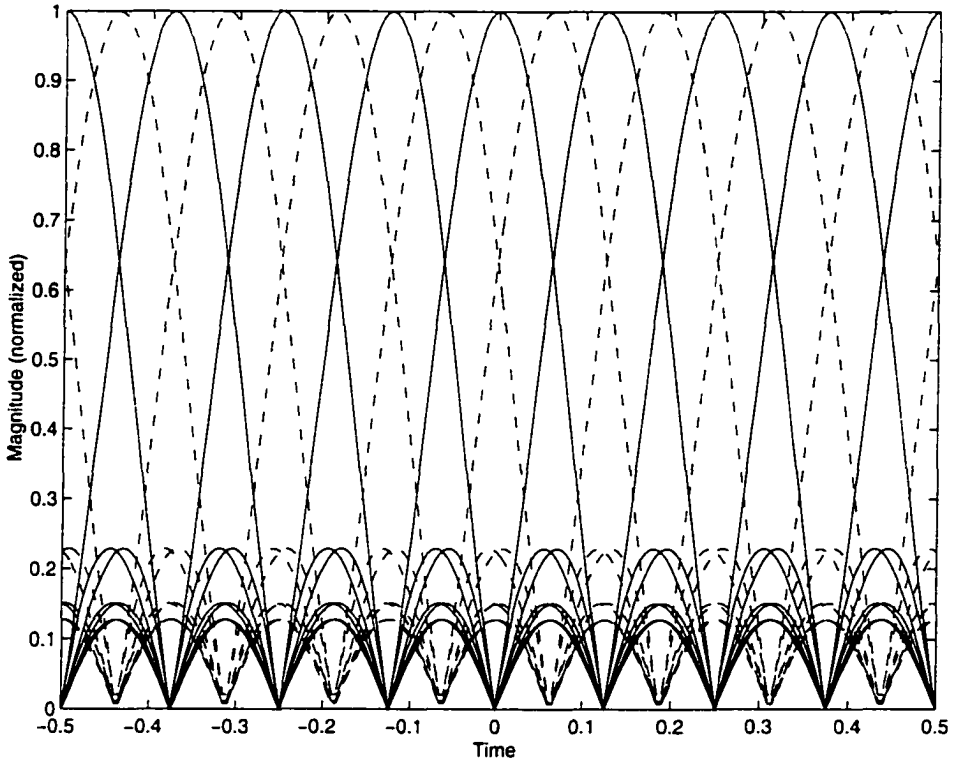

Figure 3.4: $2N$ Pseudo-orthogonal CI signals (N=8)

3.2 CI Pulse Shape

In the previous section, we introduced the CI signal and its properties. In this section, we apply the CI signal to pulse shaping by replacing traditional pulse shapes by one period of the CI signal.

Placing the CI signal presented in section 3.1, in the context of traditional communication signals, we see that the CI signal is actually a frequency sampled version of the sinc() waveform. That is, the CI signal is an approximation to the sinc() waveform generated by frequency sampling the sinc waveform using N equally spaced samples. Of course, frequency sampling leads to time repetition, which explains the periodic nature of the CI signal. The CI pulse shape is represented as

$$g(t) = \sum_{i=0}^{N-1} Ae^{j2\pi i\Delta ft}. \tag{3.20}$$

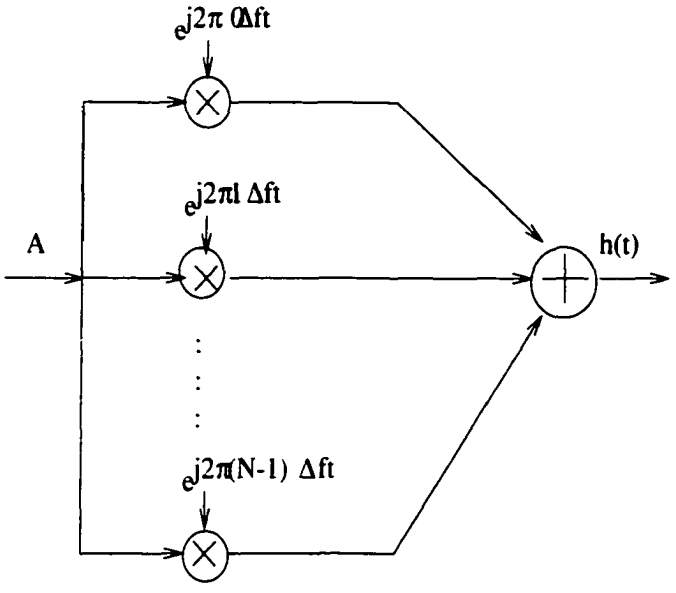

Figure 3.5: CI pulse shape generator

Figure 3.5 shows conceptually how the CI pulse shape $g(t)$ is generated. We can support N orthogonal symbols satisfying the Generalized Nyquist criterion (GNC) at the transmitter, by employing the following set of pulse shapes:

$$Set\ 1 : \{g(t), g(t - \frac{1}{N\Delta f}), \cdots, g(t - \frac{(N-1)}{N\Delta f})\} \tag{3.21}$$

Furthermore, following the derivation in section 3.1.2, we can support additional symbols in one period, via pseudo-orthogonal positioning of CI pulse shapes. The second set of N symbols are modulated by the second set of CI pulse shapes given by

$$Set\ 2 : \{g(t - \frac{1}{2N\Delta f}), g(t - \frac{1}{N\Delta f} - \frac{1}{2N\Delta f}), \cdots, g(t - \frac{(N-1)}{N\Delta f} - \frac{1}{2N\Delta f}))\} \tag{3.22}$$

The design of a TDMA system employing these CI pulse shapes is discussed in detail in chapter 6. We demonstrate that by switching to a receiver that performs frequency domain processing, this CI/TDMA system outperforms a traditional GSM system by 5-8 dB. Furthermore, we will show that by pseudo-orthogonal positioning of CI pulse shapes, the throughput can be doubled in a TDMA system with negligible loss in BER performance.

3.3 CI Spreading Code

The CI signal with its orthogonal properties can also be understood as a signature waveform in CDMA systems. Specifically, we can place the CI signal in the context of MC-CDMA, where the CI signal, $g(t)$, corresponds to: an MC-CDMA spreading code (signature waveform) $c_k(t)$ with carrier 0 to carrier $N-1$ demonstrating the spreading sequence

$$\{\beta_k^0, \beta_k^1, \cdots, \beta_k^{N-1}\} = \{+1, +1, \cdots, +1\}. \tag{3.23}$$

That is,

$$c_k(t) = \sum_{i=0}^{N-1} \beta_k^i e^{j(2\pi i \Delta f t)} \tag{3.24}$$

where $\beta_k^i = 1$ for all i.

Placing the orthogonal property of the CI signal in terms of MC-CDMA spreading codes, there exists an important alternative representation of the orthogonal set $\{g(t), g(t-1/(N\Delta f)), g(t-2/(N\Delta f)), \cdots, g(t-(N-1)/(N\Delta f))\}$. To understand this alternative representation, consider the following:

$$\begin{aligned} g(t+\frac{k}{N\Delta f}) &= \sum_{i=0}^{N-1} e^{j(2\pi i\Delta f(t+\frac{k}{N\Delta f}))} \\ &= \sum_{i=0}^{N-1} e^{j(2\pi i\Delta f t+\frac{2\pi}{N}ik)} \\ &= \sum_{i=0}^{N-1} e^{ji\Delta\theta_k} e^{j(2\pi i\Delta f t)} \end{aligned} \tag{3.25}$$

where $\Delta\theta_k = 2\pi k/N$. That is, the k^{th} CI signal in the orthogonal set $\{g(t), g(t-1/(N\Delta f)), g(t-2/(N\Delta f)), \cdots, g(t-(N-1)/(N\Delta f))\}$ is the linear combination of N carriers weighted by an appropriate "complex spreading sequence", namely $\{e^{j0}, e^{j2\pi k/N}, \cdots, e^{j(N-1)2\pi k/N}\}$. This is illustrated in Figure 3.6. In other words, the N CI signals in the orthogonal set can be viewed as N codes for MC-CDMA, i.e.,

$$\begin{aligned} \{c_k(t) &= \sum_{i=0}^{N-1} e^{j(2\pi i\Delta f t+i\Delta\theta_k)}, \quad k=0,1,\cdots,N-1\} \\ \{c_k(t) &= \sum_{i=0}^{N-1} \beta_k^i e^{j(2\pi i\Delta f t)}, \quad k=0,1,\cdots,N-1\} \end{aligned} \tag{3.26}$$

where these codes are orthogonal to one another by application of the complex spreading sequences

$$\beta_k^i = e^{ji\Delta\theta_k} = e^{ji\frac{2\pi}{N}k} \tag{3.27}$$

Here, the CI signals are understood as spreading codes for an MC-CDMA system where (1) the codes are orthogonal (providing an alternative to Hadamard Walsh codes); (2) the codes may be designed for any length N; and (3) the codes, when sent

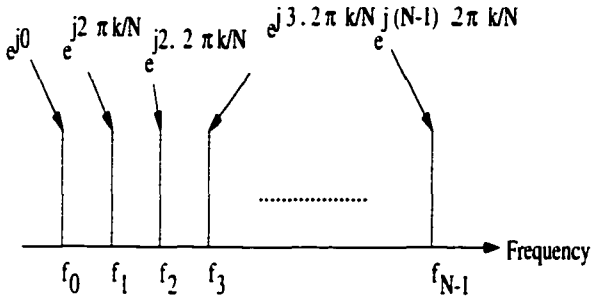

Figure 3.6: CI spreading codes

(as a set) in the time domain demonstrate low PAPR. All these details along with a complete design of MC-CDMA system based on CI codes is provided in chapters 4 and 5.

Based on the above discussion, the CI signals may be used to replace traditional *orthogonal* spreading code strategies. However, to increase network capacity CI signals must be able to replace pseudo-orthogonal spreading codes. This is possible, based on the discussion in section 3.1.2. We express those results in terms of MC-CDMA spreading codes as follows (by simply recognizing the equivalence between shifts in the time domain (τ_k) and phase offsets in the frequency domain ($\Delta\theta_k$), namely $\tau_k = \frac{\Delta\theta_k}{2\pi\Delta f}$): Consider two sets of MC-CDMA spreading codes corresponding to CI signals:

$$Set\ \ 1 : c_0(t), c_1(t), \cdots, c_{N-1}(t) \tag{3.28}$$

where $c_k(t)$ represents the multi-carrier spreading code (equation(3.29)) with carriers 0 to $N-1$ demonstrating complex spreading sequences based on equation (3.30).

$$Set\ \ 2 : c_N(t), c_{N+1}(t), \cdots, c_{2N-1}(t) \tag{3.29}$$

where $c_{N+1}(t)$ represents the multi-carrier spreading code (equation(3.29)) with carriers 0 to $N-1$ demonstrating complex spreading codes $\{\beta_k^0, \beta_k^1, \cdots, \beta_k^{N-1}\} =$

$\{e^{j0+0\cdot\Delta\theta}, e^{j(2\pi k/N+1\cdot\Delta\theta)}, \ldots, e^{j((N-1)2\pi k/N+(N-1)\cdot\Delta\theta)}\}$. From the analysis in section 3.1.2, we can conclude that the choice of $\Delta\theta$ that would minimize the root-mean-squared interference between spreading code set 1 and spreading code set 2 is

$$\Delta\theta = \zeta \cdot 2\pi\Delta f = \frac{1}{2N\Delta f} \cdot 2\pi\Delta f = \frac{\pi}{N} \tag{3.30}$$

Hence, the CI signals are understood as multi-carrier codes where (1) if orthogonal users are to be supported, N orthogonal codes may be used; and (2) if more than N users are to be supported, up to $2N$ users can be supported by introducing a second set of users which are orthogonal with one another, but pseudo-orthogonal to the first set. The CI/MC-CDMA system design is discussed in the next chapter.

3.4 Summary

In this chapter, we introduced the idea of Carrier Interferometry. The fundamental building block for CI systems, namely the CI signal was discussed in detail, and the key orthogonal and pseudo-orthogonal properties were analyzed. We also provided insight into how CI signals are used as pulse shapes, and saw how these CI signals serve as signature waveforms in CDMA systems. Specifically, we derived the orthogonal and pseudo-orthogonal pulse shapes for TDMA and complex CI codes for MC-CDMA. The design and performance of an MC-CDMA system employing these CI codes are discussed next.

Chapter 4

CI/MC-CDMA

In this chapter, we analyze an MC-CDMA system employing Carrier Interferometry (CI) codes (introduced in Section 3.3). We demonstrate that CI codes provide both flexibility and excellent bit-error- rate (BER) performance relative to traditional MC-CDMA employing Hadamard Walsh (HW) codes. We also show that it is possible to maintain good BER performance even after doubling the capacity of an MC-CDMA system via pseudo-orthogonal CI codes.

The communication channel model of interest is described in this chapter. Specifically, the frequency domain channel models for multi-carrier systems are derived from typical time domain channel models. The chapter also describes an algorithm that is useful in generating correlated fading envelopes: This enables a realistic simulation model that is used throughout the rest of this thesis.

This chapter proceeds in the following manner. We review the features of traditional MC-CDMA and discuss the benefits of incorporating Carrier Interferometry (CI) spreading codes in MC-CDMA. We then present CI/MC-CDMA signaling and the transmitter model. We also apply the notion of pseudo-orthogonal CI spreading codes to increase network capacity with zero cost in bandwidth. We then discuss the channel model in detail. Finally, we present receiver design architectures followed by performance curves assuming perfect synchronization.

4.1 Introduction

Since its introduction in the winter of 1993, MC-CDMA has been the focus of research and development efforts (e.g., [39]-[48]) and has emerged as a powerful alternative to conventional direct sequence CDMA (DS-CDMA)[73] in mobile wireless communications. In MC-CDMA, each user's data symbol is transmitted simultaneously over N narrowband subcarriers, with each subcarrier encoded with a -1 or $+1$ (as determined by an assigned spreading code). Multiple users are assigned unique, orthogonal (or pseudo-orthogonal) codes. That is, while DS-CDMA spreads in the time domain, MC-CDMA applies the same spreading sequences in the frequency domain.

The benefits offered by MC-CDMA over DS-CDMA systems were discussed in Section 2.3. In this chapter we further enhance the capability and flexibility of MC-CDMA systems via novel CI codes. Prior to this work, there had been considerable efforts in improving MC-CDMA performance and capacity by introducing new spreading codes [55]. However, as discussed in Section 1.3 these schemes suffer from certain drawbacks namely, (1) the systems either are designed to support N users using length-N orthogonal codes, *or*, support more than N users via pseudo-orthogonal codes at the cost of degraded BER performance; and (2) there is always a restriction in the choice of N (e.g., N is 2^n or $2^n \pm 1$ ($n \in I$)). The CI spreading codes of length N introduced in this paper have a unique feature which allows the CI/MC-CDMA system to (1) support N users orthogonally; (2) then, as system demand increases, codes can be selected to accommodate up to an additional N users pseudo-orthogonally. Additionally, there is no restriction on the length N of the CI code (i.e.,$N \in I$), making it more robust to the diverse requirements of wireless environments.

The following sections demonstrate the flexibility and the performance improvement achievable through CI/MC-CDMA.

4.2 Signaling and Transmitter

The transmitter for the k^{th} user in a CI/MC-CDMA system is shown in Figure 4.1. Here, the k^{th} user's spreading code corresponds to $(1, e^{j\Delta\theta_k}, e^{j2\Delta\theta_k}, \cdots, e^{j(N-1)\Delta\theta_k})$. Specifically, the input data symbol is $a_k[n]$ where n denotes the n^{th} bit interval and k denotes the k^{th} user. It is assumed that $a_k[n]$ takes on values -1 and +1 with equal probability. The transmitted signal corresponding to the input $a_k[n]$ is

$$s_k(t) = \Re e[\sum_{i=0}^{N-1} a_k[n] e^{j(2\pi f_i t + i\Delta\theta_k)} \cdot m(t - nT_b)] \tag{4.1}$$

where $f_i = f_c + i\Delta f$ and $m(t)$ is defined to be a rectangular pulse of unity height, extending from 0 to T_b. As with traditional MC-CDMA, the Δf's are selected such that the carrier frequencies $\{f_i, i = 0, 1...., N-1\}$ are orthogonal to each other, typically $\Delta f = 1/T_b$, where T_b is the bit duration.

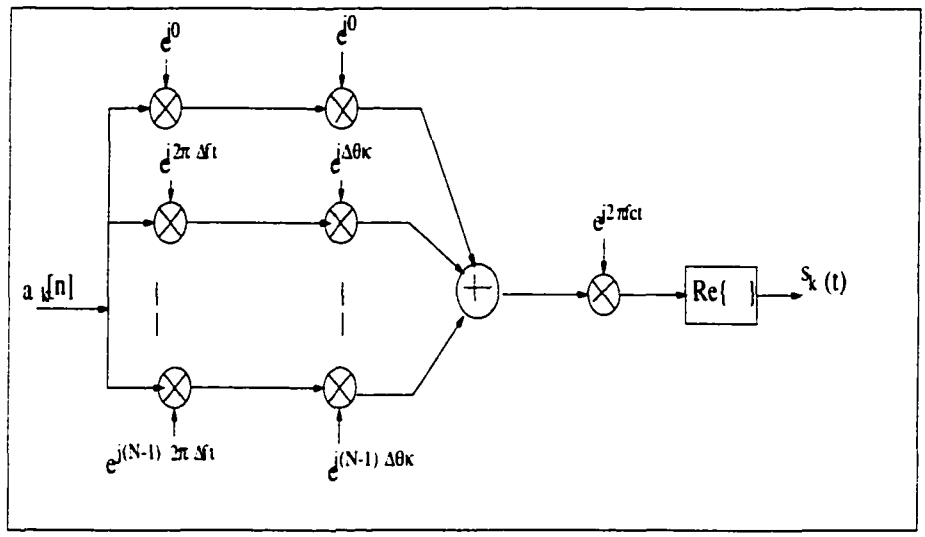

Figure 4.1: CI/MC-CDMA Transmitter for user k

The transmitted signal can also be expressed as

$$s_k(t) = \Re e[a_k[n] \cdot c_k(t) \cdot e^{j2\pi f_c t} \cdot m(t - nT_b)] \tag{4.2}$$

where $c_k(t)$ is referred to as user k's spreading sequence and corresponds to the superpositioning of N equally spaced carriers, i.e.,

$$c_k(t) = \sum_{i=0}^{N-1} e^{j(2\pi i\Delta ft + i\Delta\theta_k)}. \tag{4.3}$$

$$c_k(t) = \sum_{i=0}^{N-1} \beta_k^i e^{j2\pi i\Delta ft} \tag{4.4}$$

where (1) N refers to the number of carriers per spreading code (equal to the processing gain in a DS-CDMA system), and (2) the value β_k^i refers to the i^{th} value of the k^{th} user's spreading sequence $(\beta_k^0, \beta_k^1, \cdots, \beta_k^{N-1})$, typically a set of ± 1 values corresponding to HW codes. However, in CI codes, $(\beta_k^0, \beta_k^1, \cdots, \beta_k^{N-1})$ correspond to $(1, e^{j\Delta\theta_k}, e^{j2\Delta\theta_k}, \cdots, e^{j(N-1)\Delta\theta_k})$ (as observed when equating equations (4.4) to (4.3)).

Applying the analysis in Section 3.3, we deduce that, to support N orthogonal users in the CI/MC-CDMA system, we select the spreading code parameter $\Delta\theta_k = 2\pi k/N, k = 0, 1, 2, ... N-1$. Furthermore, if the number of users exceed N, the CI/MC-CDMA system can support N additional users by employing CI codes with $\Delta\theta_k = 2\pi k/N + \pi/N, k = N, N+1, ..., 2N-1$. It is important to note that these two sets of CI codes are pseudo-orthogonal to each other (with minimum possible cross correlation in a mean-squared sense), even though within each set of N codes, the spreading codes are orthogonal to one another.

That is, for $2N$ users on the system, each user should be assigned the spreading code $\{c_k(t), k = 0, 1, \cdots, 2N-1\}$, where

$$c_k(t) = \sum_{i=0}^{N-1} e^{j(2\pi i\Delta ft + i\Delta\theta_k)} \tag{4.5}$$

$$\Delta\theta_k = \frac{2\pi}{N}k \qquad k = 0, 1, ..., N-1 \tag{4.6}$$

$$\Delta\theta_k = \frac{2\pi}{N}k + \frac{\pi}{N} \quad k = N, N+1, ..., 2N-1 \tag{4.7}$$

In this way, CI/MC-CDMA doubles network capacity relative to orthogonal coding. The total transmitted signal with a full $2N$ users is

$$s(t) = \Re e[\sum_{k=0}^{2N-1}\sum_{i=0}^{N-1} a_k[n]e^{j(2\pi f_i t + i\Delta\theta_k)} \cdot m(t - nT_b)] \tag{4.8}$$

where $\Delta\theta_k$'s are selected as shown in equations (4.6) and (4.7).

Viewing the CI codes based on equations (4.5),(4.6) and (4.7) in the time domain leads to Figure 4.2 (with N=8). Here, the solid lines correspond to the first orthogonal set of CI codes (based on equation (4.6)). These CI codes can be thought of (conceptually) as orthogonal because when one code is at a time of mainlobe (peak energy) all other codes codes are at a time of sidelobe activity (very low energy). The second set of orthogonal codes (based on equation (4.7)) are shown by the dotted line. These codes minimize root-mean-square correlation between code sets (conceptually) because the mainlobes of these CI codes lies right between the mainlobes of the first orthogonal set. It is important to note that even though CI codes correspond to easy-to-understand waveforms in the time domain (namely interferometry patterns), it is their frequency decomposability that will serve us well in the receiver processing which is discussed in Section 4.4.

4.3 Channel Model

The transmitted signal in equation (4.8) is sent out across the channel, and, with that in mind, the channel model becomes the next focus of attention. This section provides a detailed modeling of the communication environment of interest. We focus our attention on small scale fading. Small scale fading consists of two effects: (1) a rapid fluctuation of the amplitude of a signal over short periods of time or travel distance

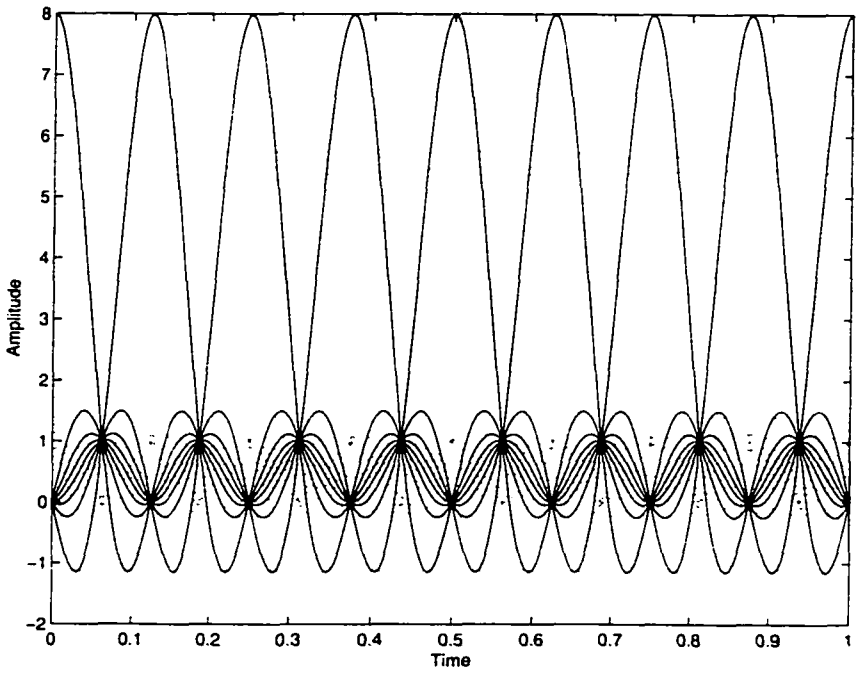

Figure 4.2: CI/MC-CDMA codes in time domain

(caused by interference between two or more versions of the transmitted signal which arrive at the receiver at slightly different times); and (2) a channel impulse response referred to as *multipath* (caused by multiple reflections that are resolvable in time).

We make the following assumptions regarding our wireless channel:

• We assume synchronicity between users, typically characteristic of the downlink in a mobile communication system. However, more and more wireless communication systems are being proposed with synchronous uplink channels, as recent efforts in 3G have focused on the creation of synchronous uplinks (e.g., [78],[79]). For example, in [79], the China Wireless Telecommunication Standard (CWTS), time division is introduced to support synchronous CDMA uplinks. The channel model studied here is of course valid for both this category of uplinks as well as downlinks.

• We assume a slowly varying frequency-selective Rayleigh fading channel, typical of the wideband channels for MC-CDMA systems. Frequency selectivity refers to the

selectivity over the entire bandwidth of transmission, and not over each subcarrier transmission; that is [80]

$$\Delta f << (\Delta f)_c < BW \tag{4.9}$$

where $(\Delta f)_c$ is the coherence bandwidth of the channel (defined as the bandwidth over which fade correlation is above 0.5) and BW is the total bandwidth of the multicarrier system. The bandwidth on each carrier being much smaller than the coherence bandwidth guarantees that the channel will be non-selective or flat on each carrier. This is similar to the models assumed for OFDM and MC-CDMA [31]-[48], where transmitting multiple narrowband subcarriers *resolves* the frequency selective channel.

• In this work, we examine frequency selectivity resulting in L fold frequency diversity over the entire bandwidth (typically, $L < N$). Here, the value L corresponds to the ratio

$$L = \frac{BW}{(\Delta f)_c} \tag{4.10}$$

• With N carriers residing over the entire bandwidth, BW, each carrier undergoes a flat fade, with the correlation between the i^{th} subcarrier fade and the j^{th} subcarrier fade characterized by [81],[82]

$$\rho_{i,j} = \frac{1}{1 + ((f_i - f_j)/(\Delta f)_c)^2}. \tag{4.11}$$

Generation of correlated fades for simulation purposes is discussed in Appendix 4A (at the end of this chapter).

The key parameter that determines the available frequency diversity benefit is coherence bandwidth. However, channel models that are provided along with wireless system standards like COST-207 GSM standard [83] and UMTS standards [84] are

based on multipath intensity profile measurements. Hence, it is important to make the transition from such time domain models to frequency domain channel models to better simulate multi-carrier systems such as CI/MC-CDMA.

In the COST-207 standard, three basic multipath channel models represent different radio propagation environments: the hilly terrain (HT) model, the typical urban (TU) model and the rural area (RA) model. These models are defined as transversal filters with time varying coefficients whose average power is determined by the multipath power delay profiles (PDPs) given in Table 4.1.

The $(\Delta f)_c$ (coherence bandwidth) can be computed from a multipath PDP by using the approximate relationship [72]

$$(\Delta f)_c \approx \frac{1}{5\sigma_\tau} \tag{4.12}$$

where σ_τ is the rms delay spread and is computed according to

$$\sigma_\tau = \sqrt{\tau' - (\tau)^2} \tag{4.13}$$

$$\tau = \frac{\sum_p \alpha_p^2 \tau_p}{\sum_p \alpha_p^2} \tag{4.14}$$

$$\tau' = \frac{\sum_p \alpha_p^2 \tau_p^2}{\sum_p \alpha_p^2} \tag{4.15}$$

Here, α_p is the power of the multipath component arriving at delay τ_p. This leads to the following coherence bandwidth results (using Table 4.1): for HT, $(\Delta f)_c$= 39.72 kHz; for RA,$(\Delta f)_c$= 2050 kHz; and for TU, $(\Delta f)_c$= 188 kHz.

We also consider two UMTS indoor channel models, Channel A and Channel B [84]. Channel A has an rms delay spread of 35 ns; and Channel B has an rms delay spread of 100 ns. These correspond to a coherence bandwidth of 5.7 MHz and 2 MHz, respectively.

Tap No.	*Typical Urban*		*Hilly Terrain*		*Rural Area*	
	$\tau(\mu s)$	α(dB)	$\tau(\mu s)$	α(dB)	$\tau(\mu s)$	$\alpha(dB)$
1	0.0	-3.0	0.0	0.0	0.0	0.0
2	0.2	0.0	0.2	-2.0	0.1	-4.0
3	0.5	-2.0	0.4	-4.0	0.2	-8.0
4	1.6	-6.0	0.6	-7.0	0.3	-12.0
5	2.3	-8.0	15.0	-6.0	0.4	-16.0
6	5.0	-10.0	17.2	-12.0	0.5	-20.0

Table 4.1: Multipath Power Delay Profiles for TU,HT and RA channels

4.4 Receiver Structures

Assuming the transmitted signal in equation (4.8), and a slow, frequency selective fading channel (Section 4.3), the received signal corresponds to

$$r(t) = \sum_{k=1}^{K} \sum_{i=0}^{N-1} \alpha_i a_k[n] \cos(2\pi f_i t + i\Delta\theta_k + \phi_i) m(t - nT_b) + \eta(t) \tag{4.16}$$

where α_i is the gain and ϕ_i the phase offset in the i^{th} carrier due to the fade; K is the total number of users utilizing the system; and $\eta(t)$ represents additive white Gaussian noise (AWGN).

The CI/MC-CDMA receiver for user k is shown in Figure 4.3. Here, the received signal is first projected onto the N orthonormal carriers that make up the transmitted signal. This leads to the output $\underline{r} = (r_0, r_1, ..., r_{N-1})$ where

$$r_i = \alpha_i a_k[n] + \sum_{j=1, j\neq k}^{K} \alpha_i a_j[n] \cos(i(\Delta\theta_j - \Delta\theta_k)) + \eta_i. \tag{4.17}$$

Here, η_i is a Gaussian random variable with mean 0 and variance $N_o/2$, and exact phase and frequency synchronization has been assumed in determining (4.17).

Next, a suitable combining strategy is used to linearly combine the r_i terms and create a decision variable, D. In a flat fading channel (i.e., $\alpha_1 = \alpha_2 = ... = \alpha_N$), a

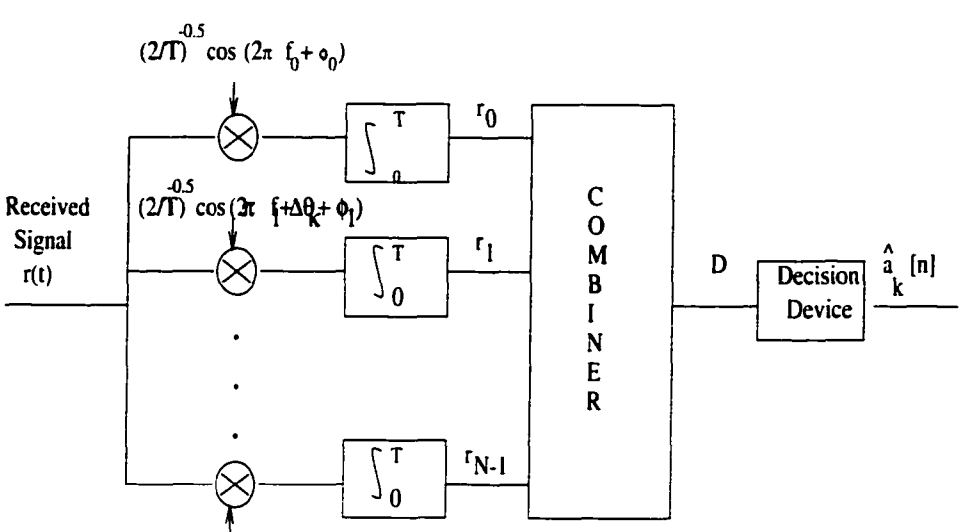

Figure 4.3: CI/MC-CDMA receiver for user k

simple addition, i.e., $D = \sum_0^{N-1} r_i$, leads to the elimination of the second term (whenever codes $c_k(t)$ and $c_j(t)$ are orthogonal) and maximizes the SNR. This combining technique is termed as Equal Gain Combining (EGC).

However, in frequency selective channels of interest here, different combining methods may be used. Two such combining strategies are discussed next.

4.4.1 Maximal Ratio Combining/ML Combining

One way to determine a weight vector is the approach of maximal ratio combining (MRC) [80]. Here, each component of the weight vector is determined separately by [85]

$$w_i = \frac{E\{a_k^* \cdot r_i/\alpha_i\}}{Var\{a_k^* \cdot r_i/\alpha_i\}} \tag{4.18}$$

where, a_k^* represents the complex conjugate of the transmitted symbol a_k (in the case of BPSK $a_k^* = a_k$); $E\{\cdot\}$ denotes the expected value; and $Var\{\cdot\}$ represents the variance.

Assuming that the desired data, a_k, is uncorrelated with both noise as well as the interference terms (since data of different users are independent), the MRC combining weight can be written as

$$w_i = \frac{\alpha_i}{M_i \alpha_i^2 + N_0/2} \tag{4.19}$$

where, M_i is given by

$$M_i = \sum_{j=1, j\neq k}^{K} \cos\left(i(\Delta\theta_j - \Delta\theta_k)\right)^2. \tag{4.20}$$

MRC is optimal and is equivalent to the maximum likelihood combining (ML combining) in the sense of minimizing probability of error when noises and interference across different carriers are uncorrelated (e.g., when only AWGN is present). In [54], this is considered optimal from the standpoint of lack of knowledge regarding the correlation between the interference terms. However, in reality the correlation among the MAI in different carriers makes MRC sub-optimal. In the next subsection we will observe that when K is large, the expression for MRC/MLC (equation (4.20)) converges to minimum mean-squared error combining (MMSEC).

4.4.2 MMSE Combining

Minimum mean square error combining (MMSEC) produces excellent performances in terms of MC-CDMA probability of error [51]. The minimum mean square error combining method approximates the transmitted symbol $a_k[n]$ from the N-length vector $\underline{r} = (r_0, r_1, ..., r_{N-1})$ (see Figure 4.3) by using the linear sum :

$$D = \sum_{i=0}^{N-1} w_i r_i \tag{4.21}$$

Based on the MMSE criterion, the estimation error must be orthogonal to all the baseband components of the received subcarriers [86]. That is,

$$E\{(a_k[n] - \sum_{i=0}^{N-1} w_i r_i) \cdot r_i\} = 0, \quad i = 0, 1, ..., N-1. \tag{4.22}$$

The solution to equation (4.22) as obtained from Weiner filter theory corresponds to [87]

$$w_i = C^{-1}A \tag{4.23}$$

where $C = E\{r_i \cdot r_i|\alpha_i\}$, $A = E\{a_k[n] \cdot r_i|\alpha_i\}$ and $E\{\cdot\}$ denotes the expected value. This operation, when applied to the r_i in CI/MC-CDMA (equation(4.17)) yields

$$C = \alpha_i^2 \sum_{j=1}^{K} \cos\left(i(\Delta\theta_j - \Delta\theta_k)\right)^2 + N_o/2 \tag{4.24}$$

$$A = \alpha_i \tag{4.25}$$

Substituting (4.24) and (4.25) in (4.23) we obtain the weights for MMSEC :

$$w_i = \frac{\alpha_i}{(\alpha_i^2 \sum_{j=1}^{K} \cos\left(i(\Delta\theta_j - \Delta\theta_k)\right)^2 + N_o/2)} \tag{4.26}$$

and; hence, from (4.21),

$$D = \sum_{i=0}^{N-1} \frac{\alpha_i}{(\alpha_i^2 \sum_{j=1}^{K} \cos\left(i(\Delta\theta_j - \Delta\theta_k)\right)^2 + N_o/2)} \cdot r_i. \tag{4.27}$$

Therefore, employing MMSEC in CI/MC-CDMA results in the decision variable

$$D = \sum_{i=0}^{N-1} r_i \cdot [\frac{\alpha_i}{(R_i\alpha_i^2 + N_o/2)}], \tag{4.28}$$

where R_i is a known constant for a given K and carrier i and corresponds to

$$R_i = \sum_{j=1}^{K} \cos\left(i(\Delta\theta_j - \Delta\theta_k)\right)^2. \tag{4.29}$$

Now, if we consider a fully loaded system, i.e., $K = N$, the R_i simplifies to

$$R_i = \begin{cases} N & i = 0, \frac{N}{2} \\ N/2 & \text{else} \end{cases} \tag{4.30}$$

It is important to note that, by constructing a receiver that processes the signal in the frequency domain rather than in the time domain, we circumvent the need for sub chip synchronism.

4.5 Performance Results

We now characterize the performance of a wireless system where: (1) MC-CDMA transmitters are constructed using CI codes as shown in Figure 4.1 and equations (4.2)-(4.8); (2) channels are slow, frequency selective fading channels characterized in Section 4.3; and (3) receivers are constructed as shown in Figure 4.3 and described in Section 4.4.

Figure 4.4 presents the average bit error rate (BER) versus number of users for $N = 32$ carriers and $SNR = 14$dB. Results are presented for a frequency selective Rayleigh fading channel with $(\Delta f)_c/BW$=0.5 (supporting L=2-fold diversity over the entire bandwidth).

In Figure 4.4, two benchmark MC-CDMA system curves are also provided. The first MC-CDMA benchmark assumes orthogonal Hadamard-Walsh (HW) codes of length 32 (dashed line) and the second assumes Gold codes (solid line) - here, length 31 Gold codes support 33 users, with a second set of Gold codes used to support additional users. Additionally, a flat dotted line is drawn which represents the matched filter lower bound (performance of a single user system exploiting the available diversity through MRC).

The BER for our proposed CI/MC-CDMA is shown on the dotted line. It slightly outperforms MC-CDMA (using HW codes) up to 32 users. While orthogonal MC-CDMA can not support additional users, CI/MC-CDMA accommodates an additional 32 users (up to 64 users) by using a second set orthogonal set of N=32 codes. If MC-CDMA is pre-selected to support additional users, by use of pseudo orthogonal Gold codes, it results in significant performance degradation relative to CI/MC-CDMA as shown by the solid line. In fact, at a BER of 0.005, the CI/MC-CDMA system supports 64 users, 4 times the number of users supported by the pseudo-orthogonal

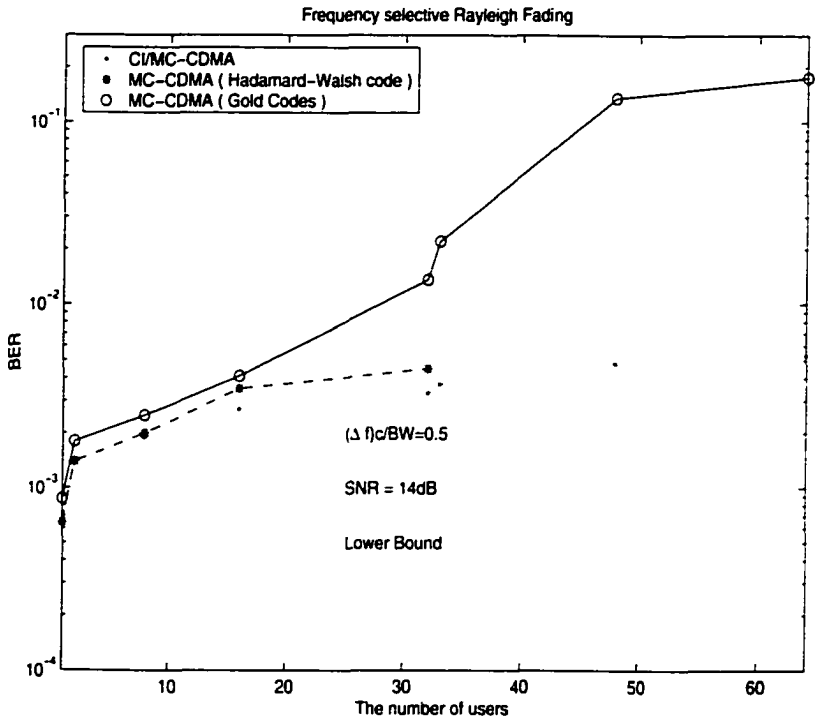

Figure 4.4: Average BER performance of CI/MC-CDMA, orthogonal MC-CDMA and pseudo-orthogonal MC-CDMA

MC-CDMA system.

It is observed that with a total of 64 users (32 orthogonal and 32 pseudo orthogonal), CI/MC-CDMA systems offer an average performance comparable to that of MC-CDMA employing Gold codes with 16 users or MC-CDMA employing HW codes with 32 users. Hence, CI/MC-CDMA enjoys approximately 300% more capacity relative to pseudo orthogonal MC-CDMA methods and 100% more relative to MC-CDMA with HW codes. Furthermore, the CI/MC-CDMA system is implemented using FFT's and IFFT's similar to MC-CDMA, resulting in comparable complexities.

4.6 Summary

In this chapter, CI/MC-CDMA, an innovation in code design for MC-CDMA, was introduced. In synchronous frequency selective Rayleigh fading channels, CI/MC-

CDMA's performance matches that of orthogonal MC-CDMA using Hadamard-Walsh codes up to the MC-CDMA $K = N$ user limit; moreover, CI/MC-CDMA provides the added flexibility of supporting $K > N$ (up to $K = 2N$) users by adding users with pseudo orthogonal codes. CI/MC-CDMA also provides added flexibility in the choice of N ($N \in I$ versus $N = 2^n$ or $N = 2^n \pm 1$ ($n \in I$)) making it more robust to the wide range of mobile system applications. In the following chapter we will discuss some practical issues that impact the design and performance of CI/MC-CDMA systems.

APPENDIX 4A : How to Generate Correlated Rayleigh Envelopes for Use in Simulations

It is well known that Rayleigh random variables are closely related to complex Gaussian random variables. To illustrate this point, consider N complex Gaussian signals $(v_1, v_2, \cdots, v_N)$ where

$$v_i = x_i + jy_i \tag{4.31}$$

and x_i, y_i are independent zero mean Gaussian random variables with variance $\frac{1}{2}\sigma_g^2$. The envelopes of $(v_1, v_2, \cdots, v_N)$, labeled $(R_1, R_2, \cdots, R_N)$, and corresponding to

$$R_i = |v_i| = \sqrt{x_i^2 + y_i^2} \tag{4.32}$$

are Rayleigh distributed.

Assume we want to generate N Rayleigh envelopes $(R_1, R_2, \cdots, R_N)$ with a normalized covariance matrix

$$\mathbf{K_R} = \begin{pmatrix} 1 & \rho_{R1,2} & \rho_{R1,3} & \cdots & \rho_{R1,N} \\ \rho_{R2,1} & 1 & \rho_{R2,3} & \cdots & \rho_{R2,N} \\ \vdots & & & & \\ \rho_{RN,1} & \rho_{RN,2} & \rho_{RN,3} & \cdots & 1 \end{pmatrix} \tag{4.33}$$

The idea underlying this work is to generate N complex Gaussian random variables $(v_1, v_2, \cdots, v_N)$ with a corresponding normalized covariance matrix

$$\mathbf{K_g} = \begin{pmatrix} 1 & \rho_{g1,2} & \rho_{g1,3} & \cdots & \rho_{g1,N} \\ \rho_{g2,1} & 1 & \rho_{g2,3} & \cdots & \rho_{g2,N} \\ \vdots & & & & \\ \rho_{gN,1} & \rho_{gN,2} & \rho_{gN,3} & \cdots & 1 \end{pmatrix}, \tag{4.34}$$

such that creation of the desired $(R_1, R_2, \cdots, R_N)$ results by taking absolute values of $(v_1, v_2, \cdots, v_N)$.

The generation of $\mathbf{K_g}$ given $\mathbf{K_R}$ is based on the following realization : the value $\rho_{Ri,j}$, the (i,j)th element of $\mathbf{K_R}$ (representing the correlation coefficient between R_i and R_j), is determined exclusively by $|\rho_{gi,j}|$, the absolute value of the (i,j)th element of $\mathbf{K_g}$ (the magnitude of the correlation coefficient between v_i and v_j). For simplicity in presentation and algorithm implementation, we assume that the elements of $\mathbf{K_g}$ ($\rho_{gi,j}$'s) are real, and consequently the value $\rho_{Ri,j}$ is determined exclusively by $\rho_{gi,j}$ (and vice-versa).

The exact analytical relationship relating $\rho_{Ri,j}$ and $\rho_{gi,j}$ is given by [88]

$$\rho_{Ri,j} = \frac{(1+|\rho_{gi,j}|)E_i(\frac{2\sqrt{|\rho_{gi,j}|}}{1+|\rho_{gi,j}|}) - \frac{\pi}{2}}{2-\frac{\pi}{2}}, \tag{4.35}$$

where $E_i(\eta)$ denotes the complete elliptic integral of the second kind with modulus η. In [88], the lack of a direct closed form solution to the $\rho_{Ri,j} - \rho_{gi,j}$ equation is resolved by the use of numerical methods, namely polynomial approximation (to evaluate the elliptical integrals).

While the results of [88] may be used to relate $\rho_{gi,j}$ to $\rho_{Ri,j}$ (using an intermediate variable λ), a new method is provided here which offers an immediate, simple, one-to-one relationship between $\rho_{gi,j}$ and $\rho_{Ri,j}$. Given $\rho_{gi,j}$:(1) create pairs of complex Gaussian samples with correlation $\rho_{gi,j}$ from pairs of uncorrelated samples by employing Cholesky Decomposition [89];(2) numerically evaluate the correlation among the envelopes of Gaussian samples with correlation coefficient $\rho_{gi,j}$ - this provides $\rho_{Ri,j}$.(3) In this way, a look-up table of values relating $\rho_{gi,j}$ and $\rho_{Ri,j}$ is available. Table 4.2 and Figure 4.5 show a table and corresponding plot relating $\rho_{gi,j}$ and $\rho_{Ri,j}$. The table and figure may be used as a quick reference to evaluate $\rho_{gi,j}$ given $\rho_{Ri,j}$ (using linear interpolation).

In this way, all elements of $\mathbf{K_R}$ can be mapped to corresponding elements in $\mathbf{K_g}$. Once $\mathbf{K_g}$ is determined, the N correlated Gaussian samples $(v_1, v_2, \cdots, v_N)$

are generated by Cholesky Decomposition [89], and the desired $(R_1, R_2, \cdots, R_N)$ are created by evaluating the envelopes of the N complex Gaussian samples.

The procedure for generating the N correlated Rayleigh fading signals is summarized by the following algorithm

Algorithm

The starting point is the desired covariance matrix of the Rayleigh envelopes $(R_1, R_2, \cdots, R_N)$, given by

$$\hat{\mathbf{K}}_{\mathbf{R}} = \begin{pmatrix} \sigma_{R1}^2 & \hat{\rho}_{R1,2} & \hat{\rho}_{R1,3} & \cdots & \hat{\rho}_{R1,N} \\ \hat{\rho}_{R2,1} & \sigma_{R2}^2 & \hat{\rho}_{R2,3} & \cdots & \hat{\rho}_{R2,N} \\ \vdots & & & & \\ \hat{\rho}_{RN,1} & \hat{\rho}_{RN,2} & \hat{\rho}_{RN,3} & \cdots & \sigma_{RN}^2 \end{pmatrix}. \tag{4.36}$$

1. Normalize this matrix to create the normalized covariance matrix

$$\mathbf{K}_{\mathbf{R}} = \begin{pmatrix} 1 & \rho_{R1,2} & \rho_{R1,3} & \cdots & \rho_{R1,N} \\ \rho_{R2,1} & 1 & \rho_{R2,3} & \cdots & \rho_{R2,N} \\ \vdots & & & & \\ \rho_{RN,1} & \rho_{RN,2} & \rho_{RN,3} & \cdots & 1 \end{pmatrix}, \tag{4.37}$$

where $\rho_{Ri,j} = \hat{\rho}_{Ri,j} / \sqrt{\sigma_{Ri}^2 \sigma_{Rj}^2}$.

2. For each cross correlation coefficient $\rho_{Ri,j}$, compute the corresponding $\rho_{gi,j}$ by (a) using Table 4.2 (and linear interpolation) or (b) relating $\rho_{Ri,j}$'s and $\rho_{gi,j}$'s as discussed earlier.

3. Form the normalized covariance matrix of complex Gaussian samples:

$$\mathbf{K}_{\mathbf{g}} = \begin{pmatrix} 1 & \rho_{g1,2} & \rho_{g1,3} & \cdots & \rho_{g1,N} \\ \rho_{g2,1} & 1 & \rho_{g2,3} & \cdots & \rho_{g1,N} \\ \vdots & & & & \\ \rho_{gN,1} & \rho_{gN,2} & \rho_{gN,3} & \cdots & 1 \end{pmatrix} \tag{4.38}$$

4. Generate N uncorrelated complex Gaussian samples $\mathbf{V} = (v_1, v_2, ..., v_N)$ each with variance σ_g^2; then, determine the coloring matrix $\mathbf{L}$ corresponding to $\mathbf{K_g}$ (the coloring matrix $\mathbf{L}$ is the lower triangular matrix such that $\mathbf{L}\mathbf{L}^{\mathbf{T}} = \mathbf{K_g}$ where $\mathbf{L}^{\mathbf{T}}$ represents the

$\rho_{gi,j}$	$\rho_{Ri,j}$	$\rho_{gi,j}$	$\rho_{Ri,j}$
0.00	0.0000	0.50	0.2227
0.05	0.0047	0.55	0.2752
0.10	0.0056	0.60	0.3327
0.15	0.0243	0.65	0.4133
0.20	0.0337	0.70	0.4562
0.25	0.0559	0.75	0.5410
0.30	0.0737	0.80	0.6073
0.35	0.0965	0.85	0.6974
0.40	0.1494	0.90	0.7913
0.45	0.1836	0.95	0.9005

Table 4.2: Correlation of Rayleigh envelopes $\rho_{Ri,j}$ for values of complex Gaussian correlation $\rho_{gi,j}$

transpose of $\mathbf{L}$) and generate correlated complex Gaussian samples using $\mathbf{W} = \mathbf{LV}$.

5. The N envelopes of the Gaussian samples in $\mathbf{W}$ correspond to Rayleigh random variables $(R'_1, R'_2, \cdots, R'_N)$ with normalized covariance matrix $\mathbf{K_R}$ and equal variance [20]

$$\sigma_R^2 = (2 - \frac{\pi}{2})\frac{1}{2}\sigma_g^2 \tag{4.39}$$

6. Create the desired Rayleigh envelopes $(R_1, R_2, \cdots, R_N)$ from the samples $(R'_1, R'_2, \cdots, R'_N)$, by evaluating $R_i = A_i \cdot R'_i$ where $A_i = \sigma_{Ri}/\sigma_R$.

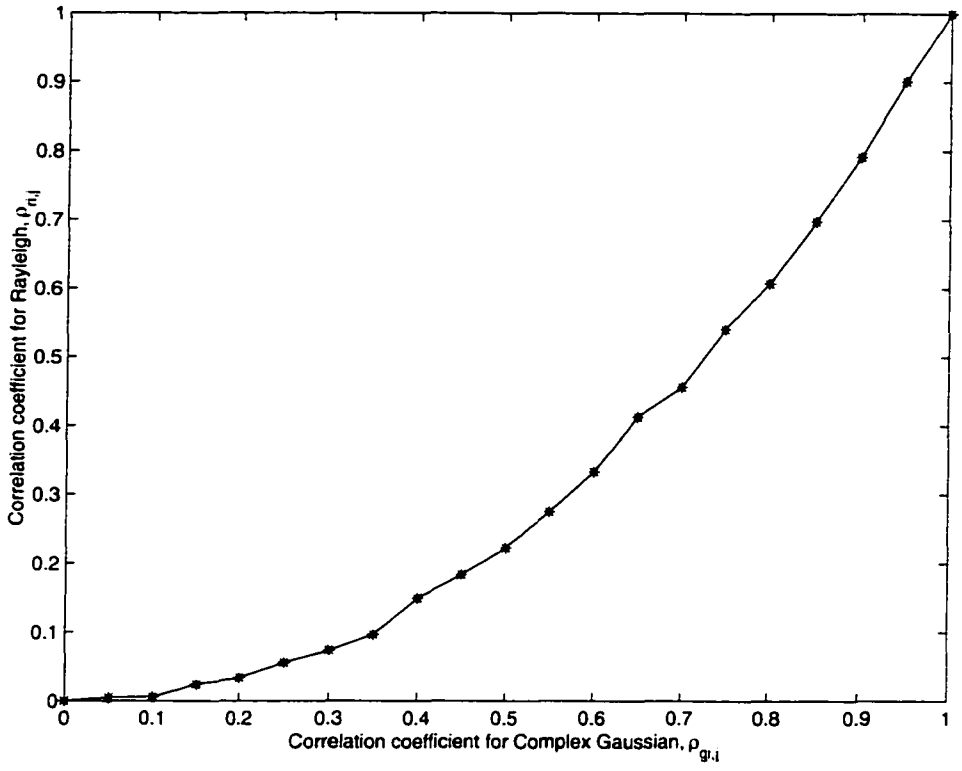

Figure 4.5: Relationship between correlation coefficients of Complex Gaussian $\rho_{gi,j}$ and Rayleigh $\rho_{Ri,j}$

Chapter 5

CI/MC-CDMA - Practical Considerations

In this chapter, we consider some practical issues that impact the design and performance of CI/MC-CDMA. We do this in three parts. First, we model the effects of phase jitter on the CI/MC-CDMA system and demonstrate its robustness via performance curves. Second, we consider the effects of frequency offsets and show that the impact of frequency offsets on CI/MC-CDMA is comparable to that in traditional MC-CDMA systems. Finally, we address the issue of crest factor [90] in CI/MC-CDMA. We show that crest factor is not a concern in CI/MC-CDMA downlink, while in the uplink, the high crest factor can be combated using simple phase encoding schemes.

5.1 Phase Jitter Effects

As we saw in Section 4.4, the channel introduces the phase offset ϕ_i on the i^{th} carrier (see equation (4.16)), which may be tracked and accounted for at the receiver using, e.g., a phase locked loop (PLL). Tracking loops are not perfect and hence a degradation in performance may result due to phase jitter.

If $\hat{\phi}_i$ is the estimate of the phase using a PLL, then $\theta_i = \phi_i - \hat{\phi}_i$, the carrier phase

error, has the Tikhonov probability density function (pdf) [91] ,

$$p(\theta_i) = \frac{exp(\rho \cos \theta_i)}{2\pi I_0(\rho)}; \quad |\theta_i| \leq \pi \tag{5.1}$$

Here, ρ is a parameter related to the tracking loop SNR and $I_0(x)$ is the modified Bessel function of the first kind. For first order tracking loops, ρ is the loop SNR and for second order loops, ρ is approximately the loop SNR for sufficiently large values [92]. Figure 5.1 plots the probability density function for this Tikhonov distributed random variable as a function of the ρ parameter. As the ρ value increases, the degree of jitter decreases. Specifically, we can calculate the rms phase jitter for different values of ρ, e.g., $\rho = 10$ corresponds to an rms phase jitter of 18.7°.

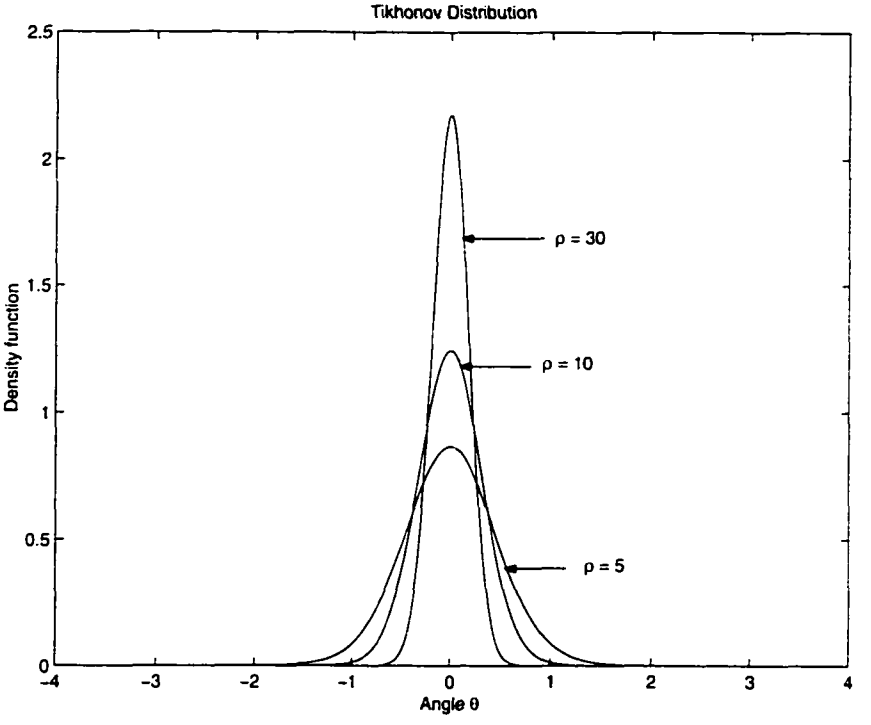

Figure 5.1: Tikhonov density function with different ρ

After demodulating the received signal using phase $\hat{\phi}_i$ on the i^{th} carrier, the received signal component r_i (see Figure 4.3, and shown in (4.17) with perfect synchro-

nization) is now given by

$$r_i = \alpha_i a_k[n] \cos\theta_i + \sum_{j=1, j\neq k}^{K} \alpha_i a_j[n] \cos\left(i(\Delta\theta_j - \Delta\theta_k) + \theta_i\right) + \eta_i \qquad (5.2)$$

where $\theta_i = \phi_i - \hat{\phi}_i$. Referring to Section 4.4, these signal components are then combined across carriers using the MMSEC of equation (4.28).

5.1.1 Performance Results

The performance of CI/MC-CDMA with phase jitter is illustrated in Figure 5.2. This figure represents simulation results under conditions identical to those used to achieve Figure 4.4, with the exception of phase jitters corresponding to $\rho = 10, 30$ and 100 (i.e., rms phase jitters of 18.7°, 10° and 5° respectively). CI/MC-CDMA demonstrates graceful performance degradation, even as phase jitters grow very large. This results because the spreading sequence of user k is $(1, e^{j\Delta\theta_k}, e^{j2\Delta\theta_k}, \cdots, e^{j(N-1)\Delta\theta_k})$ while user j's spreading sequence is $(1, e^{j\Delta\theta_j}, e^{j2\Delta\theta_j}, \cdots, e^{j(N-1)\Delta\theta_j})$, and hence, even if the value of $\Delta\theta_k$ is close to $\Delta\theta_j$ (e.g., $\Delta\theta_k - \Delta\theta_j = \epsilon$), the phase spacing between the i^{th} spreading sequence elements is $i(\Delta\theta_k - \Delta\theta_j)$ (i.e., $i \cdot \epsilon$) which is large for large values of i. Thus the CI/MC-CDMA system is more robust to phase jitters than one might expect at initial glance.

Figures 5.3 and 5.4 compare the effect of phase jitters on CI/MC-CDMA and benchmark MC-CDMA with HW and Gold codes. Figure 5.3 shows the performance with phase jitter corresponding to $\rho = 30$ and Figure 5.4 shows $\rho = 10$ results. It is observed that relative performance does not change significantly for high values of ρ. As ρ decreases (i.e., as tracking loop SNR degrades), the CI/MC-CDMA degrades at a slightly more rapid rate than its MC-CDMA counterpart, but still offers comparable benefits to those outlined in section 4.5.

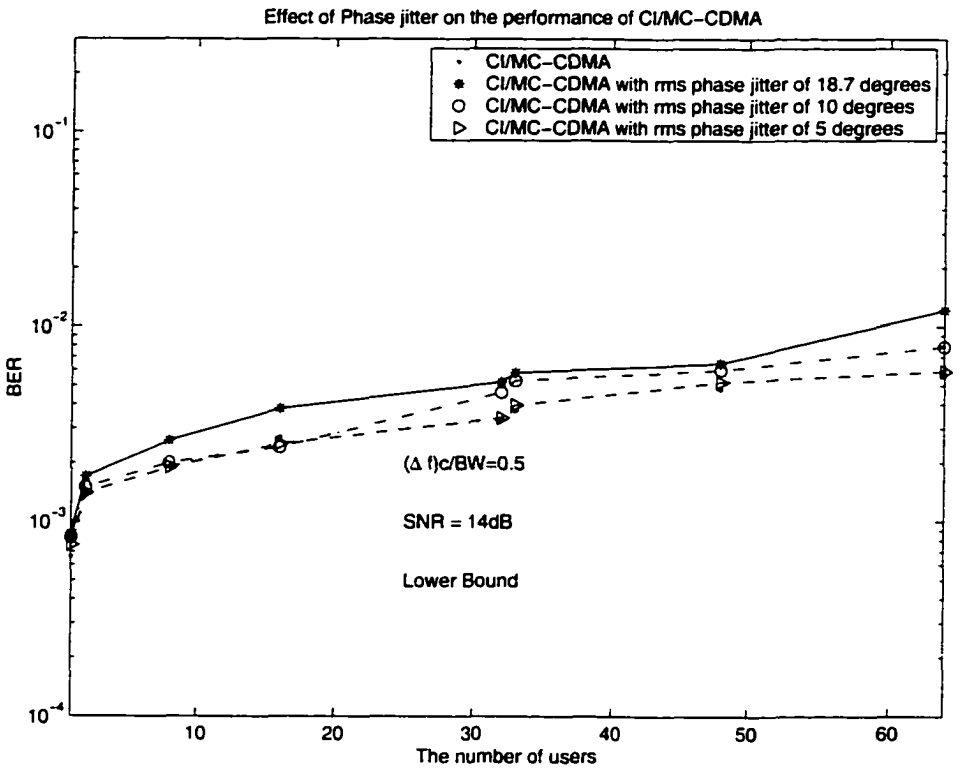

Figure 5.2: BER performance of CI/MC-CDMA in the presence of Phase Jitter

5.2 Frequency Offsets

Multi-carrier transmission schemes including traditional MC-CDMA and the newly introduced CI/MC-CDMA are particularly susceptible to performance degradations from carrier frequency offset. Two major factors are at the root of such carrier frequency offsets : (1) Doppler spread caused by a high-speed mobile and (2) offsets between the oscillator at the transmitter and that of the receiver.

Frequency offsets caused by less than perfect synchronicity between the transmitter and the receiver oscillators are present to the same degree all carriers. On the other hand, offsets due to Doppler spreads are different on each carrier (a function of the carrier's location in the spectrum). However, for mobile communication systems operating at a typical carrier frequency of e.g., 2 GHz and occupying a characteristic

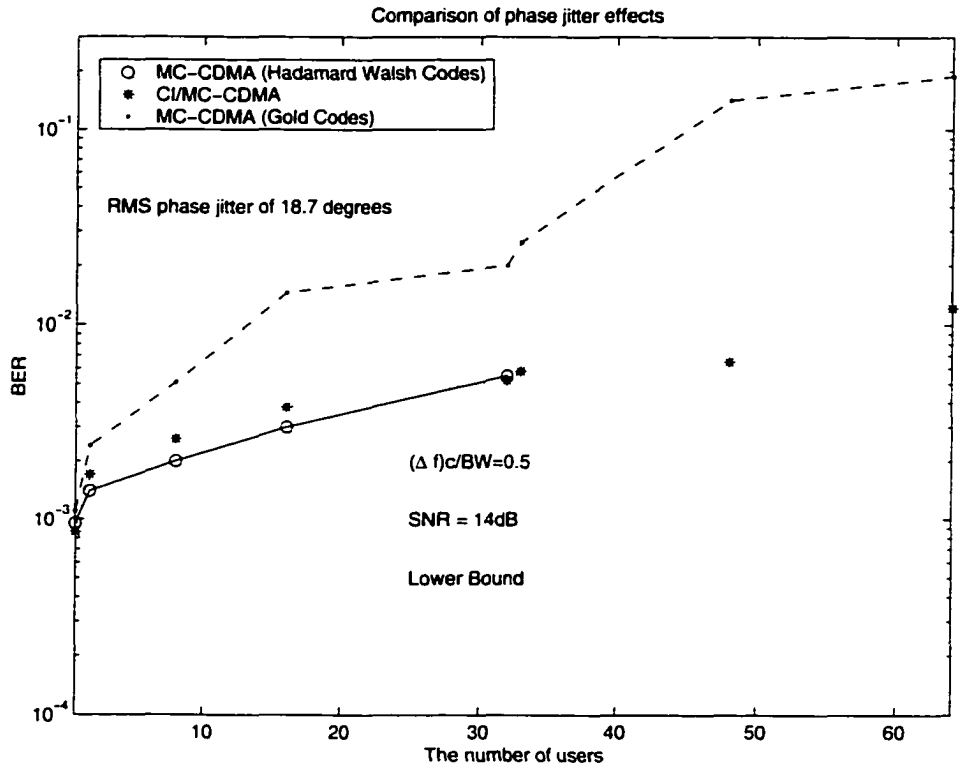

Figure 5.3: BER performance comparison of CI/MC-CDMA, orthogonal MC-CDMA and pseudo orthogonal MC-CDMA in the presence of Phase Jitter ($\rho = 10$)

1 MHz bandwidth, the maximum difference in Doppler spread among 32 carriers is in the range of 0-5 Hz, which is negligible when compared to subcarrier spacings of about 30 KHz [93]. Hence, we treat frequency offsets as a phenomenon with identical characteristics in all subchannels.

Frequency offsets in the proposed CI/MC-CDMA system results in two key adverse effects. First is the reduction of desired signal amplitude and second is the loss of carrier orthogonality which leads to the introduction of intercarrier interferences.

If Δ is the normalized frequency offset (defined as the ratio of the actual frequency offset to the subcarrier separation Δf), the decision variable D (see Figure 4.3 and equation (4.28)) is given by (analogous to [93], [94]),

$$D = S + MAI + ICI_1 + ICI_2 + AWGN \tag{5.3}$$

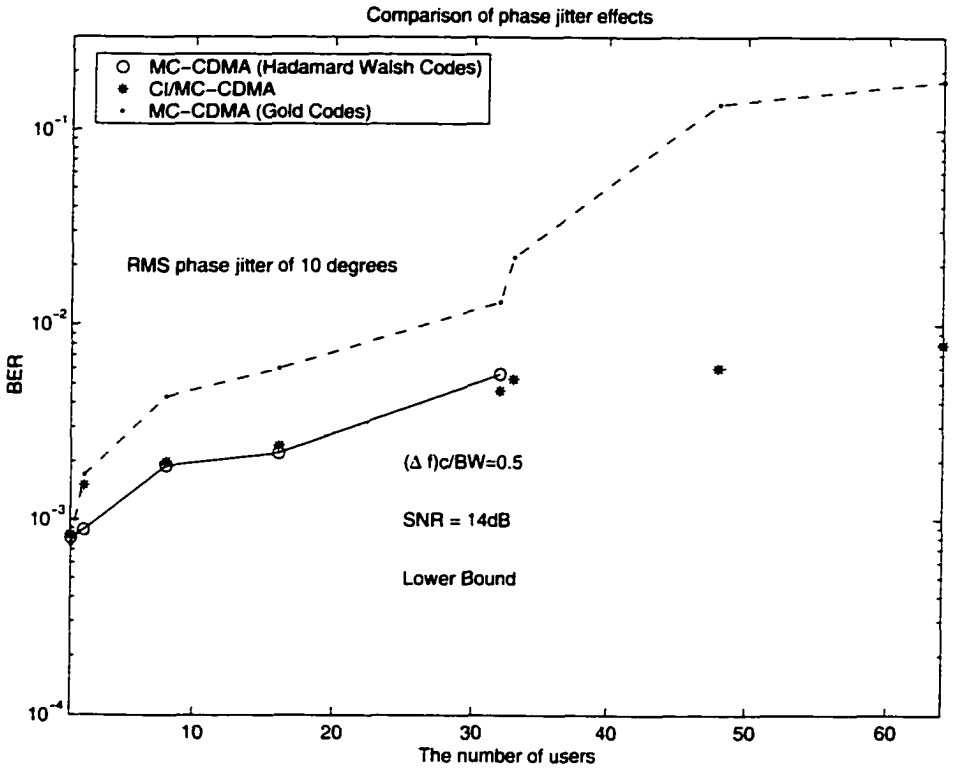

Figure 5.4: BER performance comparison of CI/MC-CDMA, orthogonal MC-CDMA and pseudo orthogonal MC-CDMA in the presence of Phase Jitter ($\rho = 30$)

where the five components correspond to

$$S = \frac{\sin \pi\Delta}{\pi\Delta} a_k[n] \sum_{i=0}^{N-1} [\frac{\alpha_i^2}{(R_i\alpha_i^2 + N_o/2)}], \tag{5.4}$$

$$MAI = \frac{\sin \pi\Delta}{\pi\Delta} \sum_{i=0}^{N-1} \sum_{j=1, j\neq k}^{K} [\frac{\alpha_i^2}{(R_i\alpha_i^2 + N_o/2)}] a_j[n] \cos\left(i(\Delta\theta_j - \Delta\theta_k)\right), \tag{5.5}$$

$$\begin{aligned} ICI_1 &= \frac{\sin \pi\Delta}{\pi} \sum_{i=0}^{N-1} \sum_{m=0, m\neq i}^{N-1} [\frac{\alpha_m^2}{(R_m\alpha_m^2 + N_o/2)}] \cdot \\ &\quad a_k[n] \cos\left(\Delta\theta_k(i-m)\right) \frac{1}{\Delta + i - m} \cdot \cos\left(\phi_m - \phi_i\right), \end{aligned} \tag{5.6}$$

$$\begin{aligned} ICI_2 &= \frac{\sin \pi\Delta}{\pi} \sum_{i=0}^{N-1} \sum_{m=0, m\neq i}^{N-1} \sum_{j=1, j\neq k}^{K} [\frac{\alpha_m^2}{(R_m\alpha_m^2 + N_o/2)}] \cdot \\ &\quad a_j[n] \cos\left(m\Delta\theta_j - i\Delta\theta_k\right) \frac{1}{\Delta + i - m} \cdot \cos\left(\phi_m - \phi_i\right), \end{aligned} \tag{5.7}$$

$$AWGN = \sum_{i=0}^{N-1} \eta_i [\frac{\alpha_i}{(R_i \alpha_i^2 + N_o/2)}]. \quad (5.8)$$

Here, S, MAI, ICI_1, ICI_2 denote the desired signal, the multi- access interference, the intercarrier interference generated from within the k^{th} user's CI code, and the intercarrier interference generated from the CI codes of the other users.

The added interference terms in equation (5.3) contribute to a degradation in performance as shown next.

5.2.1 Performance Results

Figure 5.5 plots the performance of the proposed CI/MC-CDMA in the presence of frequency offsets $\Delta = 0.1$ and 0.2. It is observed that CI/MC-CDMA is immune to 10% frequency offset while a degradation is visible for a 20% offset level. Specifically, with 20% offset, the CI/MC-CDMA system supports 16 users at a probability of error of $3 \cdot 10^{-3}$, while without frequency offsets (or with 10% offset) the system supports 32 users at that error rate. Figures 5.6 and 5.7 compare the impact of frequency offset on CI/MC-CDMA and traditional MC-CDMA with HW codes. Both systems are degraded by a comparable amount, demonstrating that CI/MC-CDMA is no more susceptible to frequency offsets than its traditional MC-CDMA counterpart. There is no significant penalty due to frequency offsets in CI/MC-CDMA and all the techniques that are used to combat this effect in traditional MC-CDMA [] are applicable to our system.

5.3 Crest Factor in CI/MC-CDMA

One concern regarding the use of MC-CDMA with CI codes is the peak-to-average power ratio (PAPR) relative to single carrier schemes. This concern arises because, in the time domain, these codes create a periodic mainlobe with sidelobe activity

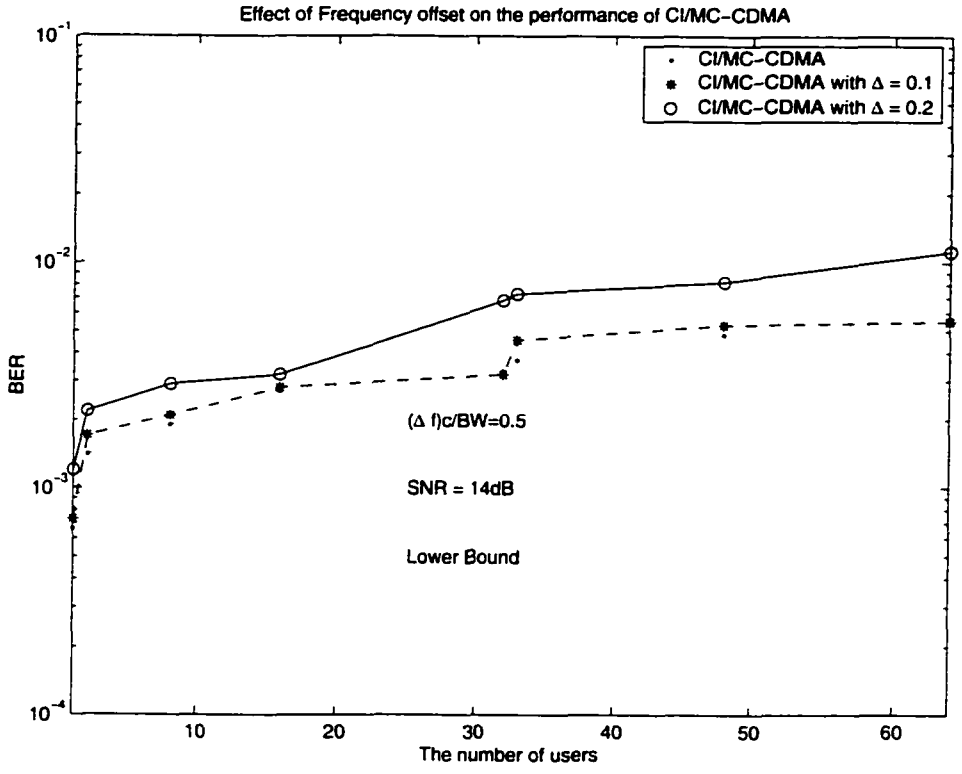

Figure 5.5: BER performance of CI/MC-CDMA in the presence of frequency offset

at intermediate times (see Figure 3.2). The correspondingly large PAPR leads to a reduced efficiency of the power amplifier, and an increased signal dynamic range requires power amplifiers with higher range of linearity.

To measure the signal compactness of the CI/MC-CDMA signal, we employ the crest factor (CF). For a multi-carrier signal $s(t)$ [90],[95]

$$CF = \frac{M^+ - M^-}{2E_{eff}} \tag{5.9}$$

where M^+ is the largest positive and M^- is the most negative value of $s(t)$. Also, E_{eff} represents the total amount of energy contained in $s(t)$ and equals $\|s\|_2$, i.e., the rms value of $s(t)$. It is clear from (5.9) that a sine wave has a crest factor of $\sqrt{2}$. Another common approximation found in the literature [90] relates crest factor

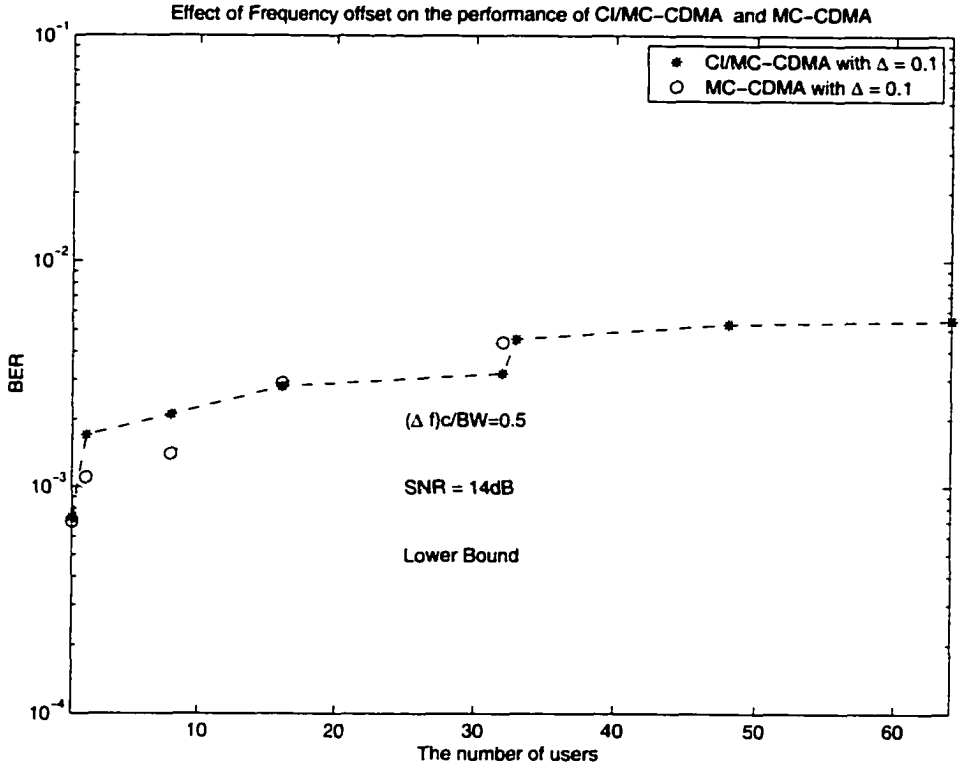

Figure 5.6: BER comparison of CI/MC-CDMA and MC-CDMA in the presence of frequency offset ($\Delta = 0.1$)

to PAPR:

$$CF_{papr} \approx \sqrt{PAPR} = \frac{\|s\|_\infty}{\|s\|_2} \tag{5.10}$$

where $\|s\|_\infty$ corresponds to the maximum absolute value of $s(t)$. In the following discussion, we provide exact CF values in accordance with (5.9) as well as $\sqrt{PAPR}$ values (see (5.10)) for CI/MC-CDMA.

5.3.1 Downlink Crest Factor

In the MC-CDMA downlink, all K user's signals are bundled together prior to transmission, leading to

$$s_{down}(t) = \sum_{k=0}^{K-1} s_k(t); \tag{5.11}$$

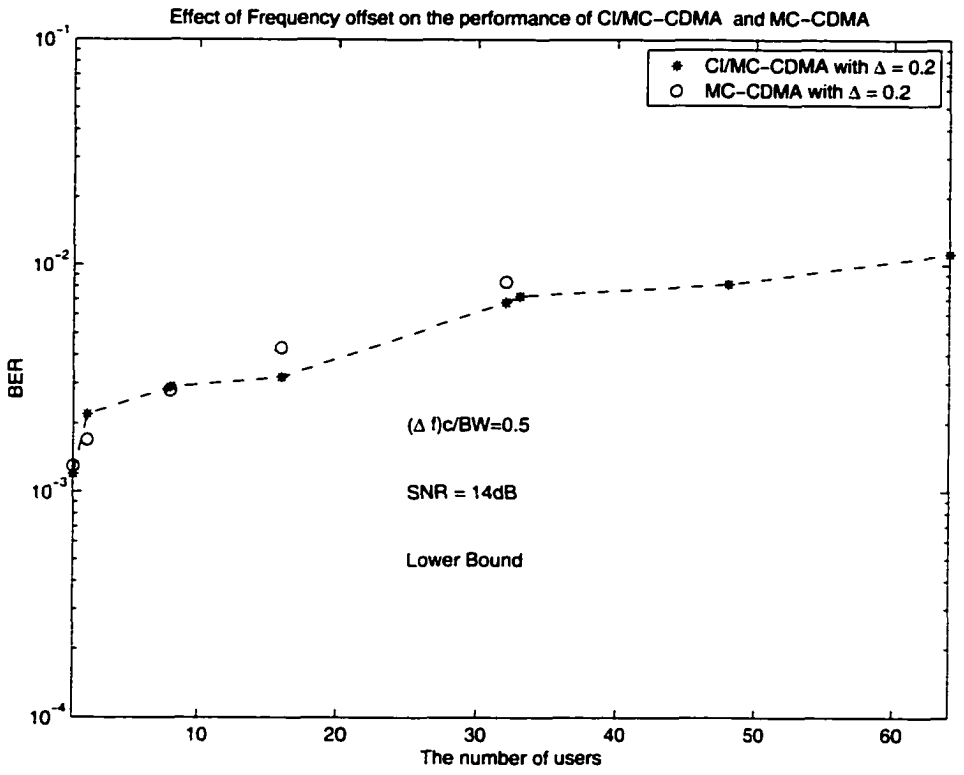

Figure 5.7: BER comparison of CI/MC-CDMA and MC-CDMA in the presence of frequency offset ($\Delta = 0.2$)

This equation is shown in greater detail in (4.8) (with $K = 2N$).

The crest factor of $s_{down}(t)$ is dependent on the binary antipodal data symbols of the users, $a_k[n]$, equally likely to be +1 or -1. The crest factor is therefore a Gaussian distributed random variable [76],[96]. Assuming $N = 32$ carriers and $K = 32$ users, the probability density functions of CF and $\sqrt{PAPR}$ for $s_{down}(t)$ are plotted in Figures 5.8 and 5.9 respectively. The corresponding cumulative distribution functions are plotted in Figures 5.10 and 5.11. These results were obtained using computer-based simulation of the transmitted signal $s_{down}(t)$ with random binary data, followed by evaluation of the CF values based on (5.9) and (5.10). It is observed that $E[CF] = 1.85$ and $E[\sqrt{PAPR}] = 1.89$, where $E[\cdot]$ refers to the numerical mean. These values are well within tolerable levels of power amplifiers. The probability of $CF \geq 2.05$ is

less than 4%, indicating that the variance of CF is low, i.e., CF rarely ventures far above its mean of 1.85. This low CF can be attributed to simultaneous transmission of all users' signals. That is, even though the signature waveform of Figure 3.2 appears to have a poor CF, the combined signal, with all signature waveforms and data symbols on them, actually improves the CF tremendously. An example of this phenomenon is shown in Figure 5.12: when bits $a_k[n]$ are '1' for all users $k \in \{0, 1, ..., N-1\}$, the combined signal (solid line) is seen to demonstrate small values of PAPR and CF.

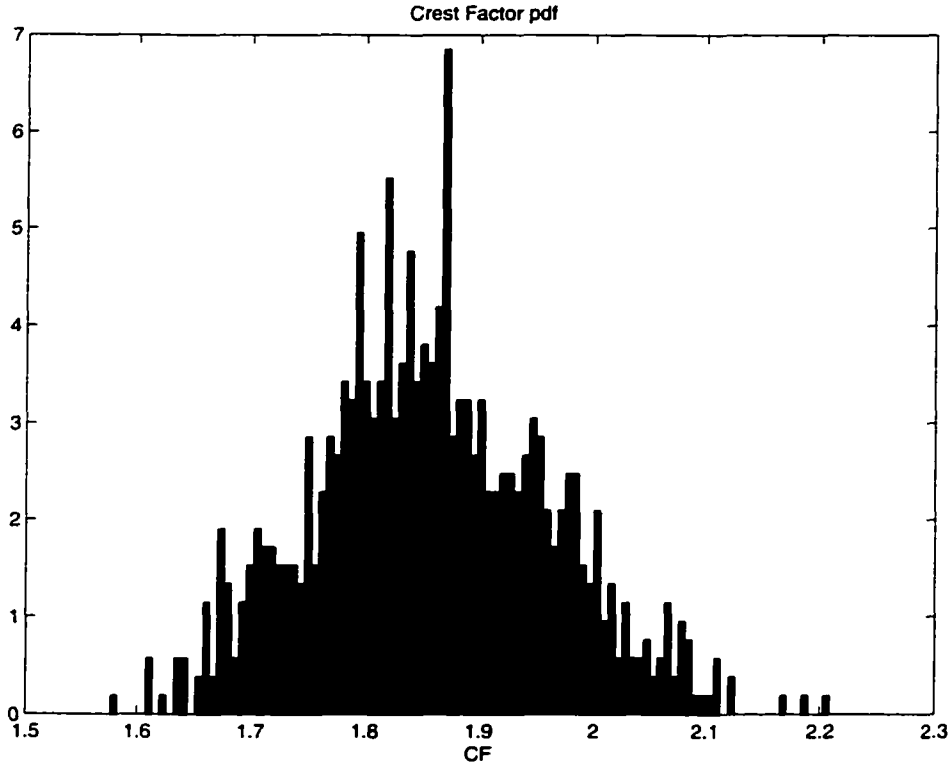

Figure 5.8: Probability density function of CF (N=32, K=32)

5.3.2 Uplink Crest Factor

We now turn our attention to the CF in the CI/MC-CDMA uplink. The signal transmitted by user k in the uplink is $s_{up}(t) = s_k(t)$ (see equation (4.1) and Figure 3.2 for details). The crest factor of $s_{up}(t)$ is shown in Table 5.1 where it is apparent

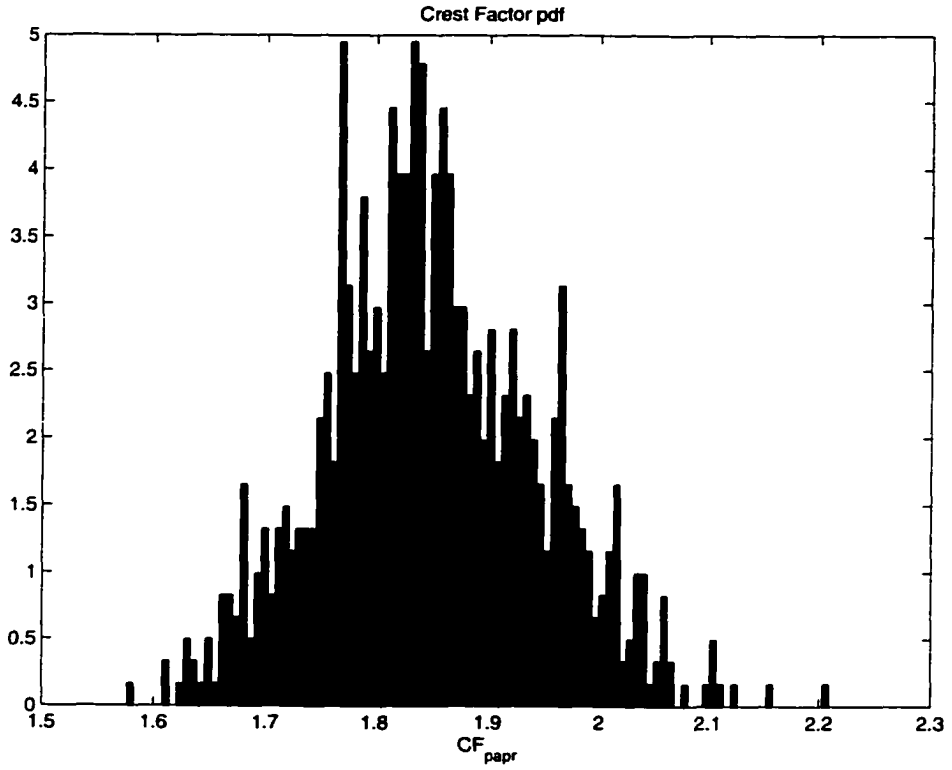

Figure 5.9: Probability density function of $\sqrt{PAPR}$ (N=32, K=32)

that CF and $\sqrt{PAPR}$ increase with increasing N. These values were calculated analytically, since the uplink CI/MC-CDMA signal envelope has a fixed maximum, minimum and rms value that does not depend on the transmitted data.

Systems built to accommodate such crest factor values would be extremely inefficient as high CF would cause the power amplifier to 'back-off' (reduce average transmission power) to avoid non-linear distortions. Hence, we employ a CF reduction technique that enables the CI/MC-CDMA system to demonstrate desirable CF values in the uplink.

5.3.3 CF Reduction Technique

In a multi-carrier signal such as the CI/MC-CDMA code of Figure 3.2 and equation (4.1), the crest factor is a function of the phase angles of the carriers. Schroeder

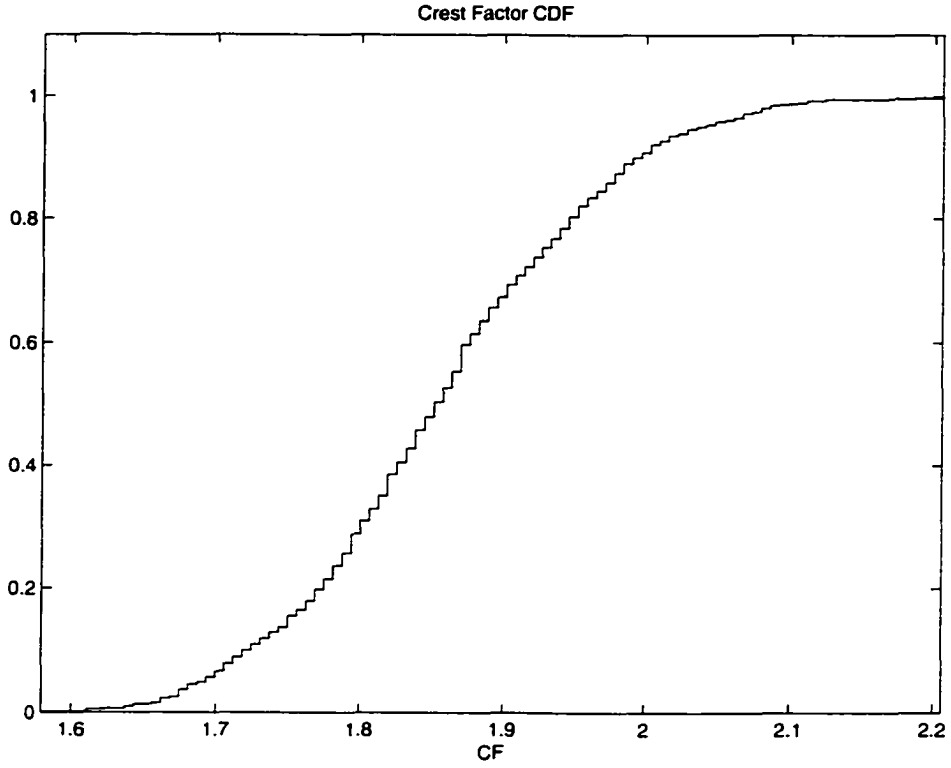

Figure 5.10: Cumulative distribution function of CF (N=32. K=32)

[97] proposed a powerful, easy-to-implement rule for phase angle adjustment that creates a multi-carrier signal with a low CF: the rule for creating low CF is effective in cases when the carriers are concentrated in a small frequency band (small relative to the center frequency), as in the case in CI/MC-CDMA. In this section, we apply Schroeder's technique to reduce CF in the CI/MC-CDMA uplink. (It is important to note that there are other techniques of phase angle adjustments ([98],[99]) that can alternatively be employed in CI/MC-CDMA systems to reduce CF).

N	CF	$\sqrt{PAPR}$
8	2.59	4.00
16	3.55	4.94
32	4.95	8.00

Table 5.1: CI/MC-CDMA Uplink CF values

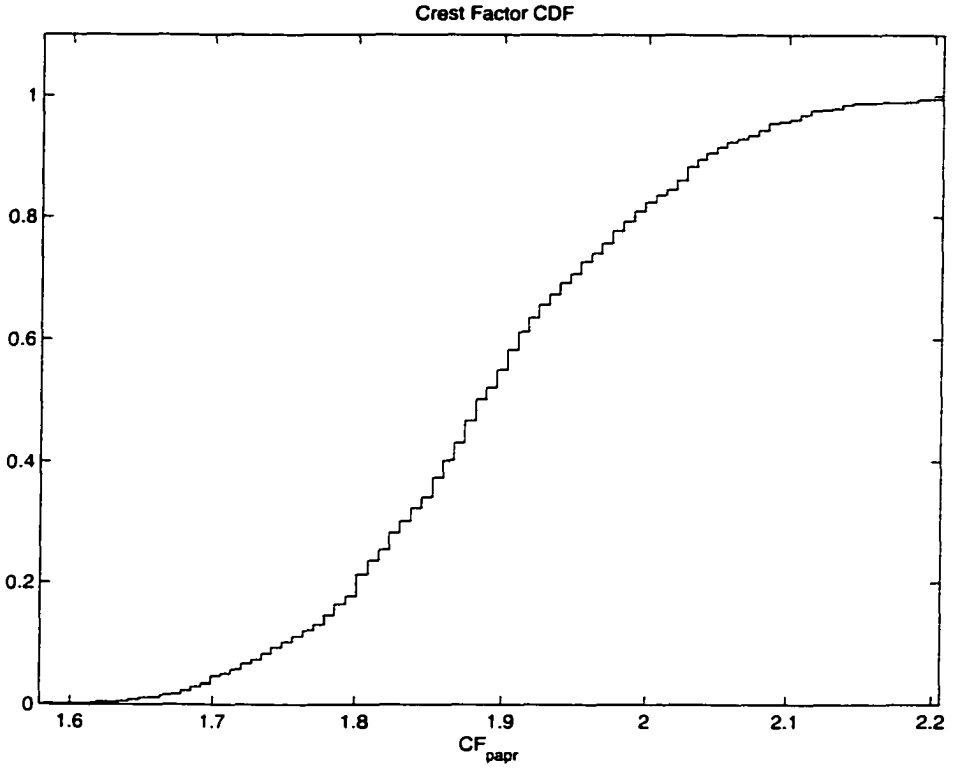

Figure 5.11: Cumulative distribution function of $\sqrt{PAPR}$ (N=32, K=32)

Referring to [97], the CF is reduced in the uplink of CI/MC-CDMA by introducing a phase offset into each carrier at the transmitter side, i.e., the code for the uplink of CI/MC-CDMA is updated from equation (4.5) to

$$c_k(t) = \sum_{i=0}^{N-1} e^{j(2\pi i \Delta f t + i\Delta\theta_k + \psi_i)} \tag{5.12}$$

where $\{\psi_0, \psi_1, ..., \psi_{N-1}\}$ are determined as follows. We start with a random phase for the first carrier, ψ_0, and calculate the phases for the $N-1$ remaining carriers $\{\psi_1, \cdots, \psi_{N-1}\}$ using [97]

$$\psi_n = \psi_0 - \frac{\pi n^2}{N}, n = 1, 2, ..., (N-1). \tag{5.13}$$

The CF for the signal in (5.12) (with the phase offsets from (5.13)) is computed and stored. Starting with a new random value for ψ_0, we repeat equation (5.13) to

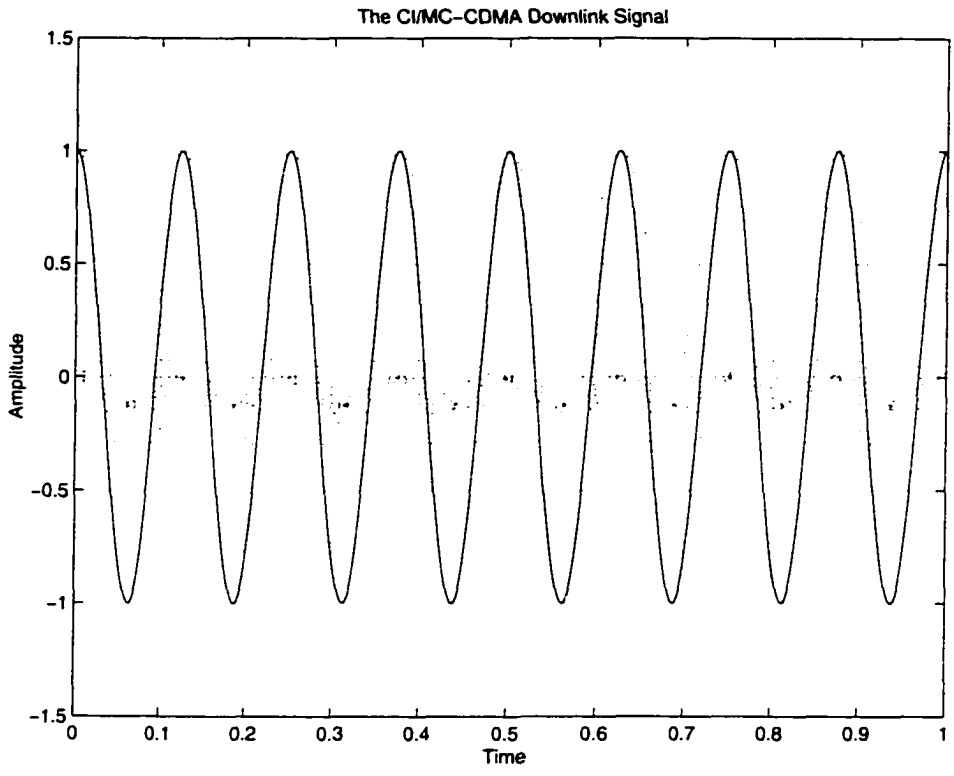

Figure 5.12: Signal Envelope of CI/MC-CDMA downlink ($a_k[n] = 1$ for all users)

determine a new $\{\psi_0, \psi_1, ..., \psi_{N-1}\}$. The CF for the signal in (5.12) with the new phase offsets are again computed. This procedure is repeated approximately 1000 times and the CF values computed are inspected to determine the $\{\psi_0, \psi_1, \cdots, \psi_{N-1}\}$ that minimized CF.

Alternately, in [97], a second method is provided where we restrict ψ_i such that $\psi_i \in \{0, \pi\}$. Here, the phase offsets are computed using

$$\psi_n = \pi \lfloor \frac{n^2}{2N} \rfloor, n = 0, 1, ..., (N-1) \tag{5.14}$$

where $\lfloor x \rfloor$ indicates the largest integer not larger than x.

The CF and $\sqrt{PAPR}$ of CI codes in (5.12) with ψ_i's generated using the Schroeder methods are presented in Table 5.2 and Table 5.3. These results were obtained for a CI/MC-CDMA system uplink employing N=8,16 and 32 carriers.

N	Method I CF	Method I $\sqrt{PAPR}$	Method II CF	Method II $\sqrt{PAPR}$
8	1.66	1.69	1.67	1.86
16	1.71	1.73	1.88	1.97
32	1.66	1.67	1.85	1.85

Table 5.2: Schroeder's methods to reduce uplink CF (Method I (any phase); Method II (0 or π))

From Table 5.2, we observe (using Shroeder's method to determine $\{\psi_0, \psi_1, \cdots, \psi_{N-1}\}$) CF values of CI codes are reduced from 4.9 to 1.6 when N=32. Even after limiting the phase offsets ψ_i such that $\psi_i \in \{0, \pi\}$, we observe an improvement from 4.9 to 1.8. Similar improvements are also seen in $\sqrt{PAPR}$ values. Specifically, the CF of the uplink is now reduced to values close to that of a single sine wave (CF of sine wave = 1.414). Hence, the CF problem of uplink CI/MC-CDMA is efficiently solved.

Finally, it is also important to note that the signature waveforms $c_k(t)$ and $c_j(t)$ in a CI/MC-CDMA system are simply time shifted versions of one other. Hence, it suffices to calculate one set of phase offsets $\{\psi_0, \psi_1, \cdots, \psi_{N-1}\}$ to reduce the CF and this set can be applied to all the users' spreading codes (as in (5.12)). (In MC-CDMA systems applying, e.g., Gold codes or Hadamard Walsh codes, the same phase offsets cannot be used for all users' spreading codes).

One attractive feature of these CI codes results by extending the use of ψ_i's (from Schroeder's method) to enhance security. Specifically, one can envision a CI system where the transmitter updates the set of phases $(\psi_0, \psi_1, \cdots, \psi_{N-1})$ it applies to the CI code (equation (5.12)). Here, the CI signal is constantly changing shape (from one low PAPR shape to another), making unwanted detection and decryption near to impossible.

i	ψ_i using Method I (in rad.)	ψ_i using Method II (in rad.)
0	0.2899	0
1	-1.2809	0
2	-3.2444	0
3	-5.9933	π
4	-3.2444	π
5	-1.2809	0
6	-0.1028	π
7	-5.9933	0

Table 5.3: ψ_n values minimizing CF in CI/MC-CDMA uplink (determined from Schroeder's method) for $N = 8$ carriers.

5.4 Summary

In this chapter, the CI/MC-CDMA system was tested in the presence of phase jitters and frequency offsets and was found to demonstrate very graceful degradations in performance at high levels of synchronization errors.

This chapter also addressed PAPR concerns in CI/MC-CDMA. An analysis of the CI/MC-CDMA downlink shows that PAPR is well within tolerable levels for today's power amplifiers. On the other hand, the CI/MC-CDMA uplink suffers from high (poor) PAPR values. However, applying Schroeder's CF reduction technique, we demonstrate that the uplink CF is easily brought to very low values (close to that of a pure sine wave).

Chapter 6

CI/TDMA

In the last two chapters, we demonstrated how Carrier Interferometry codes enhance the performance of MC-CDMA systems. In this chapter, we incorporate the Carrier Interferometry approach into TDMA systems. Specifically, we use the idea of Carrier Interferometry pulse shaping (introduced in Section 3.2) in a TDMA system.

We show that a multi-carrier implementation of TDMA via CI pulse shapes can lead to dramatic benefits in terms of probability-of-error performance and throughput. Furthermore, this approach provides a multi-carrier framework for TDMA systems that takes us one step closer to a uniform hardware platform for different multiple access techniques - a key to concepts such as software radio, global roaming, etc..

This chapter proceeds in the following manner. We first give a brief overview of the GSM system, the most commonly used TDMA architecture. We then discuss the CI/TDMA transmitter and discuss the idea of pseudo-orthogonality in TDMA systems (to enable doubling of throughput). We also analyze the bandwidth occupancy of the CI/TDMA system. We then present the novel CI/TDMA receiver. Finally, we present performance curves to demonstrate both performance and throughput gains of CI/TDMA relative to a traditional TDMA system.

6.1 Overview of GSM

Time division multiple access (TDMA) is a transmission protocol that allows users to share a communication link by assigning unique time slots to each user. Specifically, in TDMA, time is segmented into time slots that are assigned to individual users. In fixed assignment TDMA, each user transmits in one or more predetermined time slots that occur periodically. Dynamic assignment, or packet switching, assigns time slots at the time of transmission.

The Global System for Mobile Communications (GSM)[13], which is the most widespread digital cellular architecture in the world in these days of 2G and 2.5G, is based on TDMA. In typical GSM systems, each user's time slot holds 148 bits. The transmission bit rate is 270.8 kbps. Thus the bit duration $T_b = 3.69\mu s$ and the time slot duration $T_{sl} = 576.6\mu s$. A guard interval of $30.44\mu s$ is used between slots.

GSM systems use binary Gaussian minimum shift keying (GMSK) modulation. Here, information is conveyed by the phase of the transmitted signal (characterized by a constant envelope and efficient bandwidth usage). Specifically, the information bits of user p are first differentially encoded, producing an NRZ (nonreturn-to-zero) symbol stream $\underline{d}_p = d_p(i)(i = 1, 2, ..., N)$; next this symbol stream excites a transmit filter $p(t)$ with a Gaussian impulse response. The waveform at the output of the Gaussian filter may be expressed as

$$\psi_p(t) = \sum_{i=1}^{N} d_p(i) q(t - iT_b) \tag{6.1}$$

where

$$q(t) = \int_0^{T_b} p(t - \tau) m(\tau) d\tau. \tag{6.2}$$

Here, $m(\tau)$ is the rectangular waveform of the NRZ pulse and $p(t)$ is the Gaussian

pulse defined by

$$p(t) = \frac{\eta B}{\sqrt{\pi}} e^{-(\eta B t)^2}. \tag{6.3}$$

where B is the 3dB bandwidth ($BT_b = 0.3$ for GSM), and $\eta = \pi/\sqrt{2ln2} \approx 2.668$. Finally, the Gaussian filter output $\psi_p(t)$ is integrated, resulting in $\chi_p(t)$, and this serves as the phase of the transmitted waveform. The complex baseband representation of the output signal corresponds to

$$s_p(t) = e^{j\chi_p(t)}. \tag{6.4}$$

Typically, the non-linear baseband GMSK signal is approximated by a linear modulation [100] to aid in system analysis, receiver design and simulation.

GSM, like most TDMA systems, suffers from intersymbol interference (ISI) resulting from multipath. Thus, GSM receivers commonly employ a decision feedback equalizer (DFE). DFE's significantly reduce receiver complexity while only slightly compromising performance compared to maximum likelihood sequence estimators [13].

6.2 CI/TDMA Transmit Model

Figure 6.1 (a) is the conceptual representation of a traditional TDMA transmitter. Here, incoming bits are mapped to complex symbols (e.g., PSK or QAM constellation points) denoted a_k in the figure; these are then mapped to a continuous-time waveform by the pulse generator and modulated to the bandpass frequency by a mixer. In TDMA systems with CI architectures, only one change is evident at the transmitter side. CI pulse shapes replace traditional pulse shaping strategies (with N pulses per TDMA burst/slot). This leads to the N-symbol per burst transmission

$$s(t) = \sum_{k=1}^{N} \Re e[a_k g(t - (k-1)T_b) \cdot m(t) \cdot e^{j2\pi f_c t}] \tag{6.5}$$

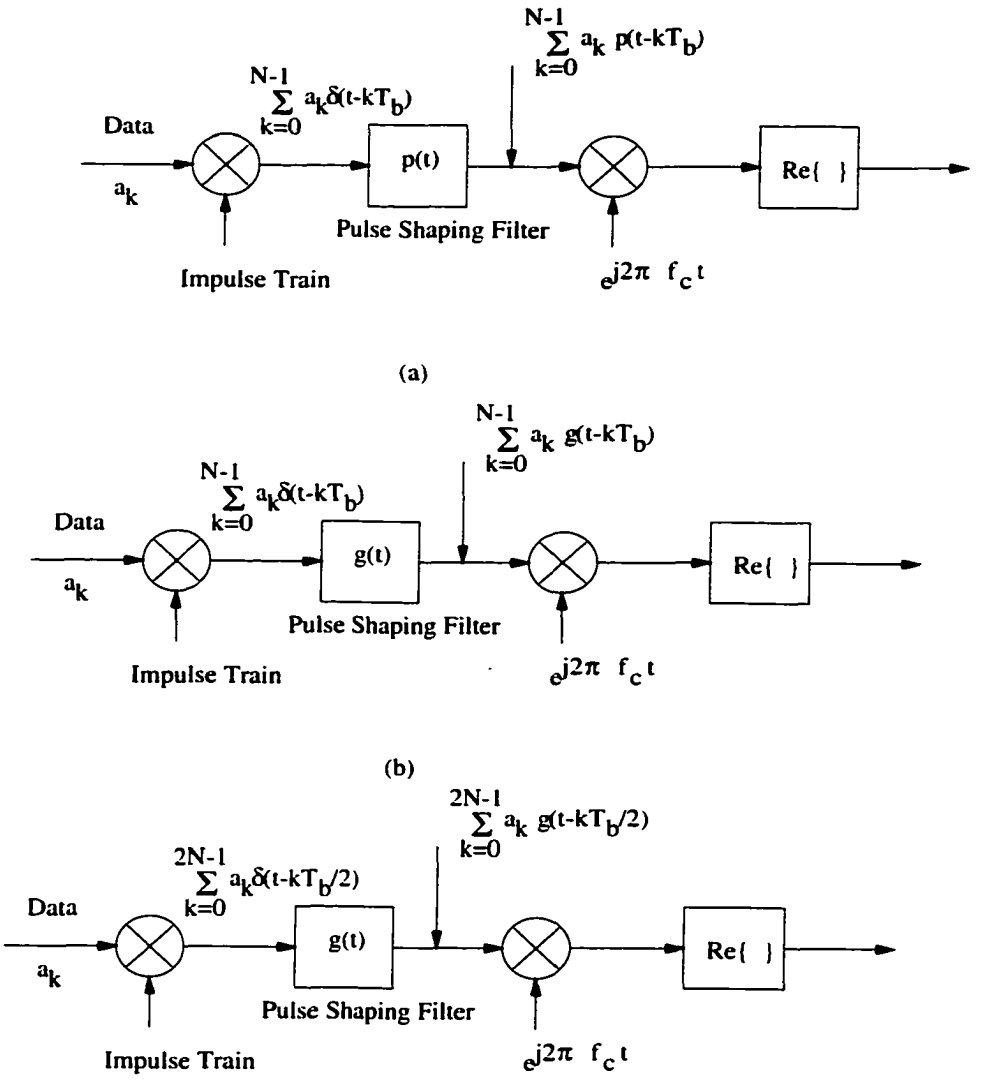

Figure 6.1: (a). Traditional TDMA transmitter (b). CI/TDMA transmitter

where a_k is the k^{th} symbol transmitted in the N symbol TDMA burst/slot; and $g(t-(k-1)T_b)\cdot m(t)$ is the k^{th} pulse shape (the CI signal $g(t-(k-1)T_b)$ time-limited to a slot duration T_{sl} by $m(t)$). From Section 3.2, $g(t)$ corresponds to

$$g(t)=\sum_{i=0}^{N-1} Ae^{j(i2\pi\Delta ft)}, \tag{6.6}$$

where $A=\sqrt{\frac{1}{N}}\sqrt{\frac{1}{T_{sl}}}$ is a constant that ensures a pulse energy of unity (over T_{sl}). This CI pulse shape extends over the entire slot duration T_{sl} (576.6μs in GSM) and not bit duration T_b (3.69μs in GSM). Also, $\Delta f=1/T_{sl}$ ensures orthogonality among the subcarriers that constitute the CI pulse shape; and N corresponds to the number of symbols per slot, e.g., 148 in GSM. It is important to note that this CI pulse shape can be implemented with ease using IFFTs.

Following the discussion in Section 3.2, the set of CI pulse shapes $\{g(t), g(t-\frac{1}{N\Delta f}),\cdots,g(t-\frac{N-1}{N\Delta f})\}$, are orthogonal to each other. Substituting $\frac{1}{N\Delta f}=T_b$ in the case of CI/TDMA, we have an orthogonal set of pulse shapes corresponding to $\{g(t), g(t-T_b),\cdots,g(t-(N-1)T_b)\}$ in one burst period NT_b. Therefore, CI pulse shapes, like sinc() pulse shapes, satisfy the generalized Nyquist criterion (GNC) for zero ISI at the transmitter side.

In CI systems, an additional change may be implemented at the transmitter side to enable throughput gains. Specifically, we can employ a second set of pseudo-orthogonal CI pulse shapes, $\{g(t-\frac{1}{2N\Delta f}), g(t-\frac{1}{N\Delta f}-\frac{1}{2N\Delta f}),\cdots,g(t-\frac{N-1}{N\Delta f}-\frac{1}{2N\Delta f})\}$, to double the number of information symbols in a burst (see Section 3.2, equation (3.22)). Substituting $\frac{1}{N\Delta f}$ by T_b, we have a second set of CI pulse shapes that correspond to $\{g(t-T_b/2), g(t-3T_b/2),\cdots,g(t-(2N-1)T_b/2)\}$. These pulse shapes are in-between the orthogonal pulse shapes in time as shown in Figure 3.4. Therefore, by positioning CI pulse shapes with time separation $T_b/2$, we support $2N$ pulse shapes per TDMA slot, and hence $2N$ symbols per slot, doubling throughput. This is anal-

ogous to the doubling of capacity in CI/MC-CDMA systems and has been discussed in detail in Section 3.2. The price, is of course, is one of reduced performance due to introduction of a controlled inter-symbol-interference at the transmitter side. With this transmission strategy, the TDMA transmitter of Figure 6.1(a) is replaced by that of Figure 6.1(c), leading to the $2N$ symbol output

$$s(t) = \sum_{k=1}^{2N} \Re e[a_k g(t - (k-1)T_b/2) \cdot m(t) \cdot e^{j2\pi f_c t}] \tag{6.7}$$

6.2.1 Bandwidth Efficiency

Next, let us compare the bandwidths of CI/TDMA systems and TDMA systems employing traditional pulse shapes. A TDMA system using Nyquist root raised cosine pulse shaping with a roll-off factor α has a total RF bandwidth $BW_{rc} = \frac{1+\alpha}{T_b} = (1+\alpha)R_b$ (where R_b is the data rate, i.e., $R_b = \frac{1}{T_b}$). If a Gaussian pulse shape is employed with BT = 0.3 (typical of GSM systems), 99% of the power is contained in bandwidth $BW_g = 1.8R_b$ [72]. To support data rate R_b, a CI/TDMA system has a bandwidth occupancy

$$BW_{CI} = N\Delta f = N \cdot \frac{1}{NT_b} = \frac{1}{T_b} = R_b \tag{6.8}$$

Thus, we see that CI/TDMA systems demonstrate the bandwidth efficiency of a sinc pulse shape. This is not a surprising result as the CI pulse shape can be perceived as a frequency sampled version of the standard sinc pulse.

Specifically, the CI/TDMA system has a spectral occupancy that is 80% less than that of GMSK (BT = 0.3), when both are designed to support identical data rates. When compared to systems employing raised cosine pulse shapes with $\alpha = 1$ (with the same data rate), the CI/TDMA system occupies only one half of BW_{rc}. Furthermore, when we consider the pseudo-orthogonal pulse shapes of Section II for doubling the data rate (without increasing BW_{CI}), the bandwidth efficiency gains (measured in

b/s/Hz) in CI/TDMA are in the order of 260%, 300% and 100% relative to GMSK (with BT = 0.3), a raised cosine pulse (with $\alpha = 1$) and a sinc pulse, respectively.

6.3 CI/TDMA Receiver Model

In CI implementations of TDMA, a more significant update in design takes place at the receiver side. Here, traditional time-based equalizers are replaced by frequency-based receiver structures. However, prior to introducing the new receiver design, it is important to note that CI/TDMA transmitters are backward compatible with existing equalizer receiver structures. That is, the transmission in the time domain appears unchanged when compared to a traditional TDMA transmitter with sinc pulse shapes. Hence, existing equalizer structures serve as adequate detectors for CI/TDMA.

A novel frequency-based receiver structure is also available, capable of significant performance improvements, some of which may be traded off for gains in throughput. We begin our novel receiver design with a description of the input to the CI/TDMA receiver. (In what follows, we will assume BPSK symbols for ease in presentation).

We assume the transmission of K symbols per slot (where K is N or $2N$), i.e., we assume the transmit signal of equation (6.5) or (6.7). Each symbol resides on a CI pulse shape composed of N frequency components. Upon transmission over a typical wideband wireless channel, the signal experiences a frequency selective Rayleigh fade. While frequency selectivity exists over the entire transmit band, each narrowband frequency component in the CI pulse shape experiences a flat fade. This is characteristic of all multi-carrier systems (including OFDM, MC-CDMA and CI/MC-CDMA), and is discussed in detail in Section 4.3. Hence, assuming the transmit signal of equation

(6.5) or (6.7), the received signal is characterized by

$$r(t) = \sum_{k=1}^{K} \Re e[a_k \{ \sum_{i=0}^{N-1} A\alpha_i e^{j(2\pi i \Delta f(t-(k-1)T_b/M)+\phi_i)} \cdot m(t) \} \cdot e^{j2\pi f_c t}] + n(t) \qquad (6.9)$$

where α_i is the gain and ϕ_i the phase offset in the i^{th} carrier of the CI pulse shape (due to the channel fade) and $n(t)$ is additive white Gaussian noise (AWGN). Here, $M = 1$ if $K = N$ and $M = 2$ if $K = 2N$. To simplify the analysis, exact phase synchronization is assumed.

Figure 6.3 illustrates the novel CI/TDMA receiver (conceptually, i.e., not in its low-complexity implementation), demonstrating detection of the j^{th}symbol. First the incoming burst, made up of frequency decomposable CI pulse shapes, is separated into N orthogonal carrier components (implementable at a low cost via an FFT), where each carrier displays a delay matched the j^{th} bit. The phase offset introduced by the channel is also removed at this stage. Each component consists of one of the subcarriers of the CI pulse shape. This results in N decision variables, one per CI pulse shape frequency component. Mathematically, the resulting decision vector corresponds to $\underline{r}_j = (r_{j,0}, r_{j,1}, ..., r_{j,N-1})$ where $r_{j,i}$, the i^{th} carrier component is

$$r_{j,i} = a_j \alpha_i A + \sum_{k=1, k\neq j}^{K} a_k \alpha_i A \cos(2\pi i \Delta f(jT_b/M - kT_b/M)) + \eta_i \qquad (6.10)$$

The first term represents the presence of the desired j^{th} symbol on the i^{th} carrier component of the CI pulse shape; the second term represents the presence (in the i^{th} carrier) of other $K-1$ symbols in a user's burst; and the final term is a zero mean Gaussian random variable representative of the noise.

Next, a suitable strategy is then applied to combine the $r_{j,i}$'s.

In the case of an AWGN channel ($\alpha_0 = \alpha_1 = \cdots = \alpha_{N-1} = 1$) or a flat fading channel ($\alpha_0 = \alpha_1 = \cdots = \alpha_{N-1}$), Equal Gain Combining (EGC) is the optimal choice for the combining strategy. EGC across carriers restores the orthogonality between

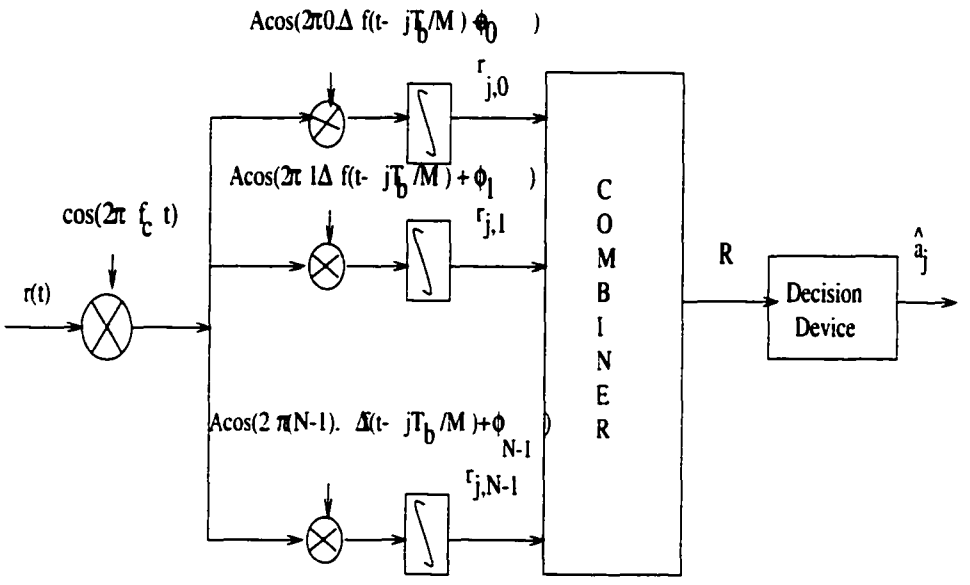

Figure 6.2: CI/TDMA Receiver structure

pulse shapes, minimizing ISI with pseudo-orthogonal pulse shapes, and minimizes noise. Here, the N carrier terms are combined as follows:

$$R_j = \sum_{i=0}^{N-1} r_{j,i} \tag{6.11}$$

However, in the presence of a frequency selective fade, orthogonality between pulse shapes can not be recreated with a simple EGC. If restoring orthogonality is a priority, the Orthogonality Restoring Combining (ORC) can be employed: this involves the scaling of $r_{j,i}$ by α_i and summing the terms, i.e.,

$$R_j = \sum_{i=0}^{N-1} r_{j,i}/\alpha_i \tag{6.12}$$

While this eliminates ISI (in the case of N CI pulse shapes per burst) or minimizes ISI (in cases of $2N$ pulse shapes per burst), it can result in substantial noise enhancement. (This is like the use of a zero forcing equalizer, which eliminates ISI at the cost of noise enhancement.)

Minimum mean square error combining (MMSEC) is a powerful alternative which

attempts to jointly minimize the second term and the noise term. In our case, employing MMSEC results in the decision variable R_j given by the linear sum (derivation is similar to that presented in Section 4.4.2)

$$R_j = \sum_{i=1}^{N} r_{j,i} \cdot [\frac{\alpha_i}{(\alpha_i^2 \sum_{p=1}^{K-1} \cos(2\pi i \Delta f(pT_b/M - jT_b/M))^2 + N_o/2)}]. \quad (6.13)$$

Note that for small α_i, the gain becomes small to avoid the excessive noise amplification, while for large α_i, it becomes proportional to the inverse of the subcarrier envelope, in order to recover the orthogonality among pulse shapes. A hard decision device provides the final output $\hat{a}_j$.

6.4 Performance Results

Figures 6.3,6.4 and 6.5 present bit error probability (BER) versus SNR performance curves for the hilly terrain (HT),rural area (RA) and typical urban (TU) channels respectively (see Section 4.3 for a detailed description of these channels). The dotted line (marked with circles) represents the CI/TDMA system results (with $N = 148$ symbols per burst) and the dashed line (marked with stars) represents a GSM system employing Gaussian pulse shaping with a DFE(6,4) receiver (and $N = 148$ symbols per burst) [13]. Both systems have identical slot duration and throughput rates.

The performance benefits of the proposed CI/TDMA system are evident from these curves. The new CI/TDMA scheme achieves more than 8dB gain in the HT channel at probability of errors in the order of 10^{-2}. Performance gains increase dramatically at lower probability of error points. In the TU channel, gains in the order of 5dB are achieved at probability of errors of 10^{-2}. Again, gains increase significantly at lower probability of errors. The performance benefit in the RA case is not as noticeable as in the HT and TU environments. This is because in RA channels, coherence bandwidth is large (delay spread is small), meaning the channel models are

closely approximated by a flat fading channel. In this case, there is little frequency diversity benefit for CI/TDMA to exploit.

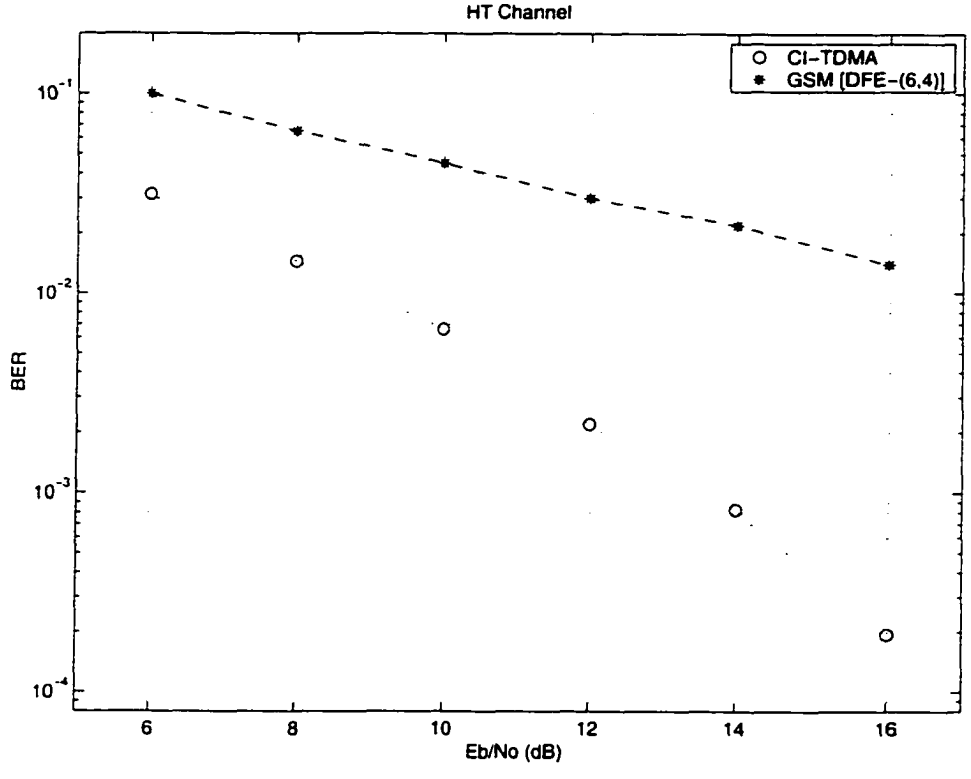

Figure 6.3: BER comparison in HT channel

These results show the dramatic performance benefits achievable in frequency selective fading channels, when replacing traditional pulse shape by a multi-carrier CI pulse and, correspondingly, changing the time-based equalizer with a frequency-based receiver. Specifically, performance degradations resulting from a limited number of taps in a digital matched filter and DFE (6,4) equalizer are overcome by a receiver employing a frequency based processing. As the number of taps in the equalizer is increased, the time based equalizer performance can be significantly improved. However, this comes at a significant cost in complexity. Here, without cost in transmit bandwidth, throughput rate or slot duration, CI/TDMA provides an efficient low cost implementation for TDMA achieving high performance by exploiting the frequency

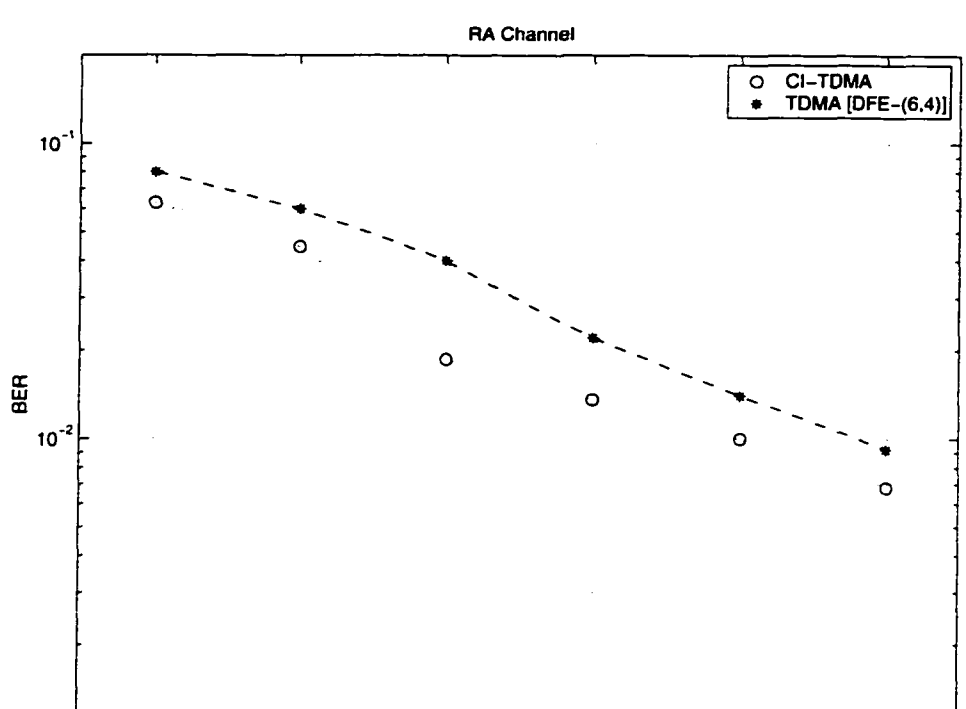

Figure 6.4: BER comparison in RA channel

domain processing. Because CI/TDMA retains all the features of a TDMA system, all higher protocol levels currently in use for TDMA are applicable to CI/TDMA as well.

Some of the performance benefits of CI/TDMA can be traded off for a doubling in throughput. This is illustrated in Figures 6.6 and 6.7, which present bit error rate (BER) versus SNR performance curves for a CI/TDMA system operating with pseudo-orthogonal bits in a burst. The dotted line marked with circles represents the performance of the CI/TDMA system with $N = 148$ orthogonal pulses. The dashed line marked with stars demonstrates the performance of the CI/TDMA system with double throughput (296 symbols per burst) via pseudo-orthogonal positioning. In both systems, a BPSK constellation is assumed. Relative to the CI/TDMA system with $N = 148$ symbols per slot, the novel CI/TDMA architecture demonstrates

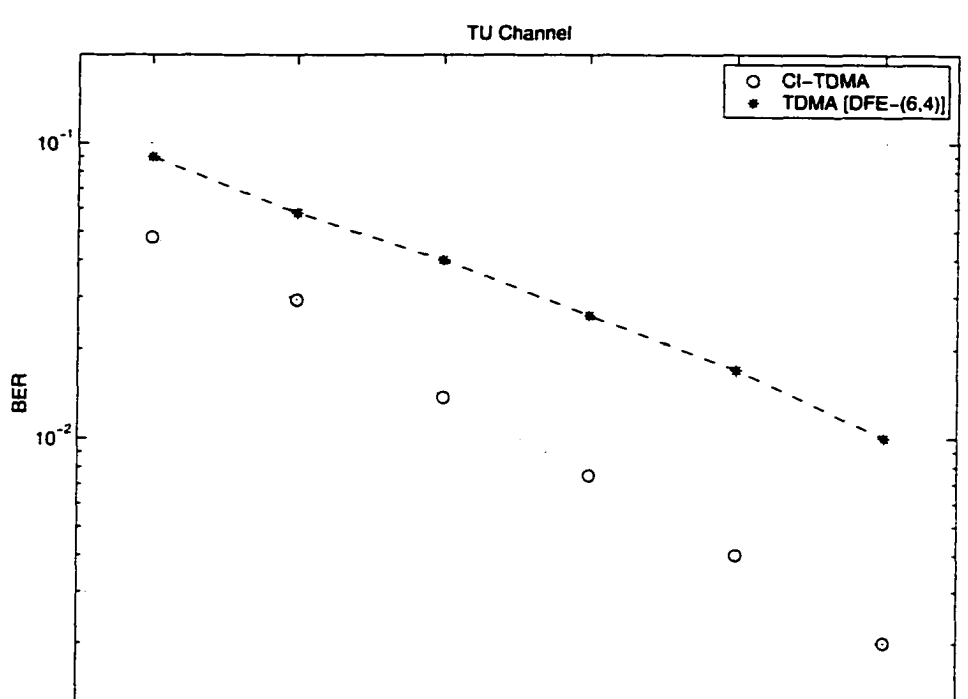

Figure 6.5: BER comparison in TU channel

degradations of 1-2 dB, a direct result from the ISI introduced at the transmitter side when employing pseudo-orthogonal pulse positioning. This performance degradation is small when compared to the benefit of doubling the throughput. Moreover, at a BER of 10^{-2} and assuming an HT channel, the CI/TDMA system with 296 CI pulses per burst achieves close to 6.5 dB gain relative to a traditional TDMA system with 148 orthogonal pulses per burst, Gaussian pulse shaping, and a DFE(6,4) equalizer at the receiver side. (In the TU channel, gains in the order of 4 dB are achieved at probability of errors in the order of 10^{-2}). These results were obtained with no increase in transmit bandwidth, or burst duration, and with no change in modulation formats. Hence, CI/TDMA provides an efficient low cost way of achieving high-throughput, while maintaining high-performance, by exploiting a frequency based signal processing.

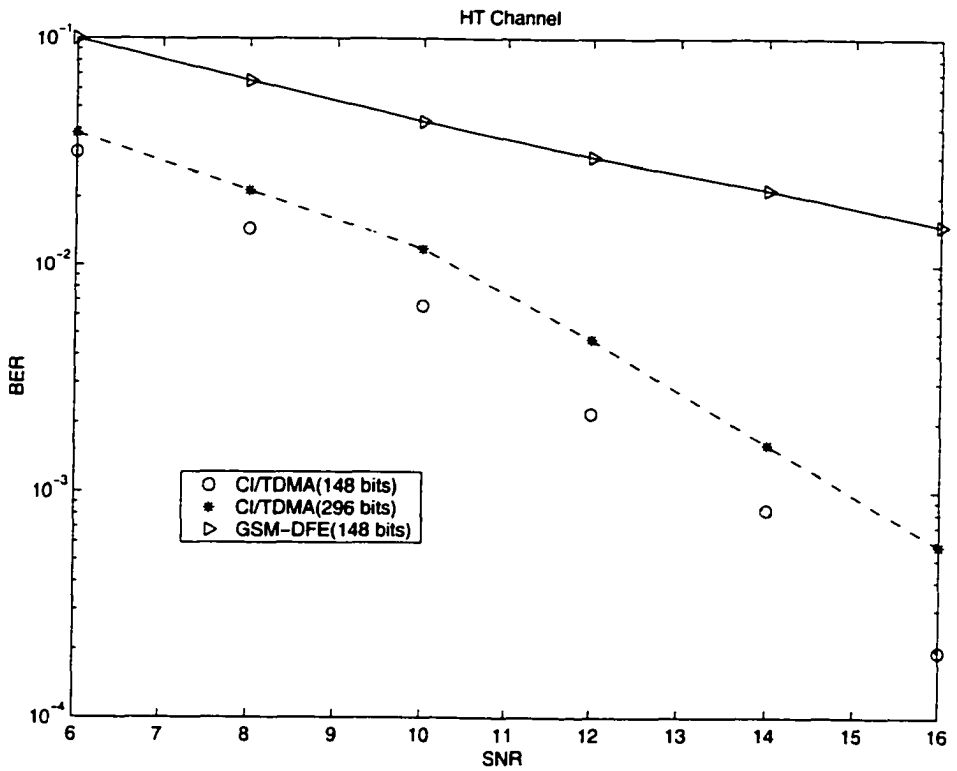

Figure 6.6: BER comparison in HT channel

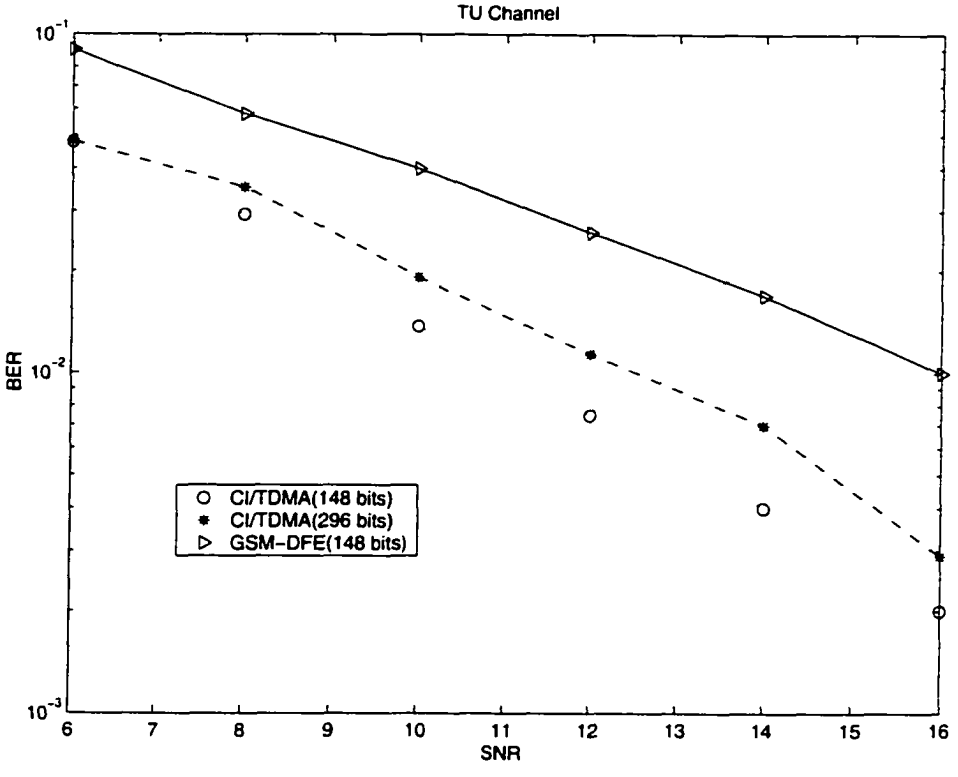

Figure 6.7: BER comparison in TU channel

6.5 Summary

In this chapter, we introduced the Carrier Interferometry Approach to TDMA systems in the form of a novel pulse shape. The resulting CI/TDMA system, with its frequency-based signal processing is bandwidth efficient, significantly enhances performance, and has the ability to double throughput by positioning CI pulse shapes pseudo-orthogonally in time. Even when the throughputs are doubled, performance still exceeds that of traditional TDMA systems. By application of the multi-carrier approach found in OFDM and MC-CDMA, and by using the pseudo-orthogonality concept that has found widespread use in DS-CDMA, TDMA systems can now benefit from significant gains in performance and throughput.

Chapter 7

CI/FSK

In Chapters 4, 5 and 6 we presented the application of Carrier Interferometry to multiple access schemes such as MC-CDMA and TDMA. The applicability of Carrier Interferometry is not limited to multiple access techniques and in this chapter we introduce this concept to modulation techniques. Specifically, we propose a novel frequency shift keying (FSK) technique that is based on a multi-carrier CI approach.

This chapter is organized as follows. We first introduce the idea and highlight the key benefits of CI/FSK. We then present the CI/FSK signal and the transmitter. This section also discusses the bandwidth occupancy of CI/FSK, provides crest factor analysis, and shows how CI/FSK can enable a doubling in throughput. Next, non-coherent and coherent detection schemes are discussed. Performance results that demonstrate the benefits of CI/FSK are presented next. Finally, we discuss the applicability of CI/FSK in Bluetooth, and we demonstrate via performance curves how CI/FSK enhances the performance and throughput in Bluetooth.

7.1 Introduction

Frequency shift keying (FSK) is a modulation technique of great practical importance. It is commonly used whenever the hardware simplicity of the receiver is of

utmost importance [101]. Recently, FSK has gained popularity with its adoption in the Bluetooth standard [12]. Bluetooth technology represents a new universal radio interface that enables electronic devices to communicate via short-range connections [102],[103].

The selection of FSK for personal area networks (such as Bluetooth) was motivated by a number of considerations. Non-coherent FSK receivers can be designed with ease and can be implemented in a cost-effective manner. Since most FSK modulation techniques result in a constant envelope, information is carried by the zero crossings of the signal alone: Hence, FSK is robust in systems that have non-linearities due to, e.g., RF amplifier effects [80].

However, FSK also has significant disadvantages. Since the BFSK (binary FSK) constellation is orthogonal rather than antipodal, it suffers from a 3 dB penalty in signal to noise ratio (SNR) for a given bit error rate (BER)(when compared to coherent BPSK). Additionally, the spectral efficiency of FSK is often lower than passband pulse amplitude modulation (PAM) and phase shift keying (PSK). Next, since the basic FSK signal is not a linear function of the data, existing linear equalization techniques cannot be used: Hence, compensation for channel distortion like selective fading is more difficult in FSK. As a result, multipath channels introduce an error floor (even in the absence of noise) [24]. These major drawbacks hinders the widespread use of FSK in wireless systems [101].

There has been considerable interest in designing FSK detectors for multipath channels (see [25]-[30]). In [25], an asymmetric raised cosine pulse shape is applied, as is a limiter discriminator receiver, improving the performance of FSK in multipath channels with small delay spreads. However, when the delay spread increases above the symbol duration, a significant error floor appears. Additionally, the system in [25] introduces a nominal degradation in spectral efficiency relative to GFSK (Gaussian

FSK). In [26], performance gains in Rayleigh fading channels with small inter-path delays are achieved via a quadratic decorrelation receiver. In [27], a generalization of FM noise-click theory is used to design an FSK receiver for detection after multipath spreading. In both [26] and [27], there is significant degradation in performance when the delay spread approaches symbol duration. A novel non-coherent equalizer for FSK is introduced in [28]. Here, ISI is combated using an approach similar to the phase-independent decorrelator multi-user detection employed in multiple access systems (where interference from other users are *tuned-out*). However, just as in multi-user detection, complexity is a limiting factor in this approach. Recently, in [29] and [30], the idea of exploiting path diversity in FSK systems is explored and it is shown to yield nominal performance gains: The impact of inter-path interference along with hardware limitations (restricting the number of RAKE fingers that can be implemented) reduces this system's ability to benefit from the available diversity.

In this chapter, we propose an enhancement to binary FSK (BFSK) that (1) provides improved spectral efficiency; *and* (2) supports enhanced BER performance; *and* (3) ensures the successful transmission of FSK over frequency selective channels, by supporting frequency diversity benefits.

Specifically, in traditional BFSK, carrier frequency $f_c + f_d$ represents binary '1' and carrier frequency $f_c - f_d$ indicates binary '0'. In the new system, we use N orthogonal in-phase subcarriers (a CI signal) around $f_c + f_d$ to represent '1' and a second set of N subcarriers (a CI signal) centered about $f_c - f_d$ to represent '0'. The total transmitted signal has an average frequency equal to either $f_c + f_d$ or $f_c - f_d$, while the envelope takes on a carrier interferometry pattern. Hence, this novel FSK system is referred to as Carrier Interferometry/FSK (CI/FSK).

We first demonstrate that CI/FSK has a spectral efficiency comparable to that of FM (frequency modulation) with a sinc(·) modulating waveform, and hence can

support higher data rates in a given bandwidth relative to BFSK. Specifically, given a total system bandwidth, BW_{total}, a CI/FSK can support data rates that are 100% and 35% higher than a traditional BFSK and GFSK (BT=0.3) system, respectively. We then analyze the crest factor [90] of the transmitted signal and show how the non-constant envelope is eliminated when a bit stream is transmitted using CI/FSK modulation: The crest factor of the CI/FSK signal, when considering transmission of a bit stream, is shown to be equal to that of a single sine wave.

Next, we demonstrate how the throughput of CI/FSK can be doubled, without bandwidth expansion and with small performance degradation, by extending the concept of pseudo-orthogonality (used with success in CDMA systems). Specifically, by positioning the CI/FSK modulated symbols pseudo-orthogonally at the transmitter, the number of transmitted symbols is doubled. This intentional introduction of inter-symbol interference (ISI) at the transmitter is effectively countered by employing the novel coherent CI/FSK receiver introduced in this work.

Finally, we demonstrate the applicability of CI/FSK in a Bluetooth system. We show significant performance improvements *and* significant data rate gains in indoor channels with both coherent and non-coherent detection. For example, we demonstrate CI/FSK's 100% gains in throughput relative to BFSK and its 35% gains relative to GFSK, without performance degradation and maintaining a low complexity non-coherent receiver structure.

7.2 CI/FSK Signaling

The main difference between traditional BFSK and CI/FSK is that CI/FSK involves a multi-carrier signal transmission. This novel FSK signaling scheme and its properties are detailed next:

7.2.1 Frequency and Time Representation

In CI/FSK, two non-overlapping frequency bands with center frequencies $f_c + f_d$ and $f_c - f_d$ convey binary information, similar to BFSK. However, unlike BFSK, the CI/FSK transmitter sends N orthogonal in-phase subcarriers centered around $f_c + f_d$ (for bit '1') or $f_c - f_d$ (for bit '0'). This is shown conceptually in Figure 1. To maintain orthogonality between subcarriers, we select $\Delta f = \frac{1}{NT_b}$, where T_b is the bit duration. This frequency spacing will create overlap between subcarriers (much like OFDM [31]; but not shown in Figure 7.1), which in turn enhances bandwidth efficiency (as discussed in subsection 7.2.4).

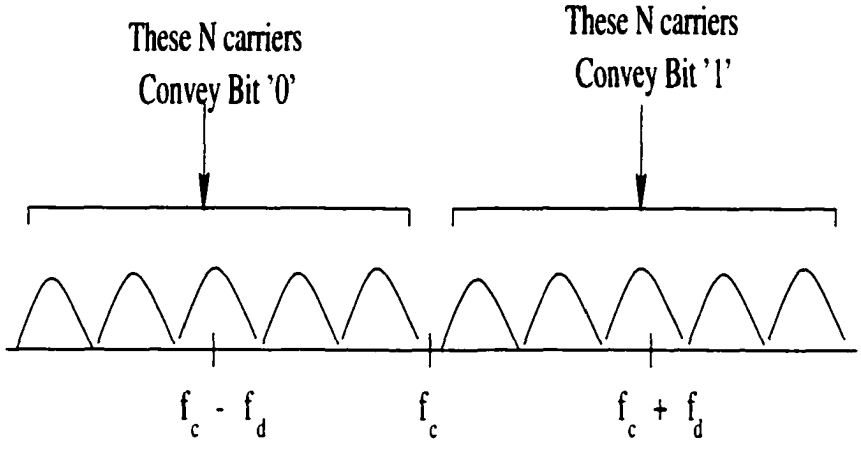

Figure 7.1: The CI/FSK signal sent for bit '0' (on the left) and bit'1' (on the right). Each signal is the linear combination of N carriers.

With N subcarriers used to represent bit '0' and bit '1', and subcarrier spacing set to $\Delta f = \frac{1}{NT_b}$, an important design parameter is the selection of N. The value of N is chosen to (1) ensure a flat fade over each subcarrier (as in OFDM systems [76]) and (2) maintain a reasonable time duration over which bit energy is spread. Referring to criteria (1), in which we require a flat fade over each subcarrier, we note that the frequency width of each subcarrier is $\Delta f = \frac{BW_{total}}{2N}$, e.g., $\Delta f = \frac{1.4}{2N}$ Mhz $= \frac{700}{N}$ kHz. Additionally, considering a typical urban wireless fading channel, channel delay

spread (T_m) may be, e.g., 2 μs, i.e., coherence bandwidth ($(\Delta f)_c$) may be on the order of 100 kHz. In this example, with subcarrier width $\Delta f = \frac{700}{N}$ kHz and $(\Delta f)_c = 100$ kHz, flat fades over each subcarrier are achieved with, e.g., $N \geq 15 (\Delta f < 2(\Delta f)_c)$. Next, referring to criteria (2), we minimize the time duration over which the bit energy is spread. As shown in the next paragraphs, bit energy is spread over duration NT_b: hence, with, e.g., $N \geq 15$ to ensure a flat fade, we select $N = 15$ to minimize the energy spread (in time) of each bit.

The CI/FSK signal for the 0^{th} bit, $a_0 \in \{-1, +1\}$, corresponds to (in the time domain)

$$s_0(t) = A \sum_{i=1}^{N} \cos\left(2\pi f_c t + a_0 (2\pi (i - \frac{1}{2})\Delta f)t\right), \quad 0 \leq t < NT_b \tag{7.1}$$

where A is a constant that determines the symbol energy. Note that the signal energy is spread over the time duration NT_b, instead of the usual T_b. Here, $s_0(t)$, the sum of a finite number of sinusoids with spacing Δf, is a periodic signal with period $1/\Delta f (1/\Delta f = NT_b)$: the limitation $0 \leq t < NT_b$ holds $s_0(t)$ to a single period.

Using simple summation rules, the CI/FSK signal in (7.1) can be expressed in time according to

$$s_0(t) = A \frac{\sin(\frac{N}{2}\Delta f t)}{\sin(\frac{1}{2}\Delta f t)} \cos\left(2\pi (f_c + a_0 \frac{N}{2}\Delta f)t\right), \quad 0 \leq t < NT_b \tag{7.2}$$

As is evident from (7.2), a single CI/FSK modulated signal does not have a constant envelope. This signal $s_0(t)$ is shown (over time duration NT_b) in the solid line of Figure 7.2. The CI/FSK signal can be rewritten in a more conventional manner via

$$s_0(t) = A \cdot E(t) \cos\left(2\pi (f_c + a_0 f_d)t\right), \quad 0 \leq t < NT_b \tag{7.3}$$

where $E(t) = \frac{\sin(\frac{N}{2}\Delta f t)}{\sin(\frac{1}{2}\Delta f t)}$ represents the carrier interferometry envelope pattern and $f_d = \frac{N}{2}\Delta f = \frac{N}{2} \cdot \frac{1}{NT_b} = \frac{1}{2T_b}$.

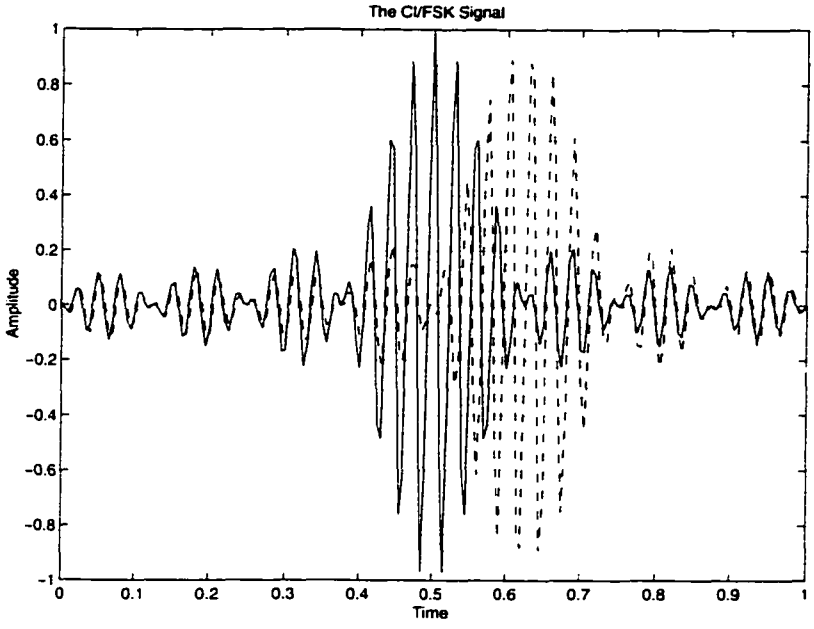

Figure 7.2: Solid line is one CI/FSK signal. Dashed line is a time shifted CI/FSK signal (shifted by a bit duration T_b)

7.2.2 Bit Stream Transmission

Next, we consider the transmission of a bit stream. Following transmission of the 0^{th} bit, the 1^{st} bit is sent as (referring to equation (7.3))

$$s_1(t) = A \cdot E(t - T_b)\cos(2\pi(f_c + a_1 f_d)t), \quad 0 \leq t < NT_b \tag{7.4}$$

This is illustrated in Figure 7.2 over duration 0 to NT_b via the dotted line. It is easily shown that

$$\int_0^{NT_b} E(t - kT_b)E(t - nT_b)dt = 0 \qquad (n \neq k). \tag{7.5}$$

Hence, a bit stream modulated using CI/FSK maintains the required condition of zero ISI (by satisfying the generalized Nyquist criterion (GNC)) at the transmitter side, i.e., $s_0(t)$ and $s_1(t)$ are orthogonal at the transmitter side. It is important to note that phase continuity is not guaranteed in CI/FSK. However, the spectral leakage

is minimal and is not viewed as a problem in CI/FSK system design. The total transmitted signal for a block of N bits then corresponds to

$$\begin{aligned} s(t) &= \sum_{k=0}^{N-1} s_k(t) \\ s(t) &= \sum_{k=0}^{N-1} A \cdot E(t - kT_b) \cos\left(2\pi(f_c + a_k f_d)t\right), \\ & \quad 0 \leq t < NT_b. \end{aligned} \tag{7.6}$$

Expressing this in terms of the multi-carrier signal of equation (7.1), $s(t)$ can alternatively be expressed via

$$\begin{aligned} s(t) &= \sum_{k=0}^{N-1} A \sum_{i=1}^{N} \cos\left(2\pi f_c t + a_k(2\pi(i - \frac{1}{2})\Delta f)(t - kT_b)\right)), \\ & \quad 0 \leq t < NT_b \end{aligned} \tag{7.7}$$

Hence, while bit energy is spread over duration NT_b via modulation to CI/FSK, N orthogonal CI/FSK symbols are located in NT_b leading to a throughput consistent with traditional FSK systems.

7.2.3 Pseudo-orthogonality in CI/FSK

Similar to the applications in CI/MC-CDMA (Section 4.2) and CI/TDMA (Section 5.2), the idea of pseudo-orthogonality can be applied to the CI/FSK system leading to doubling in system throughput. This is explained in detail below.

From equation (7.5), it is evident that the CI/FSK system supports N orthogonal modulated symbols positioned at $\{kT_b, k = 0, 1, ..., N-1\}$ in duration $t \in [0, NT_b]$. It is possible to support additional CI/FSK symbols in $t \in [0, NT_b]$ by positioning the modulated CI/FSK symbols pseudo-orthogonally, i.e., positioning CI/FSK symbols at times τ_k and τ_j such that: (1) we select $\tau_k - \tau_j < T_b$, and (2) we ensure $\int_0^{NT_b} E(t - \tau_k)E(t - \tau_j)dt \leq \epsilon$, where ϵ is some small predetermined value.

We allow the first N CI/FSK symbols to be placed orthogonally, i.e., their envelopes $E(\cdot)$ are transmitted with delays $\{\tau_k = kT_b, k = 0, 1, ..., N-1\}$. Now, if we introduce an additional delay ζ to all envelopes, i.e., replace *each* $\tau_k = kT_b$ by $\tau_k = kT_b - \zeta$ in $E(t - \tau_k)$, the set of N CI/FSK symbols remain orthogonal to one another. That is, the cross correlation between the signal envelopes remains zero as long as the difference is $\tau_m - \tau_n = (mT_b - \zeta) - (nT_b - \zeta) = (m-n)T_b$. Of course, there is correlation between an orthogonal set of N envelopes with $\zeta = 0$ and the orthogonal set of N envelopes constructed with arbitrary ζ.

We seek to support $2N$ CI/FSK symbols in duration $t \in [0, NT_b]$, by simultaneously supporting one set of N CI/FSK symbols using $E(t - kT_b - \zeta)$ with $\zeta = 0$ and another set of N CI/FSK symbols using envelopes $E(t - kT_b - \zeta)$ with $\zeta = \zeta$. That is, we intend to transmit N CI/FSK symbols in $[0, NT_b]$ using envelopes $E(t), E(t - T_b), ..., E(t - (N-1)T_b)$ and the second set of N symbols via envelopes $E(t - \zeta), E(t - T_b - \zeta), ..., E(t - (N-1)T_b - \zeta)$. To do this in an optimal fashion, we determine the value of ζ that minimizes the root mean square cross correlation between sets. Mathematical analysis (see Section 3.1.2) yields an intuitively pleasing result, namely that when positioning the $2N$ envelopes in $[0, NT_b]$, each envelope should be separated from the neighboring envelope by duration $\frac{T_b}{2}$ (i.e., $\zeta = \frac{T_b}{2}$). This is most easily understood in terms of the transmitter output :

$$s(t) = \sum_{k=0}^{2N-1} A \cdot E(t - kT_b/2) \cos(2\pi(f_c + a_k f_d)t), \quad 0 \le t < NT_b. \tag{7.8}$$

Notice that $2N$ CI/FSK symbols are positioned in the same duration $[0, NT_b]$ and the same bandwidth by separating the CI envelopes by duration $T_b/2$ rather than the usual T_b. The success of CI/FSK "channel overloading" or "oversaturation" via pseudo-orthogonal positioning of CI envelopes will depend on how well the intentional

introduction of inter-symbol-interference at the transmitter is combated by the receiver. The novel coherent receiver introduced in Section 7.3 offers a very good BER performance even after doubling throughput, as shown in Section 7.4.

7.2.4 Bandwidth Occupancy

BFSK: FSK can be understood as frequency modulation (FM) with a carefully selected modulating waveform. The bandwidth of the modulating waveform determines the total bandwidth of transmission. For traditional BFSK, the modulating waveform is a rectangular pulse. Assuming no overlap in the BFSK spectrums for binary digits 0 and 1, the bandwidth required to support data rate R_b is thus [72]

$$BW_{BFSK} = 2f_d + 2R_b = \frac{4}{T_b}. \tag{7.9}$$

CI/FSK: In CI/FSK, we space N subcarriers by $\Delta f = \frac{1}{NT_b}$ to represent each binary input, allowing an overlap among subcarriers while still maintaining subcarrier orthogonality (as in MC-CDMA). The ability to overlap subcarriers allows CI/FSK to achieve greater bandwidth efficiency. Specifically, with non-overlapping spectrum for binary digits 0 and 1, a data rate of R_b is supported with bandwidth

$$BW_{CI/FSK} = 2N\Delta f = \frac{2}{T_b}. \tag{7.10}$$

That is, CI/FSK demonstrates the spectral efficiency of FM with a sinc modulating waveform [72], and hence supports higher data rates in a given bandwidth relative to BFSK.

Specifically for a given bandwidth and considering only the spectral efficiency of CI/FSK: (1) CI/FSK supports twice the data rate of traditional BFSK; and, (2) in

addition, CI/FSK supports a 35% increase in data rate relative to GFSK as proposed in Bluetooth (since, $BW_{GFSK} = 2(\beta + 1)1.04R_b = 2.7R_b = \frac{2.7}{T_b}$ (assuming $\beta = 0.3$ as defined in the Bluetooth standard) [67]). When the doubling in throughput via pseudo-orthogonal placement of CI/FSK symbols is also taken into consideration, a bandwidth efficiency (b/s/Hz) gain of 300% and 170% is achieved relative to BFSK and Bluetooth's GFSK, respectively.

7.2.5 Crest Factor in CI/FSK

To measure the signal compactness of the CI/FSK signal, we employ the crest factor (CF): for a multi-carrier signal $u(t)$ [90]

$$CF = \frac{M^+ - M^-}{2E_{eff}} \tag{7.11}$$

where M^+ is the largest positive and M^- is the most negative value of $u(t)$. Also, $E_{eff} = \|u\|_2$ represents the energy of $u(t)$, i.e., the rms value of $u(t)$. It is clear from (7.11) that a sine wave has a crest factor of $\sqrt{2}$.

Considering a block of N CI/FSK signals over $[0, NT_b]$ with arbitrary a_k's (see equation (7.6)), the transmitted signal consists of a sum of N envelopes. It is easily shown that the sum of all N envelopes results in a single sine wave with frequency $N\Delta f$. This is illustrated in Figure 7.3. Therefore, the crest factor of the total CI/FSK transmitted signal over $[0, NT_b]$ is $\sqrt{2}$, equal to that in a traditional BFSK signal.

7.3 CI/FSK Reception

Next, we consider the reception techniques that are employed in a CI/FSK system. The non-coherent receiver for detection of CI/FSK symbols is similar to that employed in BFSK systems. The exact receiver structure is shown in Figure 7.4. It consists of two matched filters, each matched to the CI/FSK signal corresponding to a binary 1

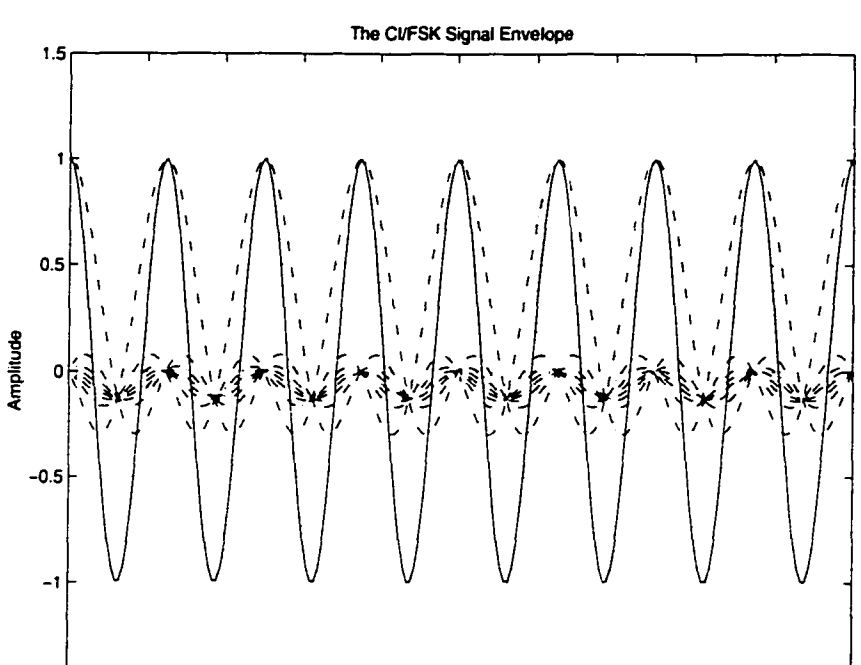

Figure 7.3: Combined CI/FSK envelope (solid line) in a transmission block

or binary 0. It is important to note that the impulse response of each matched filter extends over time duration $[0, NT_b]$ as transmitted CI/FSK symbols also extend over this time duration. A decision is made based on the relative output power of the matched filters. This receiver is both easy to implement and cost efficient.

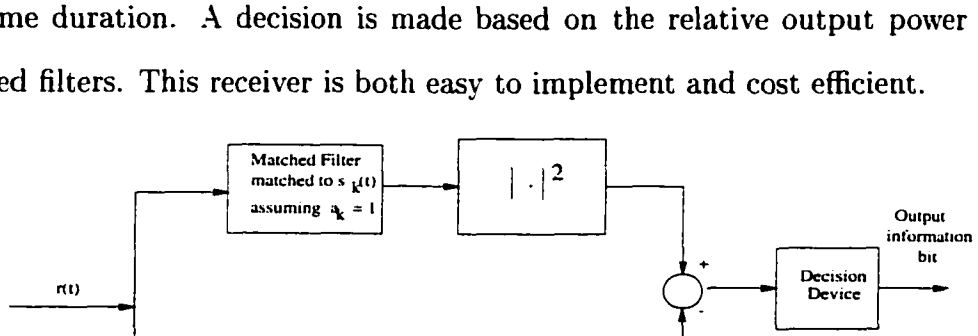

Figure 7.4: Non-coherent receiver for detection of CI/FSK symbols

Coherent reception techniques are very different in BFSK and CI/FSK systems. In

traditional BFSK, coherent reception involves the use of two matched filters, matched to the BFSK signals corresponding to a binary 1 and binary 0. Also in coherent BFSK detection, filters make use of the phase information of the received signal and the decision variable is obtained by direct comparison of the matched filter output values (instead of their respective powers).

The coherent CI/FSK receiver operates in an entirely different manner. Figure 7.5 illustrates the novel coherent receiver for CI/FSK. On the bottom branch of this receiver, the received signal is projected onto all the subcarriers constituting a binary 0. This is followed by a subcarrier combining. The combining weights are chosen to exploit frequency diversity, minimize ISI, and/or minimize noise. A similar set of operations take place on the top branch, where the subcarriers constituting a binary 1 are separated and combined. The output of the combiner from the bottom branch is then compared to the output of the combiner from the top branch, and a decision is made based on the relative size of these outputs. Details follow.

We first consider the coherent detection of the k^{th} bit in either a slow flat fading channel or an additive white Gaussian noise (AWGN) channel. We assume the transmitted signal of either equation (6) or (8). Hence, the received signal corresponds to

$$r(t) = \alpha s(t) + n(t), \qquad 0 \leq t < NT_b \tag{7.12}$$

where $s(t)$ is as represented in (7.6) or (7.8), $n(t)$ is AWGN, and α is the channel fade ($\alpha = 1$ in an AWGN channel). (Perfect phase estimation and removal has been assumed in equation (7.12)). That is,

$$r(t) = \alpha \sum_{k=0}^{K-1} AE(t - kT_b/M) \cos\left(2\pi(f_c + a_k f_d)t\right) + n(t), \qquad 0 \leq t < NT_b \tag{7.13}$$

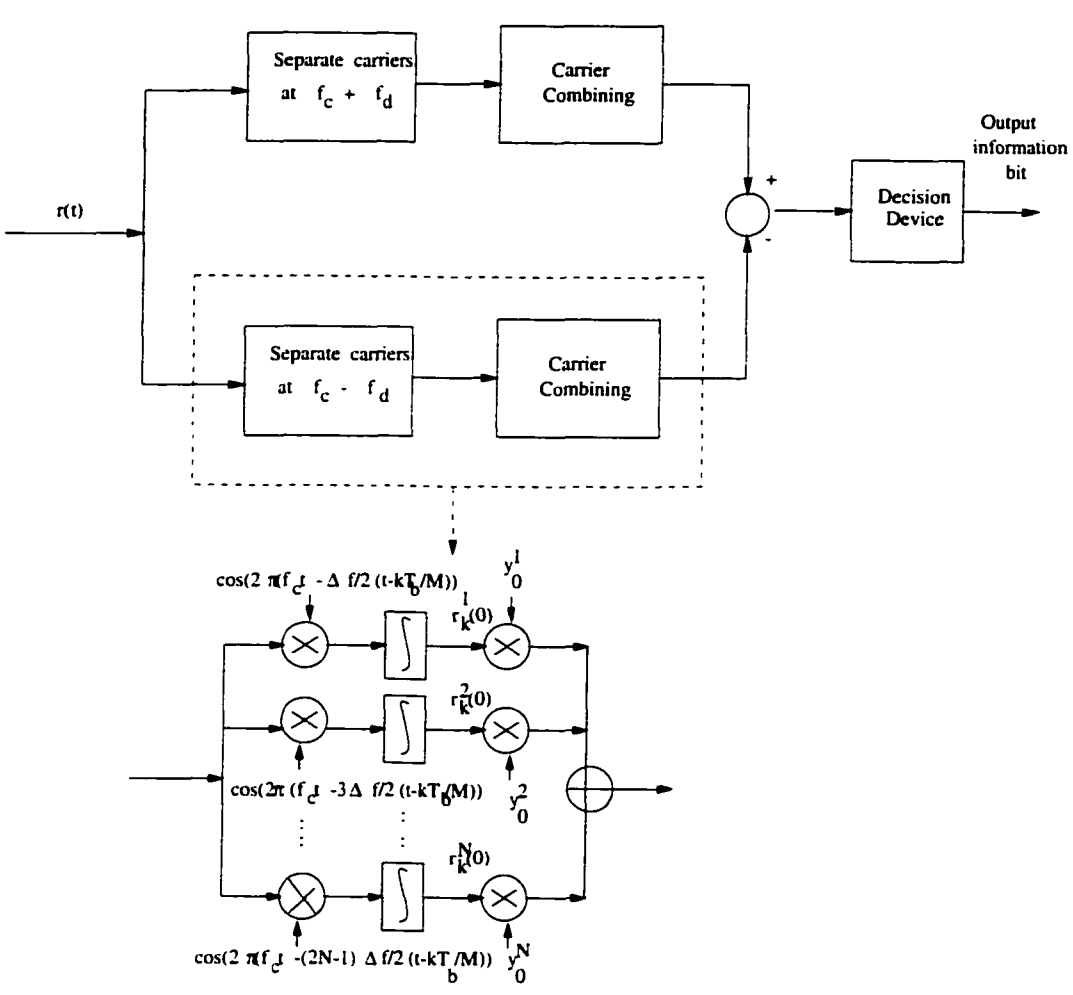

Figure 7.5: Coherent receiver for detection of CI/FSK symbols

$$r(t) = \alpha \sum_{k=0}^{K-1} A \sum_{i=1}^{N} \cos\left(2\pi f_c t + a_k(2\pi(i - \frac{1}{2})\Delta f)(t - kT_b/M))\right) + n(t), \quad 0 \leq t < NT_b \tag{7.14}$$

where $K = N$ and $M = 1$ if $s(t)$ corresponds to transmission of orthogonal CI/FSK symbols (equation (7.7)), and $K = 2N$ and $M = 2$ if $s(t)$ corresponds to pseudo-orthogonal transmission (equation(7.8)).

On the bottom branch of the receiver in Figure 7.5 (illustrated for detection of the k^{th} bit), a separation into subcarriers with delays matched to the k^{th} bit is the

first operation. This leads to the i^{th} subcarrier component

$$r_k^i(0) = \alpha A \beta_k(0) + \alpha A \sum_{j=0, j\neq k}^{K-1} \beta_j(0) \rho_{j,k}^i + \eta_i(0) \tag{7.15}$$

where $\eta_i(0)$ is a Gaussian random variable with mean 0 and variance σ_n^2. Additionally, $\beta_k(0)$ represents the presence of binary data on the bottom branch, i.e., $\beta_k(0) = 1$ if $a_k = -1$ and $\beta_k(0) = 0$ if $a_k = 1$. The second term represents the ISI due to other information bits in $[0, NT_b]$, and $\rho_{j,k}^i = \cos(2\pi i \Delta f(jT_b/M - kT_b/M))$ represents the cross correlation between the k^{th} bit and j^{th} bit in the i^{th} carrier.

The subcarrier components are combined according to (on the bottom branch)

$$D_k(0) = \sum_{i=1}^{N} r_k^i(0) \cdot y_0^i \tag{7.16}$$

In the upper branch, similar carrier decomposition and recombining is performed, leading to

$$D_k(1) = \sum_{i=1}^{N} r_k^i(1) \cdot y_1^i. \tag{7.17}$$

Here, y_0^i and y_1^i represent the combining weights in the lower branch of Figure 7.5 and the upper branch of Figure 7.5, respectively. $D_k(0)$ and $D_k(1)$ are then compared, and the final decision, $\hat{a}_k$ corresponds to $\hat{a}_k = 1$, $D_k(1) > D_k(0)$, and $\hat{a}_k = -1$ otherwise.

In the case of $K = N$ orthogonal CI/FSK symbols and an AWGN or flat fading channel, equal gain combining (EGC), i.e., $y_1^i = y_0^i = 1$, is optimal since (1) it maximizes the signal to noise ratio and (2) it eliminates the ISI entirely. In the case of $K = 2N$ pseudo-orthogonal CI/FSK symbols over AWGN or flat fading channels, a minimum mean squared error combining, which jointly minimizes the noise and ISI terms is optimal. Here,

$$\begin{aligned} y_0^i &= \frac{\alpha}{(\alpha^2 \sigma_\beta^2 \sum_{j=0}^{2N-1} (\rho_{j,k}^i)^2 + \sigma_n^2)} \\ y_1^i &= \frac{\alpha}{(\alpha^2 \sigma_\beta^2 \sum_{j=0}^{2N-1} (\rho_{j,k}^i)^2 + \sigma_n^2)} \end{aligned} \tag{7.18}$$

where $\sigma_\beta^2 = A/4$ is the variance of the Bernoulli distributed variable $\beta_n(0)$ or $\beta_n(1)$.

The novel coherent receiver can also be employed in multipath fading channels with encouraging performance results. Specifically, in CI/FSK, the frequency selectivity over the entire bandwidth is resolved by the narrowband subcarriers. This will enable the coherent CI/FSK receiver to exploit the available frequency diversity (in much the same way MC-CDMA receivers benefit from frequency diversity gains [39]-[48]). Details follow.

Assume the transmitted signal of equation (7.6) or (7.8) is sent over a frequency selective (multipath) slow fading channel. Here, frequency selectivity corresponds to selectivity over the entire transmit bandwidth, but not over each individual subcarrier making up the CI/FSK symbol. That is, the i^{th} subcarrier experiences a unique flat fade characterized by Rayleigh distributed gain α_i and phase distortion ϕ_i. (This is typical of multi-carrier signals - see, e.g., the MC-CDMA and OFDM literature [39][76]. In this case, the received signal corresponds to (assuming ideal phase tracking and removal)

$$r(t) = \sum_{k=0}^{K-1} \sum_{i=1}^{N} \alpha_i A \cos\left(2\pi f_c t + a_k (2\pi (i - \frac{1}{2})\Delta f)(t - kT_b/M)\right) + n(t) \qquad (7.19)$$

The fades on the N subcarriers corresponding to a binary '1' are correlated with one another, and also with the fades on the N subcarriers corresponding to a binary '0'. The degree of correlation is based on coherence bandwidth and is characterized as seen in [82],[81]. (Correlated fades may be generated based on the algorithm provided in [104]).

We employ the coherent receiver of Figure 7.5 to detect the k^{th} bit from the received signal of equation (7.19). Considering the bottom branch in the receiver of Figure 7.5, the received signal is first decomposed into its subcarriers, where each subcarrier displays a delay matched to the k^{th} bit. The i^{th} subcarrier component is

easily shown to correspond to

$$r_k^i(0) = \alpha_i(0)A\beta_k(0) + \alpha_i(0)A \sum_{j=0, j\neq k}^{N-1} \beta_j(0)\rho_{j,k}^i + \eta_i(0) \tag{7.20}$$

where $\alpha_i(0)$ represents the fade on the subcarrier with frequency $f_c - (i - \frac{1}{2})\Delta f$ (i.e., $\alpha_i(0)$ matches the α_i of equation (7.19) if $a_k = -1$, and $\alpha_i(0)$ represents a fade correlated with but different from the α_i of (7.19) if $a_k = +1$). All other variables in (7.20) are as defined in equation (7.15). The r_k^i terms are combined across carriers to create the decision variable $D_k(0)$ as shown in equation (7.16). A similar set of operations performed along the top branch leads to decision variable $D_k(1)$. Unlike the AWGN scenario, equal gain combining is no longer a suitable combining strategy because the introduction of carrier-dependent fades α_i destroys the orthogonality between CI/FSK symbols. Hence, we attempt to jointly exploit frequency diversity, and minimize the ISI and noise terms in equation (7.20) via a minimum mean squared error combiner. Wiener filter theory analysis yields the following weights:

$$\begin{aligned} y_0^i &= \frac{\alpha_i^0}{((\alpha_i^0)^2\sigma_\beta^2 \sum_{j=0}^{K-1}(\rho_{j,k}^i)^2 + \sigma_n^2)} \\ y_1^i &= \frac{\alpha_i^1}{((\alpha_i^1)^2\sigma_\beta^2 \sum_{j=0}^{K-1}(\rho_{j,k}^i)^2 + \sigma_n^2)} \end{aligned} \tag{7.21}$$

7.4 Performance Results

Performance results are characterized using BER (bit-error-rate) vs. SNR (signal to noise ratio) curves. Here, we compare traditional BFSK performance curves to those of (1) an orthogonal CI/FSK (O-CI/FSK) system where $N = 15$ orthogonal CI/FSK symbols are transmitted in every duration $[0, 15T_b]$ and (2) a pseudo-orthogonal CI/FSK (PO-CI/FSK) system, where $N = 30$ symbols are sent in every $[0, 15T_b]$ duration (by pseudo-orthogonal positioning of CI/FSK symbols).

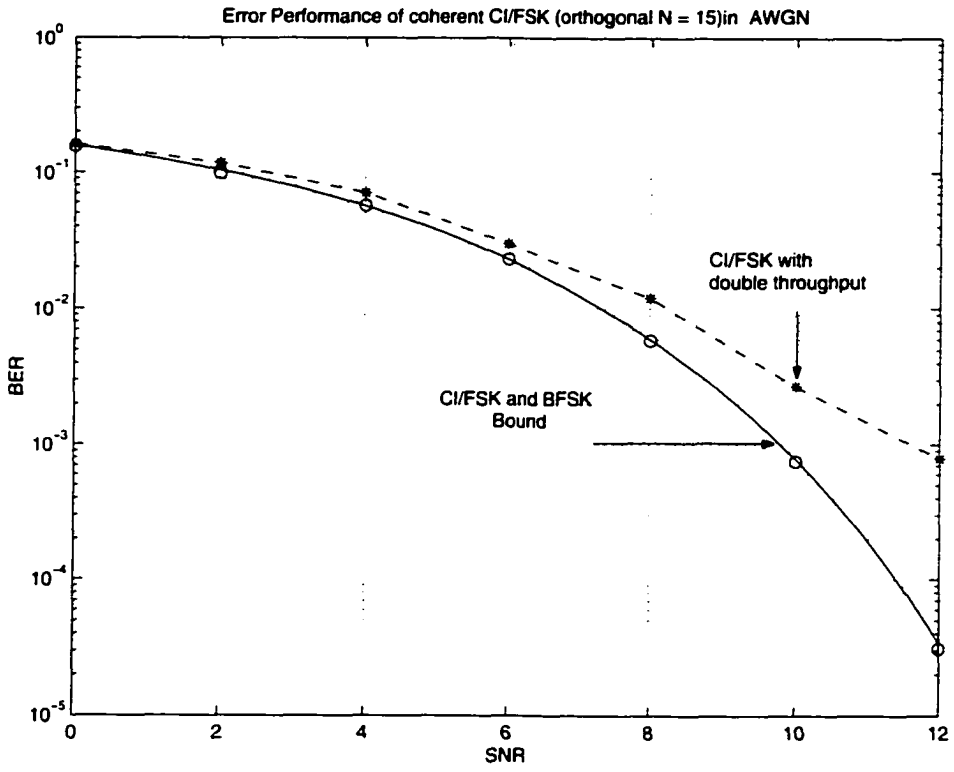

Figure 7.6: CI/FSK Performance (with double throughput) - AWGN Channel

We begin by presenting results for an AWGN channel. Figure 7.6 shows performance results for BFSK, orthogonal CI/FSK (O-CI/FSK), and pseudo-orthogonal CI/FSK (PO-CI/FSK), assuming (1) coherent detection in all cases, and (2) a total bandwidth for each system fixed at BW_{total} (the bandwidth efficiency of 0-CI/FSK then leads to doubling in throughput relative to BFSK). Performance curves for BFSK and O-CI/FSK are identical, verifying that CI/FSK's improved bandwidth efficiency comes with no degradation in performance. When PO-CI/FSK is applied, leading to a second doubling in throughput relative to BFSK, we see a small degradation in the range of 1-2 dB relative to the orthogonal case at a BER of 10^{-3}.

Next, Figures 7.7 and 7.8 represent the BER curves for O-CI/FSK and PO-CI/FSK in frequency selective channels assuming the coherent reception of Figure 7.5. Specifically, Figure 7.7 plots O-CI/FSK performance, demonstrating the im-

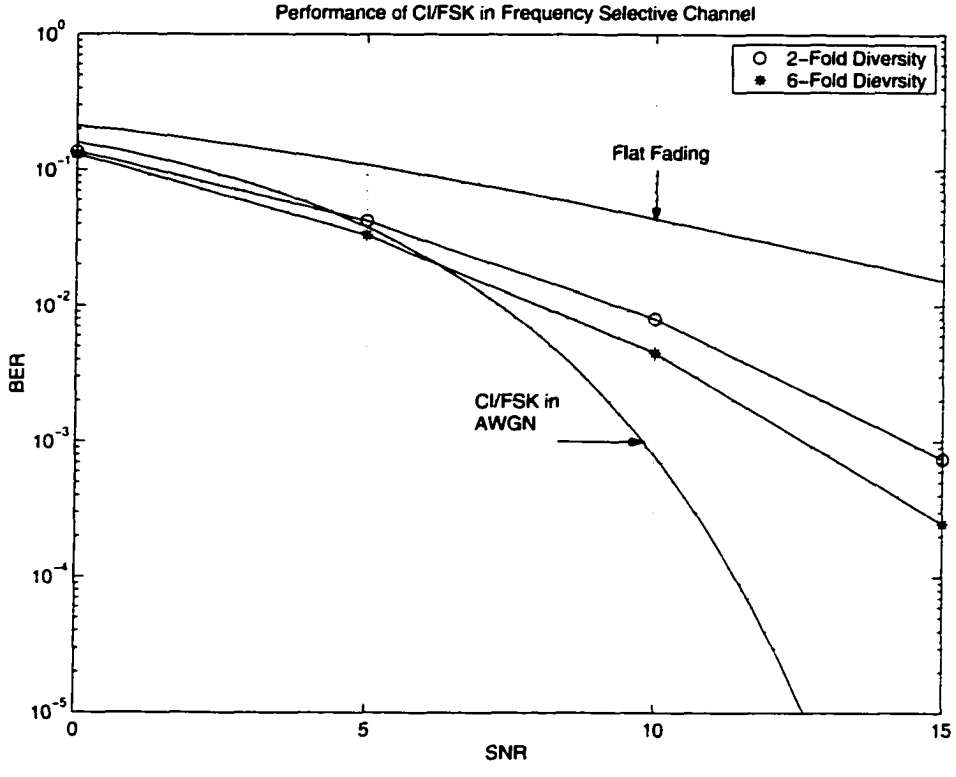

Figure 7.7: CI/FSK Performance in frequency selective channel with different degrees of diversity

provement in performance with increasing diversity (the degree of diversity, L, is defined as the ratio between the transmission bandwidth per bit ($N\Delta f$) and coherence bandwidth of the channel $(\Delta f)_c$). In Figure 7.8, PO-CI/FSK supports $2N = 30$ CI/FSK symbols in each duration $15T_b$. We observe that, in this case, performances are close to those with a 2-fold diversity gain in O-CI/FSK.

Hence, we observe that: (1) O-CI/FSK doubles throughput relative to BFSK without performance degradation due to improved spectral efficiency; (2) PO-CI/FSK supports another factor of two gain in throughput in AWGN channels with little performance degradation at a 10^{-3} error rate; (3) O-CI/FSK exploits diversity gains and drives performance away from the poor flat fading results (and toward the excellent AWGN performances); and (4) PO-CI/FSK operating over frequency selective fading

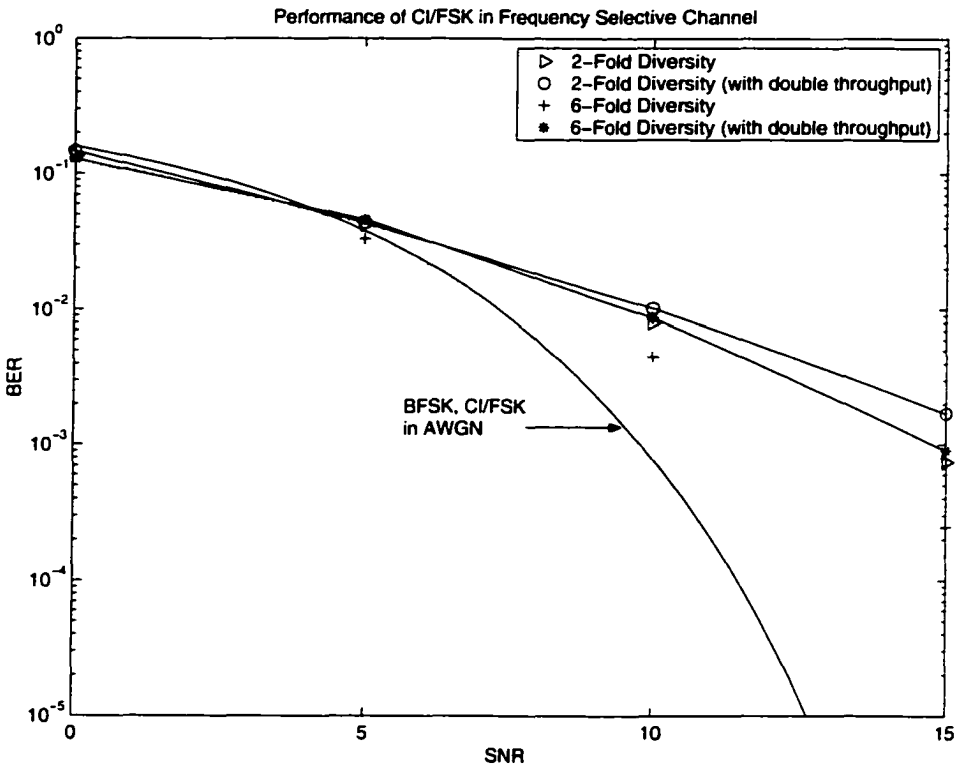

Figure 7.8: CI/FSK Performance in frequency selective channels with double throughput

channels achieves performance curves consistent with 2-fold diversity benefits.

7.5 CI/Bluetooth

Bluetooth represents a novel radio link standard supporting short range portable device inter-communication (in an ad-hoc fashion). The system is designed to operate in the unlicensed 2.4 GHz ISM band over a short range, e.g., 10m, enabling low transmission power in Bluetooth devices (in the range of 0-20 dBm). For full duplex communication, a time division duplex (TDD) scheme is mandated, where both forward and reverse links employ frequency hopping/frequency-shift-keying (FH/FSK). Specifically, 79 hop channels or carriers, each spaced by 1MHz, are defined. The hop dwell time is 625μs, i.e., the hop rate is 1600 hops/sec. GFSK with a nominal

modulation index of 0.3 is the modulation scheme of choice. Here, a binary '1' is represented by a positive frequency deviation and a binary '0' is represented by a negative frequency deviation.

We propose a change in the modulation scheme at the transmitter, (1) moving from GFSK to CI/FSK and (2) allowing for a non- overlapping '0' and '1' spectrum (possible without loss in throughput due to the increased spectral efficiency of CI/FSK). At the receiver end, we test both the usual non-coherent reception technique (Figure 7.4) and the novel coherent receiver of Figure 5. This change does not affect the Frequency Hopping (FH) architecture that operates on top of the FSK modulated signals, nor any higher layer functionality.

7.5.1 Performance and Throughput Gains

Bluetooth systems typically operate in indoor environments, where the amount of exploitable diversity is less than that in outdoor environments. The indoor channel models used for simulation are obtained from the UMTS standards [84]. The two channels considered in this work are: Channel A, with RMS delay spread of 35 ns; and Channel B, with RMS delay spread of 100 ns. These time delay spreads correspond to a coherence bandwidth, $(\Delta f)_c$, of 5.7 MHz and 2 MHz for Channels A and B, respectively (as discussed in Section 4.3).

Additionally, Bluetooth systems are intended to support data rates on the order of 700 kbps. Assuming our CI/FSK system is used to support these data rates, the total bandwidth per bit is 700 kHz. It should be noted that in the indoor UMTS channels, and assuming CI/FSK with 700 kHz bandwidths, the channel has very little diversity gain to offer: The ratio between the bandwidth per bit and the coherence bandwidth is in the range of 0.12 to 0.35.

Assuming CI/FSK operates with $N = 15$ orthogonal symbols in $[0, 15T_b]$, we

first analyze the BER performance of orthogonal CI/FSK (O-CI/FSK) with non-coherent detection. Figure 7.9 shows the performance of non-coherent O-CI/FSK, non-coherent BFSK, and non-coherent GFSK(BT=0.3) in indoor Channel A. In all cases, we hold the bandwidth per binary '0' or binary '1' fixed at 700 kHz (for a total bandwidth of 1.4 MHz). The BFSK system can only transmit 350 kbps in this frequency band (assuming no frequency overlap between the bit 0 and bit 1 frequency bands); BFSK can also support higher data rates by allowing for overlap between bit '0' and bit '1' frequency bands. Figure 7.9 shows performance curves for BFSK when both 350 kbps are sent, and when 525 kbps are transmitted. We also plot the performance of the more efficient GFSK, which can support 518 kbps in a 700 kHz per binary digit bandwidth. The performance curves verify that gains in throughput due to spectral efficiency of O-CI/FSK are available without cost in performance relative to BFSK and GFSK. When the BFSK scheme attempts to improve throughput via spectral overlap, its performance is seen to degrade relative to O-CI/FSK.

Figure 7.10 illustrates the BER performance of O-CI/FSK and PO-CI/FSK employing the novel coherent receiver in Channel A, and Figure 7.11 demonstrates the corresponding BER performances in Channel B. Figure 7.10 demonstrates: (1) the benefit of coherent receiver's cross subcarrier combining to exploit frequency diversity - a 5 dB performance improvement over the flat fading performance is observed at probability of errors between 10^{-2} and 10^{-3}; also (2) after doubling throughput via pseudo-orthogonal symbol positioning, Figure 7.10 shows that the degradation in performance is only about 1 dB. Similar gains are observed when a CI/FSK system is employed in Channel B, as illustrated in Figure 7.11. From these figures, it is evident that, in Bluetooth environments, (1) CI/FSK demonstrates the ability to exploit frequency diversity via novel coherent reception (leading to notable performance gains even in cases where little diversity gain is available); and (2) the doubling of

throughput via pseudo-orthogonal symbol positioning is available with little cost in performance.

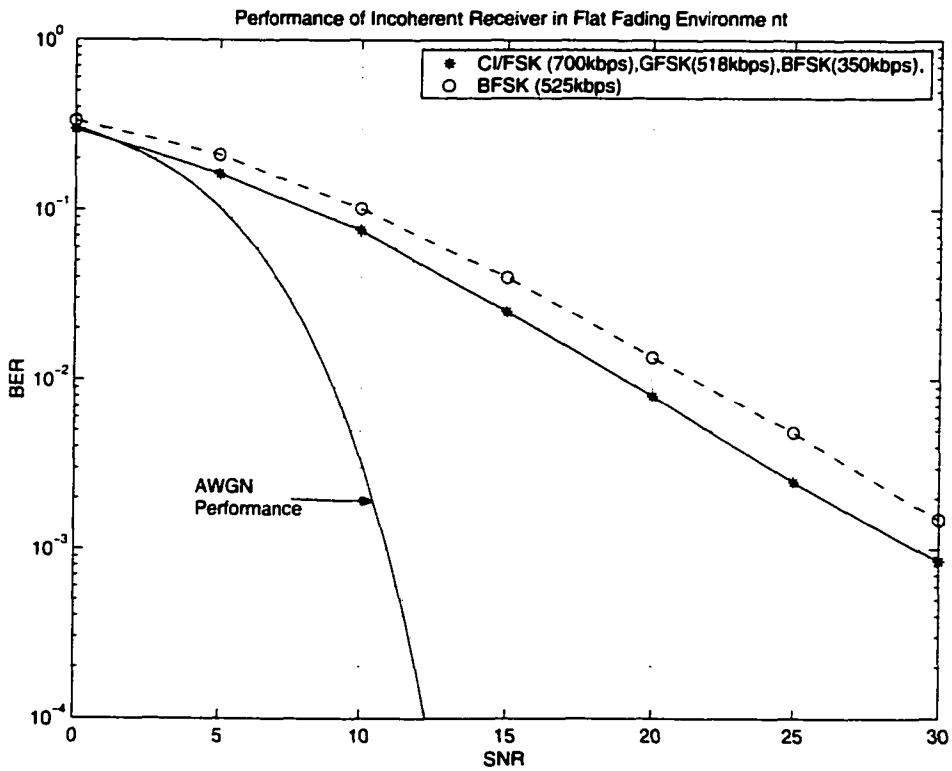

Figure 7.9: CI/FSK Performance - Non-Coherent detection

7.6 Summary

In this chapter, we presented an innovation in FSK architecture in the form of a multi-carrier implementation. Specifically, the new CI/FSK scheme involves transmission of multiple orthogonal sub-carriers around two carrier frequencies to represent binary information. This scheme is spectrally efficient relative to traditional FSK, and supports increased throughputs through pseudo-orthogonal symbol positioning.

It is also shown that the carrier interferometry envelope of the CI/FSK signal maintains excellent peak to average power ratios. The novel coherent receiver designed

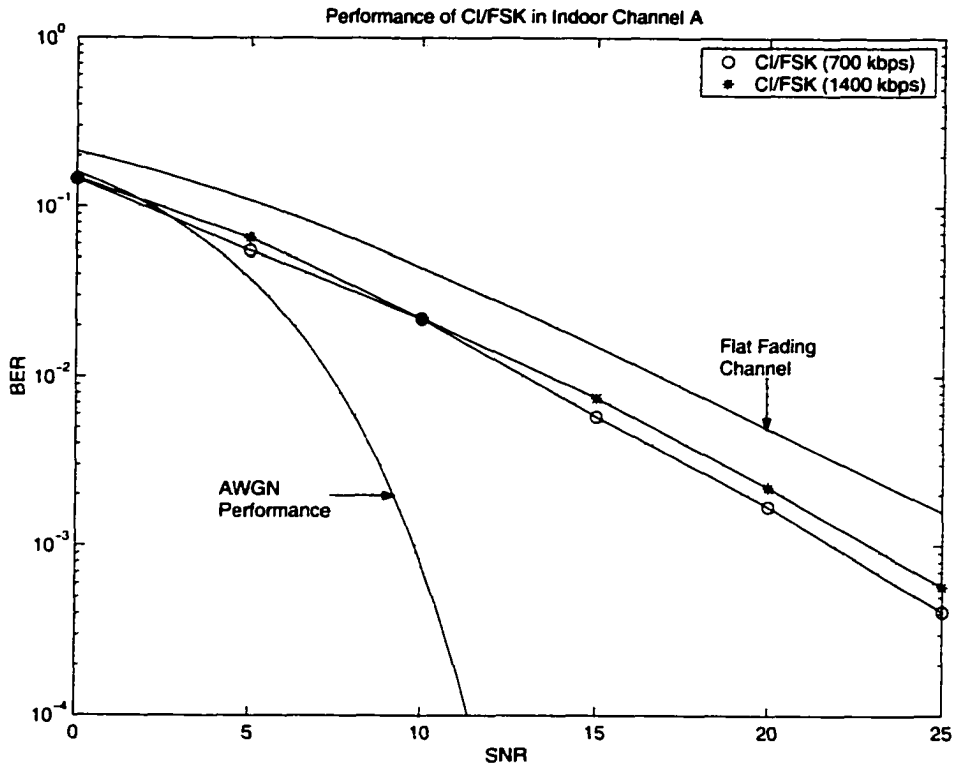

Figure 7.10: CI/FSK Performance - coherent detection in UMTS channel A

for CI/FSK makes it suitable for use in frequency selective channels, with the system benefiting from the available frequency diversity. In short, CI/FSK with both non-coherent and coherent detection demonstrates excellent BER performance at high data rates in both flat and frequency selective channels; and provides a simple means to significantly improve on the existing PAN (Bluetooth) architecture.

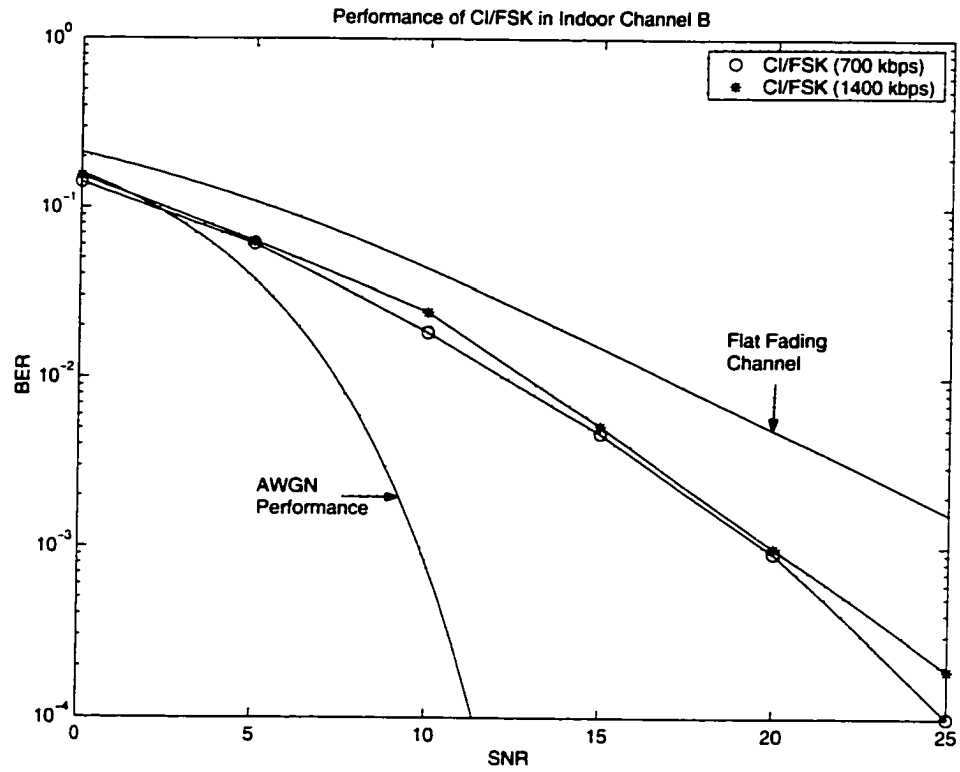

Figure 7.11: CI/FSK Performance - coherent detection in UMTS channel B

Chapter 8

Multi-Carrier Signal Synthesis and Decomposition

In chapter 6, we presented the application of Carrier Interferometry (CI) to TDMA. We demonstrated that using a multi-carrier implementation of the sinc pulse shape (that corresponds to a CI signal) along with a receiver that performs frequency domain processing, performance and throughput can be enhanced relative to a GSM system employing the Gaussian pulse shape and time-domain equalizer structure. In this chapter, we extend the multi-carrier approach to synthesize other pulse shapes (e.g., raised cosine signals).

This chapter is organized as follows. We first generalize multi-carrier signaling and highlight its key benefits. We then present the multi-carrier signal design technique and show how a practical system is designed and implemented. We also show how this approach enables a doubling in throughput via pseudo-orthogonality. Next, we present the receiver architecture that performs frequency decomposition of the signal instead of typical time-based processing. Finally, we demonstrate via performance curves how a multi-carrier design of a raised cosine pulse shape enhances performance and throughput in a GSM system.

8.1 Introduction

Signal synthesis in band-limited channels is a classic research topic (see e.g., [80]). Starting in the days of Nyquist [105], researchers have worked on designing pulse shapes and signals to suit the needs of communication environments [106]. Recent developments in DSP hardware have made it possible to implement almost any pulse shape for transmission. This has resulted in new algorithms for designing pulse shapes that match the properties of a given channel. In [107], a signal design method is proposed using projection onto convex sets. In [108], pulse shapes that satisfy Nyquist criteria at the transmitter are introduced and are shown to reduce modem costs. More pulse shape designs can be found in, e.g., [109],[110]. Considerable efforts have also been put into the use of wavelets in pulse shape design [111],[112]. Wavelet based implementations are very effective in localizing the signal in both time and frequency, and are hence well suited for environments that are both time and frequency dispersive. With the popularity of multi-carrier systems like OFDM, research has also been focusing on developing suitable pulse shapes for these systems [113]-[117]. However, in all these works ([106]-[117]), the emphasis was on developing a scheme that (1) is spectrally efficient, (2) has reduced inter-symbol-interference (ISI) or (3) enables simpler receiver designs. The prior works do not address signal synthesis with a focus on the ability to provide a common hardware platform for different systems. They have not been successful in achieving significant increases in throughputs without cost in complexity, bandwidth or performance.

In this chapter, we address the pulse shape design issue from the standpoint of providing a common multi-carrier platform. We also demonstrate increases in throughput at no cost in bandwidth and negligible cost in implementation complexity and performance.

Specifically, we show how to develop a multi-carrier implementation of basic pulse shapes such as sinc and raised cosines. The implementation is based on spectral sampling of these classic pulse shapes. To implement this at the transmitter, we propose the linear combining of discrete carriers with appropriate weighting (to approximate the traditional pulse shape in a least squares sense). At the receiver we introduce a frequency domain processor similar to that used in MC-CDMA.

The frequency sampling or spectrum sampling concept has been extensively used in signal processing applications. Specifically, this idea has been used in the design of FIR filters [118], and in perfect reconstruction circular convolution (PRCC) filters [119]. In [120][121], the application of frequency domain filters (FDF) (designed by the frequency sampling method) in interpolation of arbitrary signals is discussed. In this chapter, we apply this spectral sampling concept to pulse shape design with specific application to wireless systems. Specifically, we demonstrate that systems designed using this approach provide the following benefits:

- *High Performance* - In TDMA, using a multi-carrier implementation of, e.g., a raised cosine pulse shape and a frequency based receiver, outperform the time domain counterpart
- *High Throughput* - Using the idea of pseudo-orthogonality (discussed in Section 3.2.2) we double the throughput of the TDMA system with no cost in bandwidth.
- *Ease of Implementation* - Using IFFTs and FFTs, the transmitter and receiver structures of the multi-carrier TDMA system are implemented with minimal complexity.
- *Adaptability* - With this multi-carrier implementation, a common hardware implementation can be used for TDMA, DS-CDMA, MC-CDMA and OFDM, i.e., this signal synthesis in frequency supports a new technique for software radio.

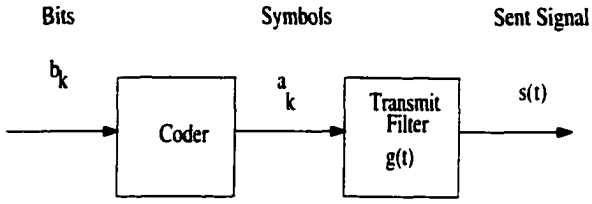

Figure 8.1: A base-band transmitter

8.2 Signal Synthesis

8.2.1 Fourier Approximation

Figure 8.1 is a simple conceptual illustration of a baseband transmitter. The impulse response $g(t)$ of the transmit filter is called the pulse shape. The output of the transmitter is the convolution of the pulse shape and the symbol sequence $\sum_{-\infty}^{\infty} a_k \delta(t-kT)$, i.e.,

$$s(t) = \sum_{k=-\infty}^{\infty} a_k g(t - kT) \tag{8.1}$$

where T is the symbol duration. The choice of pulse shape $g(t)$ determines the rate at which the symbols can be transmitted over a band-limited channel. Practical systems often use raised cosine pulses that satisfy the Nyquist criterion for zero inter-symbol-interference, i.e.,

$$g(t) = \left[\frac{\sin(\pi t/T)}{\pi t/T}\right] \frac{\cos(\alpha \pi t/T)}{1 - (2\alpha t/T)^2} \tag{8.2}$$

where $\alpha \in [0, 1]$ is the roll-off factor that determines the excess bandwidth. When $\alpha = 0$, $g(t)$ is the sinc pulse.

In practice, the pulses in (8.2) can be approximated using FIR filters by truncating the pulse at some multiple of T (though this is not a rigorous constraint)[101].

In this thesis, we propose time limiting the pulse shape to T_{obs} (and $T_{obs} = mT$, $m \in I$). Next, we approximate this time limited $g(t)$ using a truncated Fourier series

expansion. Theoretically, a time limited $g(t)$ can only be represented using an infinite Fourier series given by

$$g(t) = \sum_{i=-\infty}^{\infty} C_i e^{j2\pi i \Delta f t} \tag{8.3}$$

where C_i's are the standard Fourier coefficients, and $\Delta f = 1/T_{obs}$ (this implies the carriers are orthogonal in the time window of observation). However, since most of the frequency components beyond a certain bandwidth can be ignored (Nyquist pulses in (8.2) are band-limited), it is possible to approximate $g(t)$ as a finite sum of complex exponentials, i.e.,

$$g(t) \cong g_N(t) = \sum_{i=-P}^{P} D_i e^{j2\pi i \Delta f t} \tag{8.4}$$

The truncated Fourier series expansion of $g(t)$ (with length $N = 2P + 1$) results in a periodic $g_N(t)$ with period $1/\Delta f = T_{obs}$. As a result, we use a rectangular time window to time limit $g_N(t)$ to one period, i.e., we time limit $g_N(t)$ to T_{obs}. This translates into a sinc interpolation of the Fourier spectrum. The resulting expansion in bandwidth (due to sinc interpolation) can be shown to be negligible.

Using adequate numbers of carriers, $g(t)$ can be approximated in a least squares sense. Mathematically, we can denote the error between $g(t)$ and $g_N(t)$ via

$$\epsilon(t) = g(t) - g_N(t) \tag{8.5}$$

That is,

$$\begin{aligned} \epsilon(t) &= \sum_{i=-\infty}^{\infty} C_i e^{j2\pi i \Delta f t} - \sum_{i=-P}^{P} D_i e^{j2\pi i \Delta f t} \\ &= \sum_{i=-\infty}^{\infty} G_i e^{j2\pi i \Delta f t} \end{aligned} \tag{8.6}$$

where,

$$G_i = \begin{cases} C_i - D_i & -P \le i \le P \\ C_i & |i| > P \end{cases} \tag{8.7}$$

The mean square value of the error corresponds to $< \epsilon^2(t) >= \frac{1}{T_{obs}} \int_{-T_{obs}/2}^{T_{obs}/2} \epsilon^2(t)dt$. Assuming that $g(t)$ is real, the mean-square error value is given by [122]

$$\begin{aligned} < \epsilon^2 > &= \left\langle \left(\sum_{i=-\infty}^{\infty} G_i e^{j2\pi i \Delta f t} \right) \left(\sum_{n=-\infty}^{\infty} G_n^* e^{-j2\pi i \Delta f t} \right) \right\rangle \\ &= \sum_{i=-\infty}^{\infty} \sum_{n=-\infty}^{\infty} G_i G_n^* \left\langle e^{j2\pi(i-n)\Delta f t} \right\rangle \\ &= \sum_{i=-P}^{P} |C_i - D_i|^2 + \sum_{|i|>P} |C_i|^2 \end{aligned} \tag{8.8}$$

where the time average $< e^{j2\pi(i-n)\Delta f t} >= 0$, for $i \neq n$. Each term in this expression is positive. Therefore, to minimize $< \epsilon^2 >$ we set

$$D_i = C_i \tag{8.9}$$

This results in a minimum mean square error of

$$< \epsilon^2 >= \sum_{|i|>P} C_i^2 \tag{8.10}$$

The mean square error (MSE) decreases monotonically as the number of carriers used in the approximation grows. This is illustrated in Figure 8.2. Here, the mean-square error is plotted versus number of carriers (N) for two different values of α (0.35, 0.9). Theoretically, the MSE converges to zero asymptotically. However with $N > 25$ we observe the MSE value is small (less than 0.1) and hence, the actual signal and the multi-carrier signal converge. The MSE plays an important role in selecting N for practical system design, as discussed later.

Figure 8.3 shows a raised cosine pulse with $\alpha = 0.35$ (this corresponds to the roll-off factor specified in the IS-54 standard [123]). The lighter curve is the actual pulse shape based on equation (8.2). The darker line represents the pulse shape generated using a sum of $N = 15$ carriers. We observe that there is almost a perfect match between the signals. This is confirmed by looking at Figure 8.4, showing a close

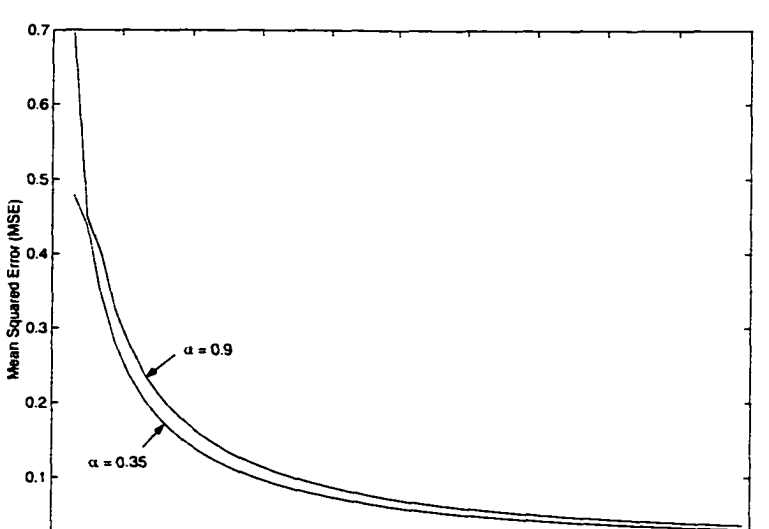

Figure 8.2: MSE of truncated Fourier series

match between the corresponding spectrums. Here the line with dots represents the multi-carrier pulse shape spectrum.

Figure 8.5 compares the sinc pulse shape (in time) with the corresponding multi-carrier implementation, and Figure 8.6 shows the same comparison for the Gaussian pulse shape. For the sinc pulse, and its approximation with $N = 20$ carriers, there is a close match between the two signals. For the Gaussian pulse shape (which is not a Nyquist pulse shape) and the $N = 47$ carrier approximation, we observe a close match in the time domain signals.

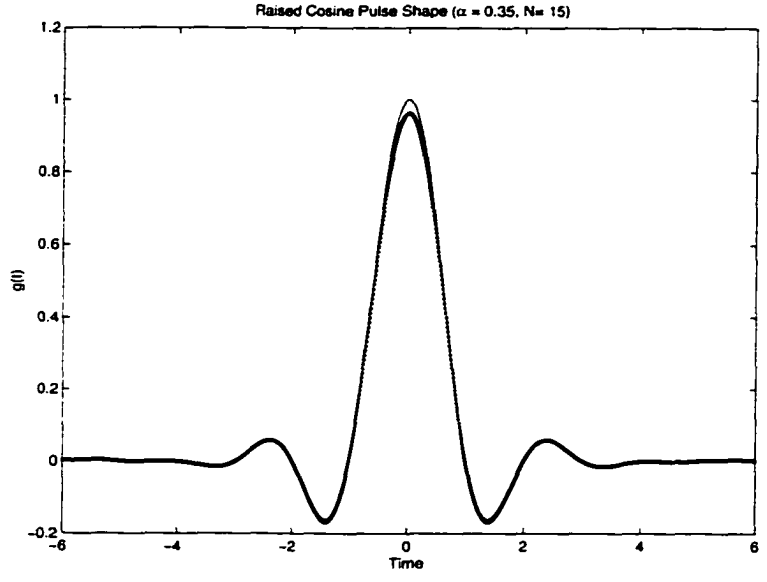

Figure 8.3: Raised cosine pulse shape ($\alpha = 0.35$) in time domain

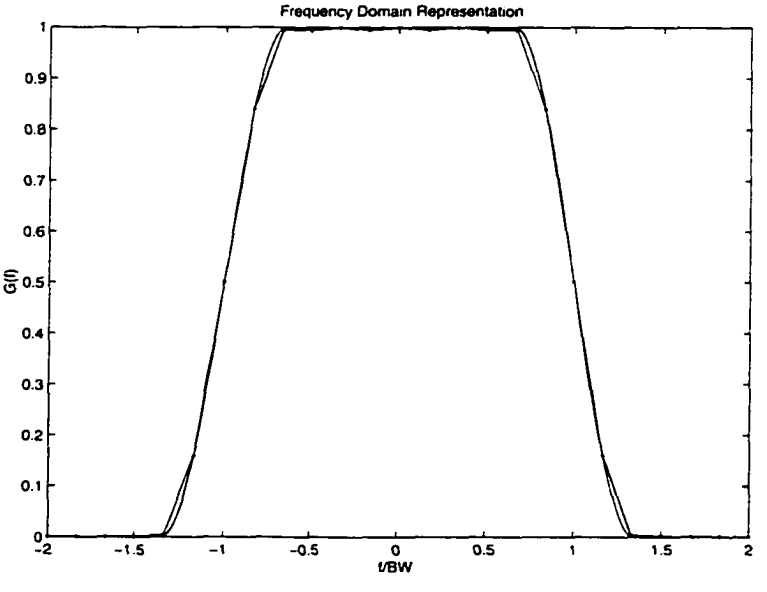

Figure 8.4: Raised cosine pulse shape ($\alpha = 0.35$) in frequency domain

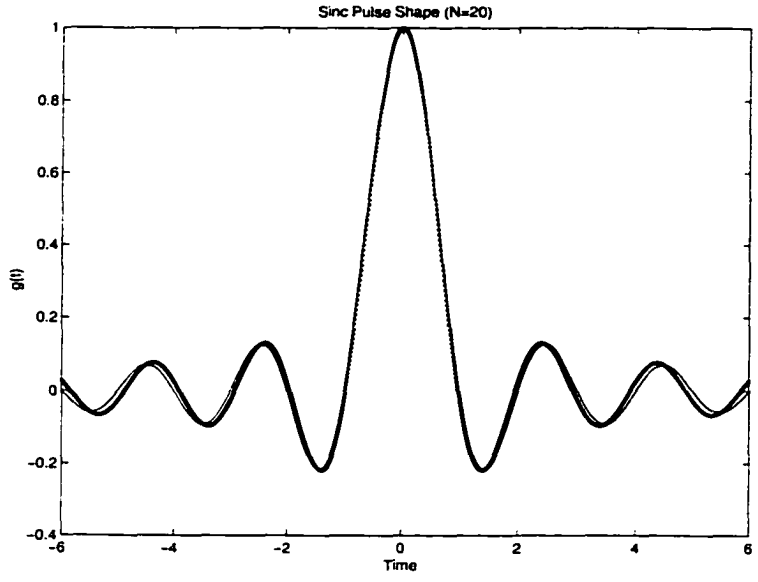

Figure 8.5: Sinc pulse shape

8.2.2 Multi-carrier Nomenclature

Generally, the pulse shape introduced in (8.4) is modulated onto a carrier frequency F_c leading to the passband representation given by

$$\begin{aligned} g_{passband}(t) &= \Re e\{g_N(t)e^{j2\pi F_c t}\} \\ &= \Re e\{\sum_{i=-P}^{P} D_i e^{j2\pi i\Delta f t} e^{j2\pi F_c t}\} \\ &= \Re e\{\sum_{i=-P}^{P} D_i e^{j2\pi(F_c+i\Delta f)t}\} \end{aligned} \tag{8.11}$$

Since, we have introduced a multi-carrier signal synthesis technique, we now shift from typical pulse shaping nomenclature to standard multi-carrier nomenclature. This provides notational convenience as well as ease in presenting time-frequency analogies. Specifically, we redefine our multi-carrier pulse shape as

$$g'(t) = \sum_{i=0}^{N-1} D_i e^{j2\pi i\Delta f t} \tag{8.12}$$

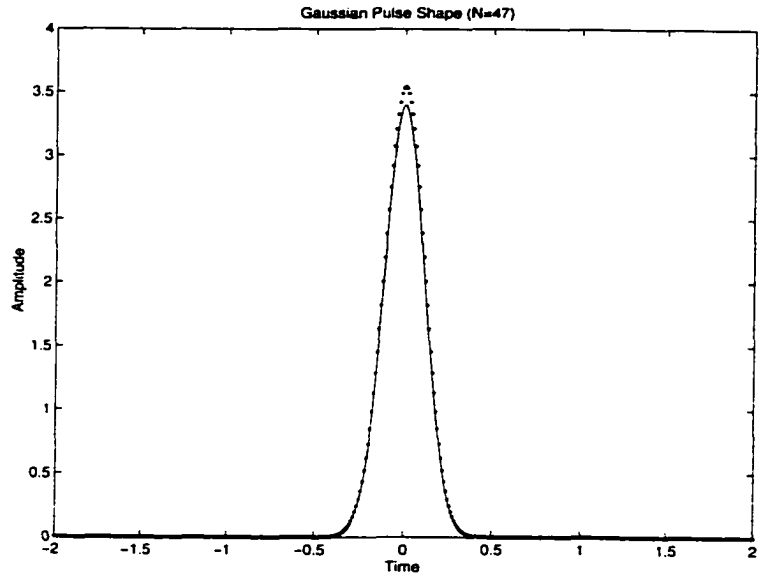

Figure 8.6: Gaussian pulse shape

Hence, from (8.11), we have

$$\begin{aligned} g_{passband}(t) &= \Re e\{g_N(t)e^{j2\pi F_c t}\} \\ &= \Re e\{g'(t)e^{j2\pi(F_c - \frac{N-1}{2}\Delta f)t}\} \\ &= \Re e\{g'(t)e^{j2\pi f_c t}\} \end{aligned} \tag{8.13}$$

where

$$f_c = F_c - \frac{N-1}{2}\Delta f. \tag{8.14}$$

Hereafter, we will denote $g_N(t) = g'(t)$, i.e.,

$$g_N(t) = \sum_{i=0}^{N-1} D_i e^{j2\pi i \Delta f t} \tag{8.15}$$

Here, $D_i = C_{i-P}, i = 0, 1, \cdots, N-1$.

8.2.3 Transmission Parameters

Assuming that we employ a multi-carrier implementation of a root raised cosine (rrc) pulse shape, the transmitted signal for the 0^{th} bit, $a_0 \in \{-1, +1\}$, corresponds to

$$\begin{aligned} s_0(t) &= \Re e\{a_0 g_N^{rrc}(t) e^{j2\pi f_c t}\}, \quad 0 \leq t < T_{obs} \\ &= a_0 \Re e\{A \sum_{i=0}^{N-1} \sqrt{D_i} e^{j2\pi(f_c + i\Delta f)t}\} \quad 0 \leq t < T_{obs} \end{aligned} \tag{8.16}$$

where A is a constant that determines the symbol energy; $\sqrt{D_i}$ denotes the multi-carrier transmit filter coefficients (D_i refers to the Fourier coefficient corresponding to the raised cosine pulse shape) and T_{obs} is the observation time of the pulse shape (set to mT_b as mentioned earlier).

As is evident from (8.16), N is an important design parameter. The value of N is chosen to (1) ensure a *good* approximation of the actual pulse shape (via weighted carriers) in a mean square sense; and (2) ensure a flat fade over each of the carriers that constitute the pulse shape.

We will also require N maintain a reasonable observation time T_{obs}, as explained next. We note that $T_{obs} = mT_b, m \in I$, and we require T_{obs} correspond to one period of the multi-carrier signal, i.e., $T_{obs} = \frac{1}{\Delta f}$ (or, alternatively, $\Delta f = \frac{1}{mT_b}$). Next, considering a multi-carrier implementation of raised cosine pulse shape with roll-off factor α, the total bandwidth corresponds to

$$BW_{total} = N\Delta f = \frac{(1+\alpha)}{T_b}. \tag{8.17}$$

Substituting for Δf, we have

$$N\frac{1}{mT_b} = \frac{(1+\alpha)}{T_b} \tag{8.18}$$

$$N = (1+\alpha)m \tag{8.19}$$

Equation (8.19) provides the final condition on N. Here, we must remember that both N and m are integers (also, $N \geq m$ since $\alpha \geq 0$). For example, if $\alpha = 0.35$, one choice of N and m that satisfies (8.19) is $N = 27$ and $m = 20$. (In the case of sinc pulse shape, the solution is trivial as $\alpha = 0$ and hence $N = m$).

Referring to criteria (1), we also select N to minimize MSE (or achieve a reasonably small value). For example, for $\alpha = 0.35$ and $N = 27$ the MSE is approximately 0.1 and the multi-carrier signal is very close to the actual pulse shape.

Finally, referring to criteria (2) which requires a flat fade over each carrier, we note that the frequency width of each carrier is $\Delta f = \frac{1}{mT_b}$. Assuming a raised cosine pulse shape with $\alpha = 0.35$ and N=27, leads to $m = 20$. With GSM data rates of 270.8 kbps, the $\Delta f = \frac{1}{20T_b}$ corresponds to 13.5 khz. For typical GSM channel models provided in Section 4.3, the coherence bandwidth of HT, TU and RA channels are 39.72 Khz, 188 Khz and 2050 Khz, respectively. Therefore flat fades are achieved with e.g., $N \geq 27$ (since $\Delta f < 2(\Delta f)_c$).

8.2.4 Symbol Stream Transmission

Assuming a block transmission strategy with block duration $T_{obs} = mT_b$, we transmit m BPSK modulated information symbols in a block. Therefore, the total transmitted signal corresponds to

$$\begin{aligned} s(t) &= \Re e\{\sum_{k=0}^{m-1} a_k g_N^{rrc}(t - kT_b)e^{j2\pi f_c t}\}, \quad 0 \leq t < mT_b \\ &= \Re e\{\sum_{k=0}^{m-1} a_k A \sum_{i=0}^{N-1} \sqrt{D_i} e^{j2\pi i \Delta f (t-kT_b)} \cdot e^{j2\pi f_c t}\}, \quad 0 \leq t < mT_b \end{aligned} \tag{8.20}$$

In the case of sinc pulse shapes, the transmitted signal is consistent with that in equation (6.5) with $m = N$ and $D_i = 1$ for all i.

Multi-carrier signal synthesis also enables a doubling in throughput via pseudo-orthogonality. Similar to the analysis in Section 3.3, we extend the idea of pseudo-

orthogonality to the raised cosine pulse shape. That is, we use two sets of raised cosine pulse shapes in T_{obs}, namely

$$\begin{aligned} Set \quad 1 \; &: \; \{g_N(t), g_N(t-T_b), \cdots, g_N(t-(m-1)T_b)\} \\ Set \quad 2 \; &: \; \{g_N(t-\zeta), g_N(t-T_b-\zeta), \cdots, g_N(t-(m-1)T_b-\zeta)\} \end{aligned} \quad (8.21)$$

and we determine the constant $\zeta (0 < \zeta < T_b)$ that minimizes the root-mean-square correlation between the two sets. This minimization is done analytically for the CI pulse shape which corresponds to the multi-carrier implementation of the sinc. There, $\zeta = T_b/2$ was the solution to this minimization. However, with a multi-carrier implementation of an arbitrary raised cosine pulse shape, this ζ is a complicated function of both the roll-off factor α and N. Therefore, the ζ is best evaluated using a numerical minimization. For example, Figure 8.7 plots the root-mean-square correllation (for symbols of set 1 and set 2 in (8.21)) with respect to ζ as a fraction of T_b, assuming $\alpha = 0.35, N = 27$ and $m = 20$. By choosing the value of ζ ($\zeta = 0.656T_b$ in this example) that minimizes the correllation function, we can transmit $2m$ symbols per block with little performance degradation.

The total transmitted signal is now represented by

$$\begin{aligned} s(t) &= \Re e\{\sum_{k=0}^{2m-1} a_k g_N^{rrc}(t-\tau_k) e^{j2\pi f_c t}\} \quad 0 \le t < mT_b \\ &= \Re e\{\sum_{k=0}^{2m-1} a_k A \sum_{i=0}^{N-1} \sqrt{D_i} e^{j2\pi i \Delta f (t-\tau_k)} \cdot e^{j2\pi f_c t}\} \quad 0 \le t < mT_b \end{aligned} \quad (8.22)$$

where

$$\tau_k = \begin{cases} kT_b & k \in \{0, 1, \cdots, m-1\} \\ (k-m)T_b + \zeta & k \in \{m, m+1, \cdots, 2m-1\} \end{cases} \quad (8.23)$$

This is analogous to the doubling of capacity in CI/MC-CDMA and in CI/TDMA. The price, of course, is one of reduced performance due to introduction of controlled ISI at the transmitter side.

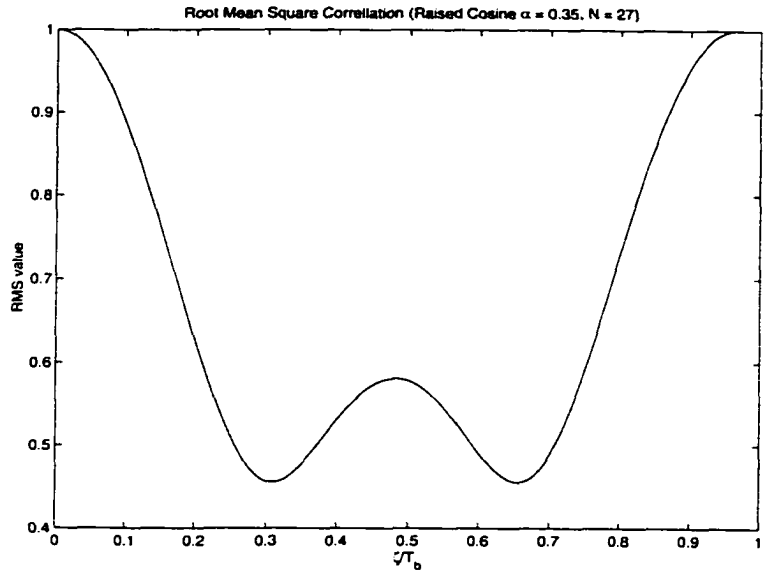

Figure 8.7: RMS correllation as function of ζ

8.2.5 Implementation

Another key benefit of multi-carrier signal synthesis is the ease in its implementation. The implementation structure differs for m-symbol per block transmission and $2m$-symbol per block transmission.

- *m-symbol Transmission*

In this case, the transmitted baseband signal corresponds to (for root raised cosine)

$$\begin{aligned} s(t) &= \sum_{k=0}^{m-1} a_k A \sum_{i=0}^{N-1} \sqrt{D_i} e^{j2\pi i \Delta f (t-kT_b)} \\ &= A \sum_{i=0}^{N-1} \sqrt{D_i} e^{j2\pi i \Delta f t} \sum_{k=0}^{m-1} a_k e^{-j2\pi i \Delta f k T_b} \\ &= \sum_{i=0}^{N-1} E_i e^{j2\pi i \Delta f t} \end{aligned} \tag{8.24}$$

where,

$$\begin{aligned} E_i &= A\sum_{k=0}^{m-1}\sqrt{D_i}a_k e^{-j2\pi i\Delta f k T_b} \\ &= A\sum_{k=0}^{m-1}\sqrt{D_i}a_k e^{-j\frac{2\pi}{m}ik} \end{aligned} \tag{8.25}$$

This vector $\mathbf{E} = (E_0, E_1, \cdots, E_{N-1})^T$ (where ^{T} refers to the matrix transpose) is obtained from the input symbol vector $\mathbf{a} = (a_0, a_1, \cdots, a_{m-1})^T$ (the input symbol vector) by employing the N x m transformation matrix

$$\Gamma = \begin{pmatrix} A\sqrt{D_0}e^{-j\frac{2\pi}{m}0\cdot 0} & A\sqrt{D_0}e^{-j\frac{2\pi}{m}0\cdot 1} & \cdots & A\sqrt{D_0}e^{-j\frac{2\pi}{m}0\cdot m-1} \\ A\sqrt{D_1}e^{-j\frac{2\pi}{m}1\cdot 0} & A\sqrt{D_1}e^{-j\frac{2\pi}{m}1\cdot 1} & \cdots & A\sqrt{D_1}e^{-j\frac{2\pi}{m}1\cdot m-1} \\ \vdots & & & \\ A\sqrt{D_{N-1}}e^{-j\frac{2\pi}{m}N-1\cdot 0} & A\sqrt{D_{N-1}}e^{-j\frac{2\pi}{m}N-1\cdot 1} & \cdots & A\sqrt{D_{N-1}}e^{-j\frac{2\pi}{m}N-1\cdot m-1} \end{pmatrix}. \tag{8.26}$$

That is,

$$\mathbf{E} = \Gamma\mathbf{a}. \tag{8.27}$$

In a digital implementation, the $s(t)$ of equation (8.24) can be sampled at times $T_{samp} = \frac{m}{N}T_b$ to yield N samples in block length $T_{obs} = mT_b$. That is, we generate

$$\begin{aligned} s(pT_{samp}) &= s(p\frac{m}{N}T_b), \qquad p = 0, 1, \cdots, N-1 \\ s(pT_{samp}) &= \sum_{i=0}^{N-1} E_i e^{j2\pi i\frac{1}{mT_b}\frac{mT_b}{N}p} \\ &= \sum_{i=0}^{N-1} E_i e^{j\frac{2\pi}{N}ip} \end{aligned} \tag{8.28}$$

This vector $\mathbf{s} = \{s(0\cdot T_{samp}), s(1\cdot T_{samp}), \cdots, s(N-1\cdot T_{samp}))\}^T$ is the inverse DFT (IFFT) of the vector $\mathbf{E}$. Therefore, the transmission vector is generated using an N-point IFFT. This is followed by a D/A (digital-to-analog) converter. The complete transmitter structure is illustrated in Figure 8.8.

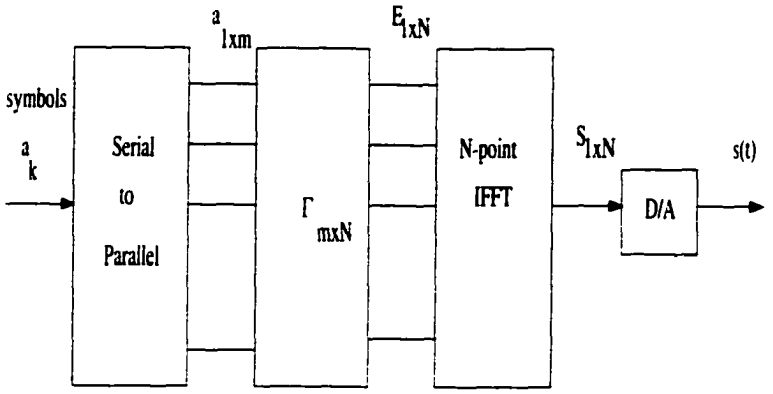

Figure 8.8: Transmitter Implementation (m symbols in a block)

It is interesting to note the case of $\alpha = 0$, i.e., $N = m$. This corresponds to a sinc waveform with $D_i = 1 \forall i$. Here, the Γ matrix transformation becomes an N-point DFT (FFT) transformation. Following the IFFT operation, we can easily verify that the transmission vector $\mathbf{s}$ in this case, satisfies Nyquist criteria for zero ISI. Since we perform two operations on the data vector $\mathbf{a}$ that are inverse of each other, the transmitter can be further simplified. Here, the transmitter consists of the incoming data feeding an ideal D/A converter.

• *2m-symbol Transmission*

With $2m$ symbols in a transmission block of length mT_b, it is necessary to make minor alterations to the transmitter. This structure is shown in Figure 8.9. Here the incoming symbols are first serial to parallel converted to yield a $2m$ long vector, $\mathbf{a} = (\mathbf{a^1}, \mathbf{a^2})^\mathbf{T}$, where $\mathbf{a^1}$ and $\mathbf{a^2}$ are m-length row vectors each. $(\mathbf{a^1})^T$ is transformed using the Γ of equation (8.26) to yield $\mathbf{E^1}$.

$$\mathbf{E^1} = \Gamma(\mathbf{a^1})^\mathbf{T} \tag{8.29}$$

The symbols in $\mathbf{a^2}$ that reside on the pseudo-orthogonally positioned raised cosine

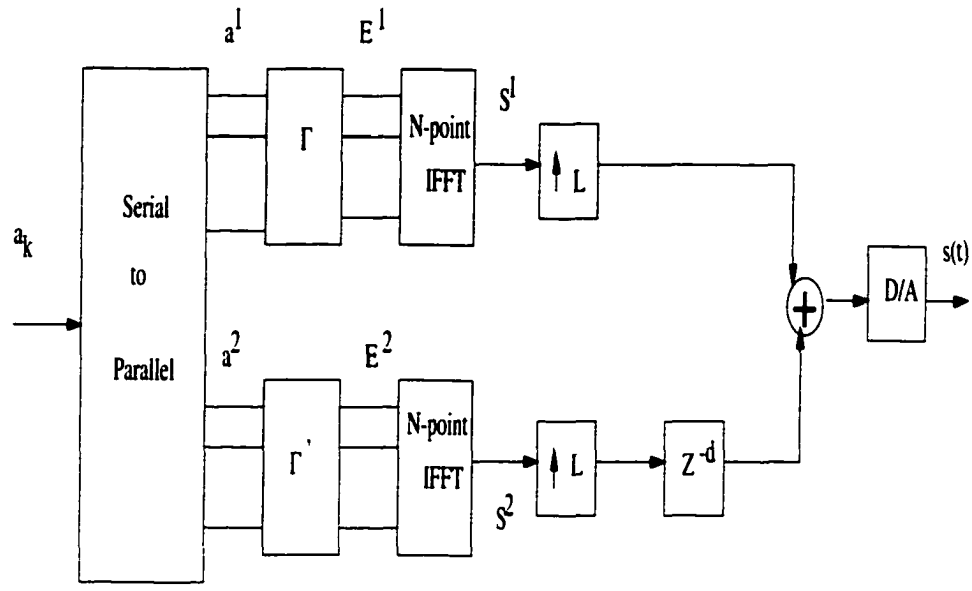

Figure 8.9: Transmitter Implementation ($2m$ symbols in a block)

pulse shapes (with $\tau_k = (k-m)T_b - \zeta, k = m, m+1, \cdots, 2m-1$), are transformed by matrix

$$\Gamma' = \begin{pmatrix} A\sqrt{D_0}e^{-j2\pi 0\cdot\Delta f\tau_m} & A\sqrt{D_0}e^{-j2\pi 1\cdot\Delta f\tau_{m+1}} & \cdots & A\sqrt{D_0}e^{-j2\pi(N-1)\cdot\Delta f\tau_{2m-1}} \\ A\sqrt{D_1}e^{-j2\pi 0\cdot\Delta f\tau_m} & A\sqrt{D_1}e^{-j2\pi 1\cdot\Delta f\tau_{m+1}} & \cdots & A\sqrt{D_1}e^{-j2\pi(N-1)\cdot\Delta f\tau_{2m-1}} \\ \vdots & & & \\ A\sqrt{D_{N-1}}e^{-j2\pi 0\cdot\Delta f\tau_m} & A\sqrt{D_{N-1}}e^{-j2\pi 1\cdot\Delta f\tau_{m+1}} & \cdots & A\sqrt{D_{N-1}}e^{-j2\pi(N-1)\cdot\Delta f\tau_{2m-1}} \end{pmatrix}. \tag{8.30}$$

That is,

$$\mathbf{E^2} = \Gamma'(\mathbf{a^2})^{\mathbf{T}}. \tag{8.31}$$

Now, similar to the m-symbol transmission case, the next stage involves the N-point inverse DFT (IFFT) of E^1 and E^2. These yield two sampled transmission vectors of length N

$$\begin{aligned} \mathbf{s^1} &= (s_0^1, s_1^1, \cdots, s_{N-1}^1) \\ \mathbf{s^2} &= (s_0^2, s_1^2, \cdots, s_{N-1}^2) \end{aligned} \tag{8.32}$$

Next, both the signal vectors are upsampled by a factor of L,($L \in I$). This upsampling factor is chosen such that $\zeta \approx d \cdot \frac{T_{samp}}{L}, d \in I$. Then, $\mathbf{s^2}$ is passed through a delay operator with delay d and then added with $\mathbf{s^1}$ to yield the transmission vector $\mathbf{s}$. This transmission vector is then sent through a D/A converter to yield the signal $s(t)$.

Once again, if we consider the case of a sinc pulse shape, the implementation simplifies. In the first stage, because $\zeta = T_b/2$ is the fractional delay between the two sets of pulse shapes, the two transformations Γ and Γ' simplify to one single transformation which corresponds to a $2N$ point DFT (FFT). The output of the $2N$ point DFT (FFT) is split into two N point sequences and the IFFT is performed. The outputs are upsampled by a factor of 2 and added together to yield the transmission vector. Finally, this signal is D/A converted.

Multi-carrier signal synthesis of pulse shapes leads to a simple and elegant implementation (consistent with other multi-carrier transmission schemes).

8.3 Signal Decomposition

8.3.1 Receiver Structure

Similar to CI/TDMA, a more significant update in design takes place at the receiver side. We replace the traditional time-based equalizer structure by a frequency-based receiver structure. This receiver is capable of significant performance improvements, some of which may be traded off for gains in throughput.

We will assume BPSK symbols for ease in presentation. We assume the transmission of $K = m$ or $K = 2m$ symbols per observation block, T_{obs}. Each of the K symbols reside on a raised cosine pulse shape composed of N frequency components. Upon transmission over a typical wideband wireless channel, the signal experiences a frequency selective Rayleigh fade. While frequency selectivity exists over the entire

transmit band, each narrowband frequency component experiences a flat fade (we select a sufficiently large N to ensure this (see Section 8.2.3)). This is characteristic of all multi-carrier systems and is discussed in detail in Section 4.3. Hence, assuming the transmit signal of (8.20) or (8.22), the received signal is characterized by

$$r(t) = \sum_{k=0}^{K-1} \Re e\{a_k[\sum_{i=0}^{N-1} \alpha_i A\sqrt{D_i} e^{j(2\pi i\Delta f(t-\tau_k)+\phi_i)}] \cdot e^{j2\pi f_c t}\} + n(t) \tag{8.33}$$

where α_i is the gain and ϕ_i is the phase offset in the i^{th} carrier of the multi-carrier pulse shape (due to channel fade) and $n(t)$ is AWGN. Here, K is either equal to m (in which case $\tau_k = kT_b$) or K is equal to $2m$ (in which case τ_k is given by equation (8.23)).

We now detail the detection of the j^{th} bit as shown in Figure 8.10. We assume perfect synchronization and phase correction. As seen in Figure 8.10, the first stage of the novel receiver, separates the received signal into its corresponding carrier components (by applying suitable delays τ_j to detect the j^{th} bit, and appropriate gains on each carrier ($\sqrt{D_i}$) to satisfy Nyquist criterion). This results in N decision variables, one per frequency component of the multi-carrier pulse shape. Mathematically, the i^{th} frequency component during the detection of the j^{th} bit, corresponds to

$$r_{j,i} = a_j \alpha_i A D_i + \sum_{k=0, k\neq j}^{K-1} a_k \alpha_i A D_i \cos\left(2\pi i \Delta f(\tau_k - \tau_j)\right) + \eta_i \tag{8.34}$$

Here, the first term contains the desired information symbol. The second term is the ISI on the i^{th} carrier and η_i represent the Gaussian random variable with variance $D_i \cdot \sigma_n^2$.

Next, a suitable strategy is applied to combine the $r_{j,i}$'s. Once again, similar to the designs presented in earlier chapters, we employ minimum mean square error combining (MMSEC) to jointly minimize the ISI and the noise term. In this case, employing MMSEC results in the decision variable R_j given by the linear sum (derivation is

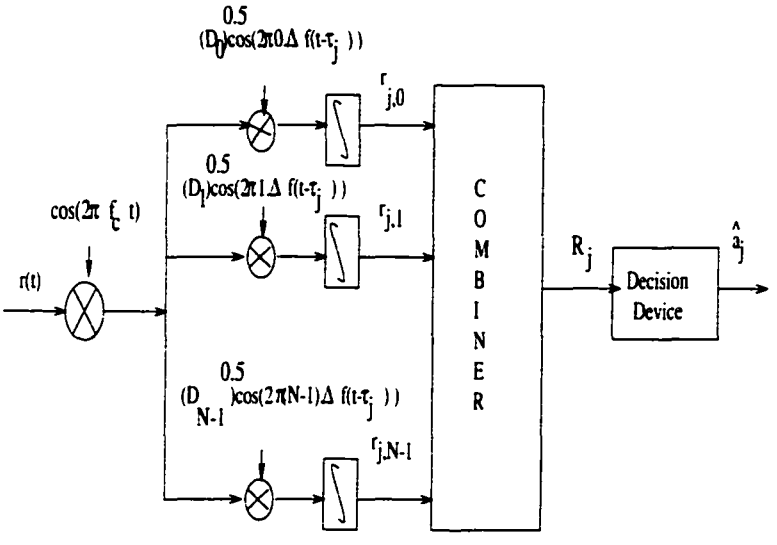

Figure 8.10: Receiver structure for multi-carrier TDMA

similar to that presented in Section 4.4.2)

$$R_j = \sum_{i=0}^{N-1} r_{j,i} \cdot \frac{\alpha_i A^2 D_i}{\left(\alpha_i^2 A^2 D_i \sum_{p=0}^{K-1} \cos\left(2\pi i \Delta f(\tau_p - \tau_j)\right)^2 + \sigma_n^2\right)}. \tag{8.35}$$

Then R_j is fed into a hard decision device where the final decision is rendered.

8.3.2 Implementation

Just as the transmitter was implemented using elegant transformations and IFFTs there is a simple low-complexity implementation of the receiver explained above. It can be easily shown that this frequency domain receiver does the reverse operation of the transmitter explained in section 8.2.5. Once again let us consider two cases - m symbol transmission and $2m$ symbol transmission.

- *m-symbol Transmission*

The receiver implementation is illustrated in Figure 8.11. The received signal $r(t)$ is first A/D (analog-to-digital) converted and is sampled at $T_{Samp} = \frac{m}{N} T_b$. Thus, we have N samples in a block length of mT_b. The first operation undoes the effect of the IFFT at the transmitter, and hence it is an N-point FFT. This corresponds to

decomposition into the frequency carriers. The i^{th} element of the output vector of the FFT corresponds to

$$r_i = \alpha_i \sqrt{D_i} A \sum_{k=0}^{m-1} a_k e^{-j\frac{2\pi}{m}ik} + n_i \tag{8.36}$$

where n_i is a Gaussian random variable representing the band-limited noise on the i^{th} carrier. This vector $\mathbf{r} = (r_0, r_1, \cdots, r_{N-1})^T$ is multiplied by a matrix transform that negates the effect of Γ at the transmitter, i.e., in terms of the receiver of Figure 8.10, it applies the appropriate delay for each bit and the appropriate gain $\sqrt{D_i}$. This matrix also takes into consideration the ISI and noise term by incorporating weights to minimize them (this weighting is analogous to the one represented in equation (8.35)). This matrix corresponds to

$$\Lambda = \begin{pmatrix} w_0^0\sqrt{D_0}e^{j\frac{2\pi}{m}0\cdot 0} & w_1^0\sqrt{D_1}e^{j\frac{2\pi}{m}1\cdot 0} & \cdots & w_{N-1}^0\sqrt{D_{N-1}}e^{j\frac{2\pi}{m}(N-1)\cdot 0} \\ w_0^1\sqrt{D_0}e^{j\frac{2\pi}{m}0\cdot 1} & w_1^1\sqrt{D_1}e^{j\frac{2\pi}{m}1\cdot 1} & \cdots & w_{N-1}^1\sqrt{D_{N-1}}e^{j\frac{2\pi}{m}(N-1)\cdot 1} \\ \vdots & & & \\ w_0^{m-1}\sqrt{D_0}e^{j\frac{2\pi}{m}0\cdot m-1} & w_1^{m-1}\sqrt{D_1}e^{j\frac{2\pi}{m}0\cdot m-1} & \cdots & w_{N-1}^{m-1}\sqrt{D_{N-1}}e^{j\frac{2\pi}{m}(N-1)\cdot m-1} \end{pmatrix}. \tag{8.37}$$

Assuming MMSEC, the weights w_i^j, the weight for i^{th} carrier during the detection of the j^{th} bit, corresponds to (from (8.35))

$$w_i^j = \frac{\alpha_i A^2 D_i}{(\alpha_i^2 A^2 D_i \sum_{p=0}^{m-1} \cos\left(\frac{2\pi}{N} i(p-j)\right)^2 + \sigma_n^2)} \tag{8.38}$$

Thus the decision vector D is given by

$$\mathbf{D} = \Lambda \mathbf{r} \tag{8.39}$$

The m-length decision vector is then parallel to serial converted and put through a decision device that outputs the vector $\hat{\mathbf{a}}$, the decision vector on the transmitted symbol vector $\mathbf{a}$.

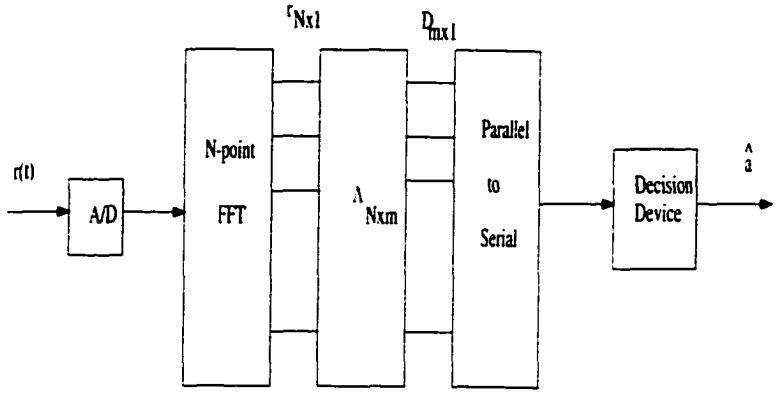

Figure 8.11: Receiver implementation (m symbols in a block)

• *$2m$-symbol Transmission*

The receiver implementation is illustrated in Figure 8.12. Once again, the received continuous time signal $r(t)$ is first A/D converted. The output sequence is then downsampled by a factor of L. Also, a delayed version of the output of the A/D (delayed by l) is also downsampled by L. Similar to the m-symbol case, an FFT is performed on both the sequences to yield two column vectors $\mathbf{r^1}$ and $\mathbf{r^2}$ of length N.

The vector r^1 is transformed using Λ from (8.37) to yield the decision vector D^1. It is important to note that the MMSEC weights in the matrix Λ are now different from that in (8.39). They correspond to

$$w_i^j = \frac{\alpha_i A^2 D_i}{(\alpha_i^2 A^2 D_i \sum_{p=0}^{2m-1} \cos\left(2\pi i \Delta f(\tau_p - \tau_j)\right)^2 + \sigma_n^2)} \tag{8.40}$$

a direct result of the presence of $2m$ bits (and not m bits). Similarly the vector r^2 is transformed using Λ'. This matrix is represented as

$$\Lambda' = \begin{pmatrix} w_0^m \sqrt{D_0} e^{j2\pi 0 \cdot \Delta f \tau_m} & w_1^m \sqrt{D_1} e^{j2\pi 1 \cdot \Delta f \tau_m} & \cdots & w_{N-1}^{2m-1} \sqrt{D_{N-1}} e^{j2\pi(N-1)\cdot \Delta f \tau_m} \\ w_0^{m+1} \sqrt{D_0} e^{j2\pi 0 \cdot \Delta f \tau_{m+1}} & w_1^{m+1} \sqrt{D_1} e^{j2\pi 1 \cdot \Delta f \tau_{m+1}} & \cdots & w_{N-1}^{2m-1} \sqrt{D_{N-1}} e^{j2\pi(N-1)\cdot \Delta f \tau_{m+1}} \\ \vdots & & & \\ w_0^{2m-1} \sqrt{D_0} e^{j2\pi 0 \cdot \Delta f \tau_{2m-1}} & w_1^{2m-1} \sqrt{D_1} e^{j2\pi 1 \cdot \Delta f \tau_{2m-1}} & \cdots & w_{N-1}^{2m-1} \sqrt{D_{N-1}} e^{j2\pi(N-1)\cdot \Delta f \tau_{2m-1}} \end{pmatrix} \tag{8.41}$$

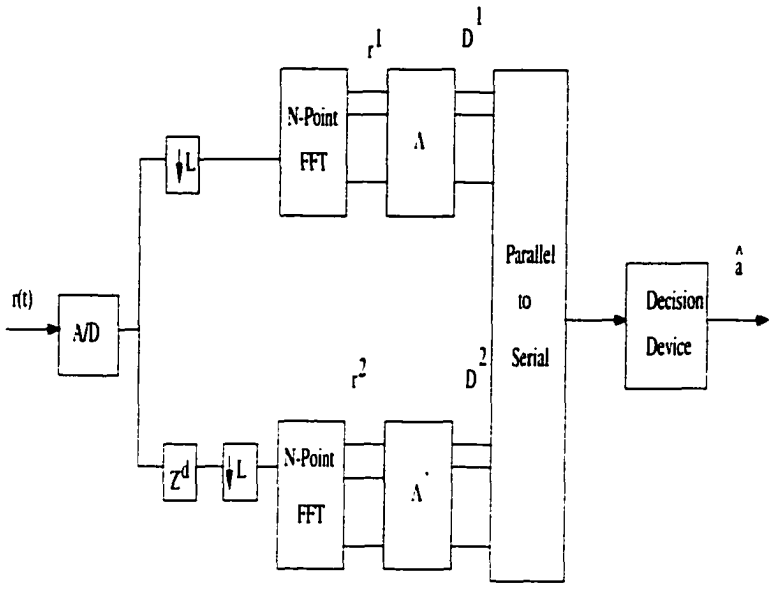

Figure 8.12: Receiver implementation ($2m$ symbols in a block)

Here, w_i^j is the same as given in equation (8.41). From Figure 8.12, we observe

$$\begin{aligned} \mathbf{D^1} &= \Lambda \mathbf{r^1} \\ \mathbf{D^2} &= \Lambda' \mathbf{r^2} \end{aligned} \tag{8.42}$$

The combined decision vector of length $2m$ now corresponds to $\mathbf{D} = ((\mathbf{D^1})^T, (\mathbf{D^2})^T)^T$. This is parallel to serial converted and then passed through a decision device to yield $\hat{\mathbf{a}}$.

Thus, the multi-carrier signal decomposition can be efficiently implemented.

8.4 Performance Results

Figures 8.13, 8.14 and 8.15 present bit error probability (BER) versus SNR performance curves for the HT, TU and RA channels respectively (see Section 4.3 for a detailed description of these channels). The dotted line marked with triangles represent the performance of a TDMA system employing a multi-carrier raised cosine pulse shape with $\alpha = 0.35$. Based on the analysis in Section 8.2.1, we choose $N = 27$

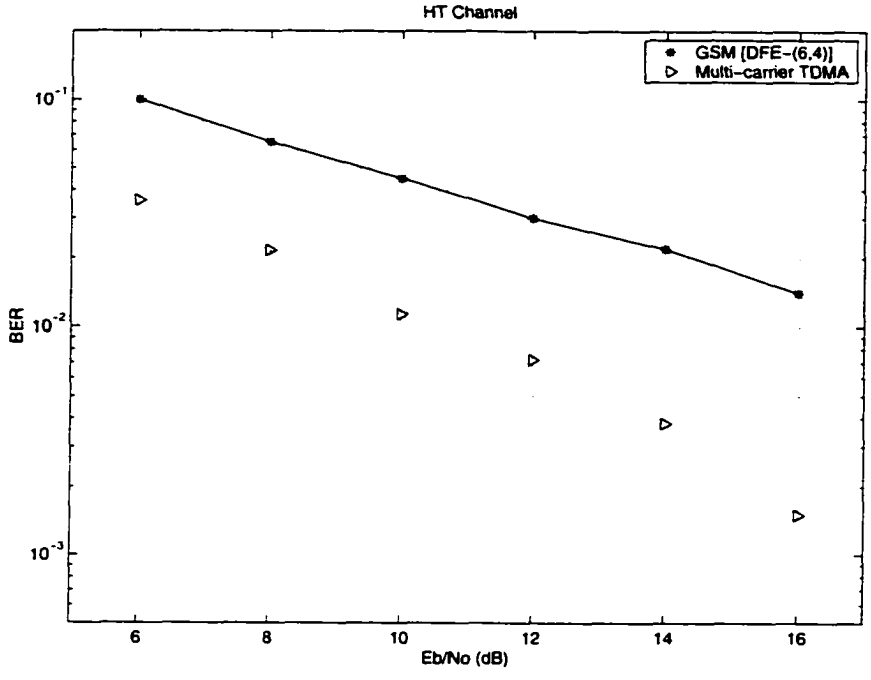

Figure 8.13: BER performance in HT channel

carriers and $m = 20$ BPSK symbols per observation block. This system is designed to support a GSM data rate of 270.8 kbps and the receiver from Section 8.3.1 is employed. The solid line (marked with stars) represents a GSM system employing Gaussian pulse shaping with a DFE(6,4) receiver [13].

The performance benefit of switching to multi-carrier pulse shapes is evident from these curves. The new system achieves close to 6 dB gains in the HT channel at probability of errors in the order of 10^{-2}. Performance gains increase dramatically at lower probability of error points. In the TU channel, gains in the order of 4 dB are achieved at probability of errors of 10^{-2}. Again, gains increase significantly at lower probability of errors. The performance benefit in the RA case is not as noticeable as in the HT and TU channel. This is consistent with the results for CI/TDMA in chapter 6, and results because, RA channels have a very large coherence bandwidth, leading to very little exploitable frequency diversity.

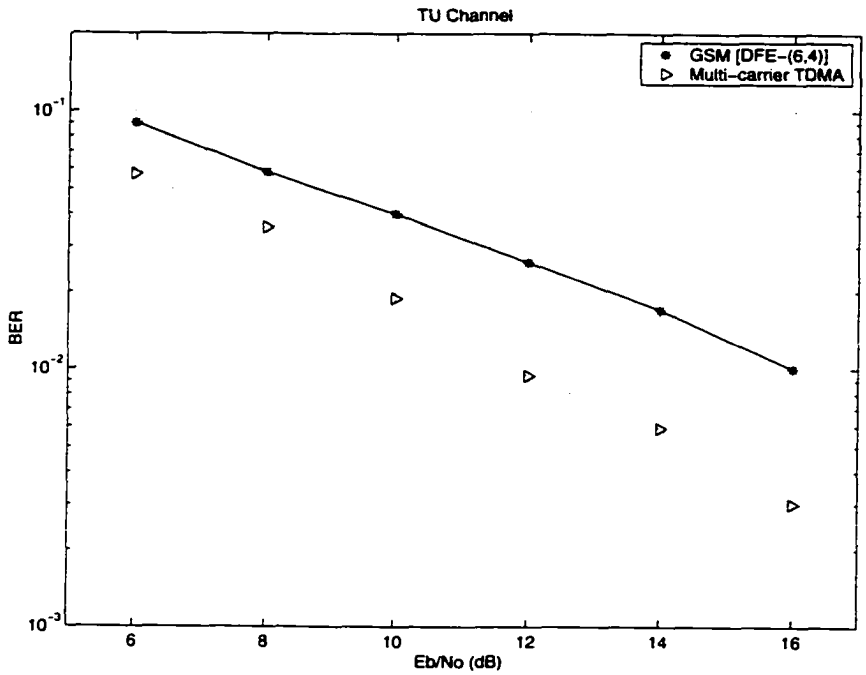

Figure 8.14: BER performance in TU channel

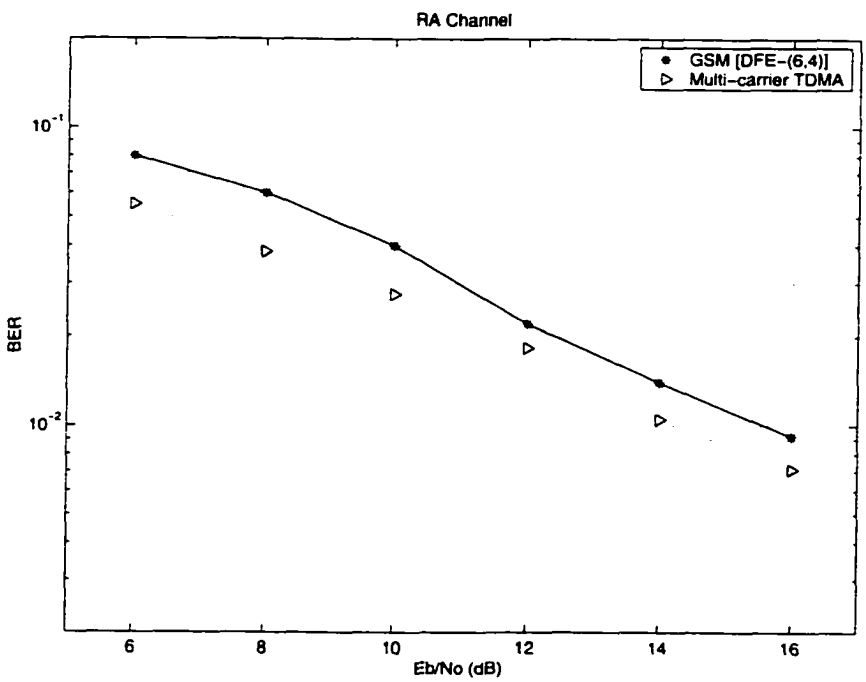

Figure 8.15: BER performance in RA channel

These results show the dramatic performance benefits achievable in frequency selective fading channels, when replacing traditional raised cosine pulse shape by a multi-carrier implementation of the same, and, correspondingly, changing the time-based equalizer receiver with a frequency-based receiver. Some of the performance benefits can be traded off for a doubling in throughput via pseudo-orthogonality as discussed in Section 8.2.3. This is illustrated in Figures 8.16 and 8.17, which present the BER versus SNR curves in HT and TU channels, respectively. The dashed line with circles demonstrates the performance of the multi-carrier TDMA system with double throughput ($2m = 40$ BPSK symbols per observation block and $2 \cdot 270.8$kbps $= 541.6$ kbps). Relative to the multi-carrier system with the original throughput of 270.8 kbps, the novel pseudo-orthogonal TDMA system demonstrates degradations of 5 dB, a direct result of ISI introduced at the transmitter side. However, the pseudo-orthogonal TDMA system supporting 541.6 kbps outperforms the GSM system (supporting 270.8 kbps) by 1 dB. (In the TU channels the gains are less than 0.1-1 dB relative to the standard GSM system). These results were obtained with no increase in transmit bandwidth, or slot duration and with no change in modulation formats. Hence, multi-carrier signal synthesis along with frequency decomposition at the receiver end provides an efficient means to double throughput and maintain good BER performance.

8.5 Summary

In this chapter, we extend the idea of spectral sampling to pulses such as raised cosine pulse shapes. A TDMA system based on multi-carrier signal synthesis and decomposition, was designed. We demonstrated that this TDMA system, with its frequency based signal processing significantly enhances performance, and has the ability to double throughput via pseudo-orthogonality. Even when the throughputs are dou-

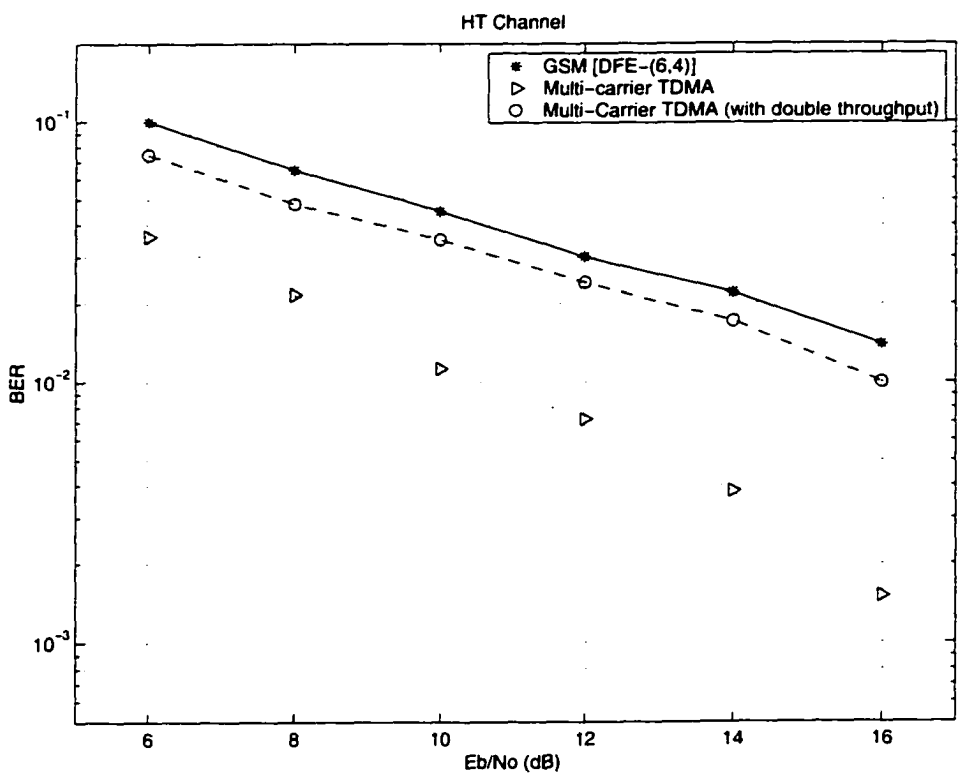

Figure 8.16: BER performance with double throughput in HT channel

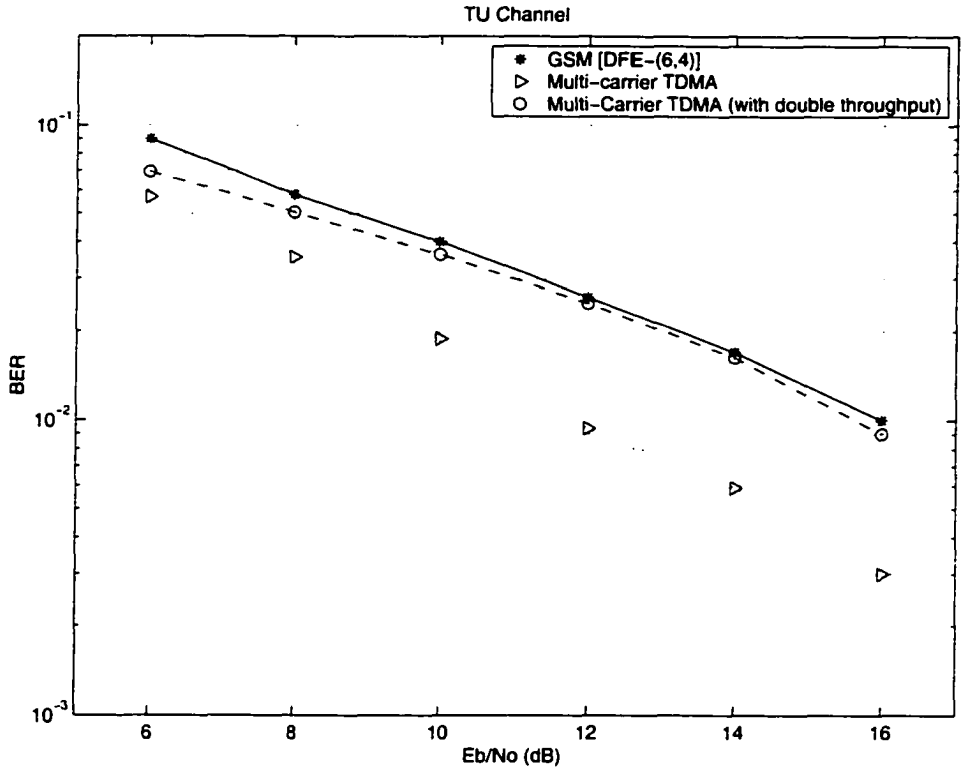

Figure 8.17: BER performance with double throughput in TU channel

bled, performance still exceeds that of traditional TDMA systems. Furthermore, we demonstrated the simplicity in implementation of this multi-carrier system by developing elegant IFFT and FFT based implementations of both the transmitter and receiver. Thus, the application of multi-carrier signal synthesis not only helps create a uniform multi-carrier framework between different wireless systems like TDMA, DS-CDMA and MC-CDMA, but also improves the performance and capacity of these systems.

Chapter 9

Conclusions

This chapter concludes this dissertation with a brief discussion of the work to date, highlighting the contributions, and a preview of possible research for the future.

9.1 Discussion and Contributions

In this thesis, we introduce the Carrier Interferometry (CI) framework. We explain how a common multi-carrier platform based on CI can be designed for MC-CDMA, TDMA and FSK systems. We demonstrate how, in each and every scenario, the proposed CI approach is able to reduce complexity and outperform existing receiver structures in multipath fading channels, due to better exploitation of channel diversity. Furthermore, we demonstrate how this approach can result in increases in network capacity (measured in terms of number of users or throughput per user).

First, we introduced the Carrier Interferometry concept and presented the fundamental building block of this approach, the CI signal. We presented the orthogonal and pseudo-orthogonal properties of this signal and discussed its applicability to multiple access schemes.

Next, the CI approach was incorporated into MC-CDMA via complex CI spreading codes. We demonstrated that CI codes provide both flexibility and excellent bit-error-

rate (BER) performance relative to traditional MC-CDMA employing Hadamard Walsh (HW) codes. In synchronous frequency selective Rayleigh fading channels, CI/MC-CDMA's performance is close to but better than that of orthogonal MC-CDMA using Hadamard-Walsh codes up to the MC-CDMA $K = N$ user limit; moreover, CI/MC-CDMA provides the added flexibility of supporting $K > N$ (up to $K = 2N$) users by adding users with pseudo orthogonal codes. This doubling in capacity is achieved with no cost in bit-error-rate performance. CI/MC-CDMA also provides added flexibility in the choice of N ($N \in I$ versus $N = 2^n$ or $N = 2^n \pm 1$ ($n \in I$)) making it more robust to the wide range of mobile system applications. We also derive the minimum-mean-squared error and maximal ratio combining receivers for CI/MC-CDMA.

Next, the CI/MC-CDMA system was tested in the presence of phase jitters and frequency offsets and was found to demonstrate very graceful degradations in performance in the presence of synchronization errors. We also addressed the signal compactness issue in CI/MC-CDMA: An analysis of the CI/MC-CDMA downlink shows that crest factor is not a concern, while CI/MC-CDMA uplink suffers from poor crest factor values. With this in mind, Schroeder's crest factor reduction technique is applied and shown to reduce the uplink crest factor to very low values (close to that of a pure sine wave), making it a non-issue in the uplink as well.

This thesis then introduced the Carrier Interferometry signal as a pulse shape in TDMA systems. We showed that a multi-carrier implementation of GSM via CI pulse shapes can lead to dramatic benefits in terms of probability-of-error performance (5-8 dB gains relative to GSM system employing a DFE (6,4)). CI/TDMA, with its frequency-based signal processing is (1) bandwidth efficient, and (2) has the ability to double throughput by positioning CI pulse shapes pseudo-orthogonally in time. Even when the throughputs are doubled, performance still exceeds that of traditional

TDMA systems (4-6 dB gains relative to GSM employing a DFE(6,4)).

This thesis then applied the CI approach to FSK modulation to enhance performance and throughput. Specifically, the new scheme is (1) spectrally efficient relative to traditional FSK, and (2) supports increased throughputs through pseudo-orthogonal symbol positioning. It is also shown that (3) the carrier interferometry envelope of the CI/FSK signal maintains excellent peak to average power ratios. (4) The novel coherent receiver designed for CI/FSK makes it suitable for use in frequency selective channels, with the system benefiting from the available frequency diversity.

Finally, we extend the idea of CI to general pulse shaping theory. We developed a multi-carrier implementation of common Nyquist pulses like raised cosine and Gaussian pulse shapes. The multi-carrier synthesis, based on a time limited truncated Fourier series approximation of the actual pulse shapes, enables the design of receivers that perform frequency domain processing (as in OFDM, MC-CDMA). The time domain equalizer receivers are replaced by receivers that decompose the signal into its constituent carriers and recombine them coherently. This receiver structure exploits frequency diversity and maintains a common hardware implementation relative to MC-CDMA, CI/TDMA and other CI based systems.

Thus, we demonstrated that CI can serve as a "fundamental element," enabling all systems to be recreated by novel implementation of this one "element". As shown in this thesis, CI not only provides a common signal architecture for different multiple access techniques, it also vastly improves the performance and capacity of those techniques.

9.2 Future Work

This section presents possible avenues for future research. This future work can be divided into two categories: work on the CI based systems introduced in this thesis, and work on new applications of this technology.

9.2.1 CI-Based Systems

Further work can be carried out on the CI based systems that we have introduced to date.

- *Asynchronous Transmission*

  First, we can characterize the performance of CI based systems in asynchronous uplinks.

- *Jamming Resistance*

  We have yet to consider the effects of narrow-band and wide-band jammers in CI/MC-CDMA and CI/TDMA systems. This work in the future, can provide insights into the reliability offered by CI based systems.

- *Multi-user Detection*

  In a multi-user environment, the truly optimal receivers are the multi-user detectors. We will analyze the applicability of multi-user detection (MUD) techniques to CI based systems. There is also scope for developing novel multi-stage MUDs, specifically designed for CI based systems, that can help enhance both performance and capacity. The MUD techniques, traditionally applied only to CDMA based systems can be extended to CI/TDMA. Here, we can extrapolate the ideas of MUDs to multi-symbol detection to help improve performance and throughput.

- *Modulation Format*

  We have assumed BPSK transmission throughout this work. In the future, we

can analyze and test the CI based systems with other modulation formats such as QPSK, differential PSK, QAM etc.

9.2.2 Applications

The ideas introduced in this thesis can be used in a variety of novel applications.

• *Zero Bandwidth Expansion Channel Coding*

In chapter 3, we suggested the use of $2N$ CI signals to represent $2N$ information symbols by exploiting the pseudo-orthogonal properties of the CI signal. Specifically, this translates into the simultaneous use of N CI spreading codes and N offset CI spreading codes in MC-CDMA. In the future, we can explore the idea of using the N offset CI codes to transmit redundancy bits generated via a rate $1/2$ channel coder. By doing this, the BER performance of MC-CDMA can be dramatically improved via channel coding, while still maintaining high throughputs and identical bandwidth. This idea can also be extended to systems employing pseudo-orthogonal CI pulse shapes. Here, the pseudo-orthogonal pulses are used to transmit redundancy bits generated by the channel coder.

• *Optical Fiber Applications*

The CI approach introduced in this thesis lends itself well to optical fiber communications. This is a direction of future research that has tremendous potential. Specifically, we can explore the use of coherent multi-wavelength transmission in dispersion limited fibers. By employing reception techniques similar to frequency domain processing in wireless systems, rather than traditional time domain equalizer structures, we can analyze the performance and throughput benefits that can be achieved.

In summary, we have introduced a fundamental technology that can play a big part in the wireless future and illustrated some of the many research directions that will be considered next. There is no doubt that research on Carrier Interferometry

systems and applications will continue to be important in the years to come.

REFERENCES

[1] W. Webb, *Future of wireless communications.* Artech House Publishers, 1st ed., May 2001.

[2] A. Dornan, *The essential guide to wireless communications applications.* Prentice Hall, 1st ed., May 2001.

[3] X.Revws, A.Gelonch, and F.Casadevall, "Software radio implementation of a DS-CDMA indoor subsystem based on FPGA devices," in *Proceedings of IEEE International Conference on Personal, Indoor and Mobile Radio Communications*, vol. 1, pp. 86–90, Sep. 2001.

[4] M.Laddomada, F.Daneshgaran, M.Mondin, and R.M.Hickling, "A PC based software receiver using a novel front-end technology," *IEEE Communications Magazine*, vol. 39,no. 8, pp. 136–145, Aug. 2001.

[5] V.Bose, R.Hu, and R.Morris, "Dynamic physical layers for wireless networks using software radio," in *Proceedings of IEEE International Conference on Acoustics, Speech and Signal Processing*, vol. 4, pp. 2045–2048, 2001.

[6] S.Zhao, C.Luo, X.Su, and M.Zhao, "A flexible waveform synthesis method for software radio," in *Proceedings of IEEE Vehicular Technology Conference*, vol. 3, pp. 1907–1911, Spring 2001.

[7] S.P.Korah and S.A.Mcdonald, "Towards the implementation of a WCDMA AAA receiver on an FPGA software radio platform," in *Proceedings of IEEE Vehicular Technology Conference*, vol. 3, pp. 1917–1921, Spring 2001.

[8] N.J.Drew and M.M.Dillinger, "Evolution toward a reconfigurable user equipment," *IEEE Communications Magazine*, vol. 39, no. 2, pp. 158–164, Feb. 2001.

[9] K.Zangi and R.Koilpillai, "Software radio issues in cellular base stations," *IEEE Journal on Selected Areas in Communications*, vol. 17, pp. 561–573, Apr. 1999.

[10] V.Bose, M.Ismert, M.Welborn, and J.Guttag, "Virtual radios," *IEEE Journal on Selected Areas in Communications*, vol. 17, no. 4, pp. 591–602, April 1999.

[11] J.Wang, M.Zhao, X.Xu, and Y.Yao, "Hardware platform of the software radio," in *Proceedings of IEEE International Conference on Personal, Indoor and Mobile Radio Communications*, vol. 1, pp. 11–15, 1999.

[12] Bluetooth SIG group, *Specification of the Bluetooth system*, July 1999.

[13] B.A.Bjerke, J.G.Proakis, M.K.Lee, and Z.Zvonar, "A comparison of decision feedback equalization and data directed estimation technique for the GSM system," in *IEEE 6th International conference on Universal personal communications*, vol. 1, pp. 84–88, 1997.

[14] M.Rupp and A.Bahai, "Training and tracking of adaptive DFE algorithms under IS-136," in *Proceedings of the First IEEE Workshop on signal processing advances in wireless communications, SPAWC*, pp. 341–344, 1997.

[15] J.Tellado-Mourelo, E. Wesel, and J.M.Cioffi, "Adaptive DFE for GMSK in indoor radio channels," *IEEE Journal on Selected Areas in Communications*, vol. 14, no. 3, pp. 492–501, Apr. 1996.

[16] M.Rahnema, "Channel equalization for the GSM system," in *Proceedings of IEEE International Conference on Personal, Indoor and Mobile Radio Communications*, vol. 3, pp. 878–882, 1996.

[17] G.D.Aria, R.Piermarini, and V.Zingarelli, "Fast adaptive equalizers for narrowband TDMA mobile radio," *IEEE Transactions on Vehicular Technology*, pp. 392–404, May 1991.

[18] F.Vanhaverbeke, M.Moeneclaey, and H.Sari, "An excess signaling concept with Walsh-Hadamard spreading and joint detection," in *Proceedings of Globecom 2000 Conference Record*, vol. 2, pp. 906–909, Nov. 2000.

[19] R.E.Learned, A. Willisky, and D.M.Boroson, "Low complexity joint detection for oversaturated multiple access communications," *IEEE Transactions on Signal Processing*, vol. 45, pp. 113–122, Jan. 1997.

[20] S.Verdu, *Multiuser detection.* Cambridge University Press, 1 ed., Sep. 1998.

[21] L.B.Nelson and H.V.Poor, "Iterative multiuser receivers for CDMA channels: An EM based approach," *IEEE Transactions on Communications*, vol. 44, no. 12, pp. 1700–1718, Dec. 1996.

[22] P.Patel and J.Holtzman, "Analysis of a simple successive interference cancellation scheme in DS/CDMA system," *IEEE Journal on Selected Areas in Communications*, vol. 12,no. 5, pp. 796–807, June 1996.

[23] U.Madhow and L.Honig, "MMSE interference suppression for direct-sequence spread spectrum CDMA," *IEEE Transactions on Communications*, vol. COM-42, no. 12, pp. 3178–3188, Dec. 1994.

[24] K.S.Juo, U.S.Goni, and A. Turkmani, "Comparitive evaluation of the performance of anti-multipath modulation techniques for digital mobile radio sys-

tems," in *Proceedings of IEEE Vehicular Technology Conference*, pp. 1557–1561, June 1994.

[25] P.S.K.Leung, "Asymmetric-Raised-Cosine frequency shift keying (ARC-FSK)-A New Modulation with superior anti-multipath characteristics for mobile and personal communications systems," in *Proceedings of 4th IEEE International conference on Universal Personal Communications*, pp. 117–122, 1995.

[26] F.Danila and H.Leib, "FSK and DPSK over unresolved multipath Rayleigh fading channels," in *Proceedings of IEEE International Conference on Personal, Indoor and Mobile Radio Communications*, vol. 2, pp. 477–481, 1195.

[27] R.Petrovic and A.F.Molisch, "Reduction of multipath effects for FSK with frequency discriminator detection," in *Proceedings of IEEE International Conference on Personal, Indoor and Mobile Radio Communications*, vol. 3, pp. 943–948, 1997.

[28] M.K.Varanasi, "Non-coherent equalization for multipulse modulation," in *Proceedings of IEEE International conference on Personal Wireless Communications*, pp. 218–222, 1997.

[29] V.A.Aalo and J.Zhang, "Performance of maximal ratio combining diversity in a Nakagami fading channel with co-channel interference," in *Proceedings of IEEE Wireless Communications and Networking Conference, WCNC '99*, vol. 1, pp. 1–5, 1999.

[30] Y.Xin, S.Zhang, M.K.Simon, and M.S.Alouini, "Average BER performance of non-coherent orthogonal M-FSK over Nakagami fading channels," in *Proceedings of IEEE Wireless Communications and Networking Conference, WCNC '00*, vol. 3, pp. 1065–1069, 2000.

[31] T.De Couasnan *et. al*, "OFDM for digital TV broadcasting," *Signal Processing*, vol. 39, pp. 1–32, 1994.

[32] A. Hac, *Multimedia Applications Support for Wireless ATM Networks.* Prentice Hall PTR, 2000.

[33] B. Flock, M.Alard, and C.Berrou, "Coded orthogonal frequency division multiplex," *Proceedings of the IEEE*, vol. 83, no. 6, June 1995.

[34] M.Alard and R.Lasalle, "Principle of modulation and channel coding for digital broadcasting for mobile receivers," *EBU Technical Review*, pp. 168–190, Aug. 1987.

[35] A.Ruiz and J.M.Cioffi, "Discrete multiple tone modulation with coset coding for the spectrally shaped channel," *IEEE Transactions on Communications*, vol. 40, no. 2, pp. 1012–1029, June 1992.

[36] E.Classes and H.Meyer, "Frequency synchronization algorithms for OFDM systems suitable for communication over frequency selective fading channels," in *Proceedings of IEEE Vehicular Technology Conference*, vol. 3, pp. 1655–1659, 1994.

[37] E.G.Larsson and J.Li, "Preamble design for multiple-antenna OFDM-based WLANs with null subcarriers," *IEEE Signal Processing Letters*, vol. 8, no. 11, pp. 285–288, Nov. 2001.

[38] H.Sari, G.Karam, and I. J. Claude, "Transmsission techniques for digital terrestrial TV broadcasting," *IEEE Communications Magazine*, vol. 33, no. 2, pp. 100–109, Feb. 1995.

[39] N.Yee, J.P.Linnartz, and G.Fettweis, "Multi-carrier CDMA in indoor wireless radio," in *Proceedings of IEEE International Conference on Personal, Indoor and Mobile Radio Communications*, pp. 109–113, Dec. 1993.

[40] S.Hara and R.Prasad, "DS-CDMA, MC-CDMA and MT-CDMA for mobile multi-media communications," in *Proceedings of IEEE Vehicular Technology Conference*, pp. 1106–1110, Apr. 1996.

[41] K.Fazel, S.Kaiser, and M.Schnell, "A flexible and high performance mobile communications system based on orthogonal multi-carrier SSMA," *Wireless Personal Communications*, pp. 295–305, 1996.

[42] T.Mueller, K.Brueninghauss, and H.Rohling, "Performance of coherent OFDM-CDMA for broadband mobile communications," *Wireless Personal Communications*, pp. 1665–1669, 1995.

[43] N.Yee and J.P.Linnartz, "Controlled equalization of multi-carrier CDMA in an indoor Ricean fading channel," in *Proceedings of IEEE Vehicular Technology Conference*, pp. 1665–1669, 1994.

[44] J.M.G.Linnartz, "Performance analysis of synchronous MC-CDMA in mobile Rayleigh channel with both delay and doppler spreads," *IEEE Transactions on Vehicular Technology*, vol. 50,no. 6, pp. 1375–1387, Nov. 2001.

[45] P.Zong, J.Wang, and Y.Bar-ness, "Partial sampling MMSE interference suppression in asynchronous multi-carrier CDMA system," *IEEE Journal on Selected Areas in Communications*, vol. 19, no. 8, pp. 1605–1613, Aug. 2001.

[46] L.Brunel, "Design of a high-speed MC-CDMA for broadband mobile radio communications," in *Proceedings of IEEE International Conference on Personal, Indoor and Mobile Radio Communications*, vol. 1, pp. 16–20, Oct. 2001.

[47] W.Zhao, X.Lu, and J.Zhu, "M-ary MC-CDMA system for 4G," in *Proceedings of IEEE Vehicular Technology Conference*, vol. 4, pp. 2234–2238, Fall 2001.

[48] R.Wang and S.Chen, "Performance of MC-CDMA based on wavelet packets in Rayleigh multipath fading channel," *IEE Electronics Letters*, vol. 36, no. 12, pp. 1070–1072, June 2000.

[49] Bob O'Hara and A.Petrick, *The IEEE 802.11 Handbook: A designer's companion.* IEEE Press, 1999.

[50] B.G.Evans and K.Baughan, "Visions of 4G," *Electronics and Communication Engineering Journal*, vol. 12, no. 6, pp. 293–303, Dec. 2000.

[51] S.Hara and R.Prasad, "Overview of multi-carrier CDMA," *IEEE Communications Magazine*, vol. 35, no. 12, pp. 126–133, Dec. 1997.

[52] R. Prasad, *Universal Wireless Mobile Personal Communications.* Artech House, 1998.

[53] S.Zhou, G.B.Giannakis, and A.Swami, "Comparison of digital multi-carrier with direct sequence spread spectrum in the presence of multipath," in *Proceedings of IEEE International Conference on Acoustics, Speech and Signal Processing*, vol. IV, pp. 2225–2228, May 2001.

[54] Z. Wu, *High performance multi-carrier technologies with expanded applicability to CDMA systems (DS-CDMA and MC-CDMA).* PhD thesis, Colorado State University, Fort Collins, Colorado, Spring 2002.

[55] B.M.Popovic, "Spreading sequences for multicarrier CDMA systems," *IEEE Transactions on Communications*, vol. 47, no. 6, pp. 918–926, June 1999.

[56] C.R.Nassar, B.Natarajan, Z.Wu, D.Wiegandt, S.A.Zekavat, and S.Shattil, *Multi-carrier technologies for wireless communication.* Kluwer Academic Publishers, 1 ed., 2002.

[57] B.Natarajan, C.R.Nassar, S.Shattil, M.Michelini, and Z.Wu, "High performance MC-CDMA via Carrier Interferometry codes," *IEEE Transactions on Vehicular Technology*, vol. 50, no. 6, pp. 1344–1354, Nov. 2001.

[58] C.R.Nassar, B.Natarajan, and S.Shattil, "Introduction of Carrier Interference to spread spectrum multiple access," in *Proceedings of the IEEE Emerging Technologies Symposium on Wireless Communications and Systems*, Apr. 1999.

[59] Z.Wu, B.Natarajan, C. Nassar, and S.Shattil, "High performance, high capacity MC-CDMA via Carrier Interferometry," in *Proceedings of IEEE International Conference on Personal, Indoor and Mobile Radio Communications*, vol. 2, pp. 11–16, Oct. 2001.

[60] B.Natarajan, Z.Wu, and C. Nassar, "Large set of CI spreading codes for high-capacity MC-CDMA," *submitted to IEEE Transactions on Communications*, 2002.

[61] C.R.Nassar, B.Natarajan, D.Wiegandt, and Z.Wu, "Multi-carrier technology platform for wireless communications: Part II," *accepted for publication in Wireless Communications Magazine*, 2002.

[62] B.Natarajan, C.R.Nassar, and S.Shattil, "Innovative pulse shaping for high performance wireless TDMA," *IEEE Communication Letters*, vol. 5, no. 9, pp. 372–374, Sep. 2001.

[63] B.Natarajan, C.R.Nassar, and S.Shattil, "Exploiting frequency diversity in TDMA through Carrier Interferometry," in *Proceedings of Wireless 2000*, vol. 2, pp. 1799–1803, July 2002.

[64] B.Natarajan, C.R.Nassar, and S.Shattil, "Throughput enhancement in TDMA through Carrier Interference pulse shaping," in *Proceedings of IEEE Vehicular Technology Conference*, vol. 4, pp. 1799–1803, Fall 2000.

[65] C.R.Nassar, B.Natarajan, and Z.Wu, "Multi-carrier technology platform for wireless communications: Part I," *accepted for publication in Wireless Communications Magazine*, 2002.

[66] B.Natarajan, C.R.Nassar, and S.Shattil, "High-capacity, high-throughput TDMA through pseudo-orthogonal Carrier Interferometry pulse shaping," *submitted to IEEE Transactions on Wireless Communications*, 2002.

[67] B.Natarajan, C.R.Nassar, and S.Shattil, "Enhanced Bluetooth and IEEE 802.11(FH) via multicarrier implementation of the physical layer," in *Proceedings of the IEEE Emerging Technologies Symposium*, pp. 129–133, Sep. 2001.

[68] B.Natarajan, C.R.Nassar, and S.Shattil, "High data rate FSK via multi-carrier implementations for wireless personal area networks," in *submitted to ITCOM*, 2002.

[69] B.Natarajan, C.R.Nassar, and S.Shattil, "CI/FSK: Bandwidth efficient FSK for high performance, high throughput and enhanced applicability," *submitted to IEEE Transactions on Communications*, 2002.

[70] B.Natarajan and C.R.Nassar, "Multi-carrier signal synthesis and decomposition for high performance, high throughput TDMA," *to be submitted to IEEE Transactions on Communications*, 2002.

[71] B.Natarajan and C.R.Nassar, "Crest factor considerations in MC-CDMA with Carrier Interferometry codes," in *Proceedings of IEEE Pacific Rim Conference*, vol. 2, pp. 445–448, Aug. 2001.

[72] T.S.Rappaport, *Wireless Communications - Principles and Practice.* Prentice Hall, 1 ed., 1996.

[73] A.J.Viterbi, *CDMA: Principles of spread spectrum communication.* Addison Wesley Publishing Company, 1 ed., 1995.

[74] J.Korhonen, *Introduction to 3G mobile communications.* Artech House Publishing Company, 1 ed., 2001.

[75] R.Prasad, *CDMA for Wireless Personal Communications.* Artech House Publishing Company, 1 ed., 1996.

[76] R. V. Nee and R.Prasad, *OFDM for wireless multimedia communications.* Artech house Publishing Company, 1 ed., 2000.

[77] W.H.Steel, *Interferometry.* Cambridge University Press, 1 ed., 1967.

[78] F.Kleer, S.Hara, and R.Prasad, *CDMA Techniques for Third Generation Mobile Systems*, pp. 185–215. Kluwer Academic Publishers, 1 ed., 1999.

[79] *TS C101 V3.0.0 - China Wireless Telecommunications Standard (CWTS) Physical Layer - General Description*, 1999.

[80] J.G.Proakis, *Digital Communications.* McGraw-Hill, 3 ed., 1995.

[81] W.Xu and L.B.Milstein, "Performance of multicarrier DS CDMA Systems in the presence of correlated fading," in *Proceedings of IEEE Vehicular Technology Conference*, pp. 2050–2054, May 1997.

[82] W.C.Jakes, *Microwave Mobile Communications.* IEEE Press, 1994.

[83] C. of the European Community, *COST-207: Digital land mobile radio communications, Final report of the COST-Project 207*, 1989.

[84] *TR 101 112-Universal mobile telecommunications system (UMTS)*, 1997.

[85] T.M.Lok, T.F.Wong, and J.S.Lehnert, "Blind adaptive signal reception for MC-CDMA systems with interference suppression," in *Military Communications Conference, MILCOM*, vol. 3, pp. 752–756, 1998.

[86] Leon-Garcia, *Probability and Random Processes for Electrical Engineering.* Addison Wesley Publishing Company, 2 ed., 1994.

[87] S.Haykin, *Adaptive Filter Theory.* Prentice Hall, 1991.

[88] R.B.Ertel and J.H.Reed, "Generation of two equal power correlated Rayleigh fading envelopes," *IEEE Communications Letters*, vol. 2,no. 10, pp. 276–278, Oct. 1998.

[89] E.Kreysig, *Advanced Engineering Mathematics.* John Wiley & Sons, 8 ed., 1998.

[90] B.M.Popovic, "Synthesis of power efficient multitone signals with flat amplitude spectrum," *IEEE Transactions on Communications*, vol. 39, pp. 1031–1033, July 1991.

[91] H.Leib and S.Pasupathy, "Trellis-coded MPSK with reference phase errors," *IEEE Transactions on Communications*, vol. COM-35, no. 9, Sep. 1987.

[92] W.C.Lindsey and M. Simon, *Telecommunication Systems Engineering.* Prentice Hall, 1973.

[93] Y.Kim, S.Choi, C.You, and D.Hong, "Effect of carrier frequency offset on the performance of an MC-CDMA system and its countermeasure using pulse

shaping," in *Proceedings of IEEE International Conference on Communications*, vol. 1, pp. 167–171, June 1999.

[94] P.H.Moose, "A technique for orthogonal frequency division multiplexing frequency offset correction," *IEEE Transactions on Communications*, vol. 42, no. 10, pp. 2908–2914, Oct. 1994.

[95] E. Ouderaa, J.Schoukens, and J.Renneboog, "Peak factor minimization of input and output signals of linear systems," *IEEE Transactions on Instrumentation and Measurement*, vol. 37, no. 2, pp. 207–212, June 1988.

[96] K.Fazel and S.Kaiser, "Analysis of non-linear distortions on MC-CDMA," in *Proceedings of International Conference on Communications*, vol. 2, pp. 1028–1034, 1998.

[97] M.R.Schroeder, "Synthesis of low-peak-factor signals and binary sequences with low autocorrelation," *IEEE Transactions on Information Theory*, vol. IT-16, pp. 85–89, Jan. 1970.

[98] A. V. den Boss, "A new method for synthesis of low-peak-factor signal," *IEEE Transactions on Acoustics, Speech, Signal Processing*, vol. ASSP-35, no. 1, pp. 120–122, Jan. 1987.

[99] V.Aue and G.P.Fettweis, "Multi-carrier spread spectrum modulation with reduced dynamic range," in *Proceedings of IEEE Vehicular Technology Conference*, pp. 914–917, May 1996.

[100] P.A.Laurent, "Exact and approximate construction of digital phase modulations by superposition of amplitude modulated pulses," *IEEE Transactions on Communications*, pp. 150–160, Feb. 1986.

[101] E.A.Lee and D.G.Messerschmitt, *Digital Communications.* Kluwer Academic Publishers, 1990.

[102] J.C.Haartsen and S.Mattisson, "Bluetooth- a new low-power radio interface providing short-range connectivity," *Proceedings of the IEEE*, vol. 88, no. 10, pp. 1651–1661, Oct. 2000.

[103] C.Bisdikian, "An overview of the Bluetooth wireless technology," *IEEE Communications Magazine*, vol. 39, no. 12, pp. 86–94, Dec. 2001.

[104] B.Natarajan, C.R.Nassar, and V.Chandrasekhar, "Generation of correlated Rayleigh fading envelopes for spread spectrum applications," *IEEE Communications Letters*, vol. 4, no. 1, pp. 9–12, Jan. 2000.

[105] H.Nyquist, "Certain topics in telegraph transmission theory," *Transactions AIEE*, vol. 47, pp. 617–644, Apr. 1928.

[106] M.Sablatash, J.L.Lodge, and K.W.Moreland, "Theory and methods for design of pulse shapes for broadcast teletext," *IEEE Transactions on Broadcasting*, vol. 35, no. 1, pp. 40–55, Mar. 1989.

[107] R.A.Nobakht and M. Civanlar, "Optimal pulse shape design for digital communication systems by projections onto convex sets," *IEEE Transactions on Communications*, vol. 43, no. 12, pp. 2874–2877, Dec. 1995.

[108] X.Xia, "A family of pulse-shaping filters with ISI free matched and unmatched filter properties," *IEEE Transactions on Communications*, vol. 45, no. 10, pp. 1157–1158, Oct. 1997.

[109] E.H.Satorius and J.J.Mulligan, "Pulse shape design considerations for self synchronizing systems," in *Proceedings of 25th Asilomar Conference on Signals, Systems and Computers*, vol. 2, pp. 1170–1174, 1991.

[110] N.C.Beaulieu, C.C.Tan, and M.O.Damen, "A better than Nyquist pulse," *IEEE Communications Letters*, vol. 5, no. 9, pp. 576–580, Sep. 2001.

[111] W.W.Jones, "Multi-scale wavelet modulation," in *Proceedings of the 26th Southeastern Symposium on System theory*, pp. 576–580, 1994.

[112] P.P.Gandhi, S.S.Rao, and R.S.Pappu, "Wavelets for waveform coding of digital symbols," *IEEE Transactions on Signal Processing*, vol. 45, no. 9, pp. 2387–2390, Sep. 1997.

[113] S.H.Mueller-Weinfurtner, "Optimum Nyquist windowing in OFDM receivers," *IEEE Transactions on Communications*, vol. 49, no. 2, pp. 417–420, Mar. 2001.

[114] P.Guinand and J.Lodge, "Optimal pulse shape design for OFDM transmission with few subcarriers," in *Proceedings of Canadian Conference on Electrical and Computer Engineering*, vol. 1, pp. 17–19, 1995.

[115] H.Bolcskei, P.Duhamel, and R.Hleiss, "Design of pulse shaping OFDM/OQAM systems for high data rate transmission over wireless channels," in *Proceedings of IEEE International Conference on Communications*, vol. 1, pp. 559–564, 1999.

[116] A.Vahlin and N.Holte, "Optimum finite duration pulses for OFDM," *IEEE Transactions on Communications*, vol. 4, pp. 10–14, Jan. 1996.

[117] W.Ma, P.C.Ching, and K.M.Wong, "Maximum likelihood detection for multicarrier systems employing non-orthogonal pulse shapes," in *Proceedings of IEEE International Conference on Acoustics, Speech and Signal Processing*, vol. 5, pp. 2489–2492, 2000.

[118] X.P.Chen and S.L.Lu, "FIR filter design:frequency sampling method based on evolutionary programming," in *Proceedings of 2000 Congress on Evolutionary computation*, vol. 1, pp. 575–579, 2000.

[119] A.S.Bopardikar, R.M.Rao, and B.S.Adiga, "Matched sampling systems, relation to wavelets and implementation using PRCC filter banks," *IEEE Transactions on signal processing*, vol. 48, no. 8, pp. 2269–2278, Aug. 2000.

[120] T.J.Cavicchi, "DFT Time-domain interpolation," *Proceedings of Inst. Elect. Eng.*, vol. 139, no. 3, pp. 207–211, June 1992.

[121] G.D.Cain, N.P.Murthy, and A.Tarczynski, "Evaluation of several variable FIR fractional sample delay filters," in *Proceedings of IEEE International Conference on Acoustics, Speech and Signal Processing*, pp. 621–624, Apr. 1994.

[122] A. Poularikas and S.Seely, *Signals and Systems.* PWS-Kent Publishing, 2 ed., 1990.

[123] J.S.Lee and L.E.Miller, *CDMA System Engineering Handbook.* Artech House Publishers, 1 ed., 1998.